(-)-Indolactam V and MO47: Reducing Heterogeneity in Human iPSC Culture



A thesis submitted in partial fulfilment of the requirements for the degree of MSc by Research in Pharmacology

Maximilian Schüßler
St. John's College
Department of Pharmacology

Supervisor: Professor Angela J. Russell
Departments of Chemistry and Pharmacology

Abstract

The induction of induced pluripotent stem cells (iPSCs) presents a paradigm shift for cell therapies, disease modelling, drug screenings and toxicology. Notably, the first clinical trials are attempting to bring iPSC derived therapy from bench to bedside. Consequently, the demand for iPSCs has seen a considerable surge, and thereby incentivised the scale-up from 2D to 3D culturing systems. Current iPSC culture in 2D is contact-dependent. This gives rise to a lack of uniformity in iPSC cultures: cells that experience overcompaction in the centre or a lack of external cues at the edge of iPSC colonies grow with different properties, and are prone to differentiation. Colony-independent culture is promising to reduce heterogeneity in 2D culture, enabling more reproducible iPSC growth, optimised differentiation and passaging. This research project argues for a chemical approach to improve 2D culturing: the disruption of iPSC colonies and cell-cell aggregates via two structurally related protein kinase C (PKC) activators, namely (-)-Indolactam V and MO47. As a proof-of-principle, the phenotypic effects of the small molecules were examined in 2D culture. Subsequently, the mechanism of action (MoA) of each compound was investigated by focusing on PKC and E-cadherin. Finally, we assessed whether serial treatment with MO47 would impair key iPSC characteristics. Treatment with MO47 and (-)-Indolactam V resulted in the disruption of iPSC colonies and the induction of a spread phenotype. The findings support a model, in which rearrangements of the actin cytoskeleton are accompanied by the flattening of the cytoplasm. This phenotype was strong, reproducible and reversible. Combined treatment of the PKC activators with the PKC inhibitor Gö6983 resulted in the disruption of these phenotypes. We could not confirm E-cadherin cleavage or internalisation via endocytosis as an underlying MoA. Importantly, the study provides strong evidence for the preservation of iPSC characteristics upon serial treatment with MO47. The spontaneous differentiation of MO47 treated iPSCs to endoderm, mesoderm and ectoderm *in vitro* resulted in the upregulation of gene signatures for all three germ layers (ScoreCard). These findings were corroborated by the successful directed differentiation to the ectodermal (cortical neurons) and the mesodermal (macrophages) lineage. Finally, the study paves the way to further studies in 3D culture with the question as to whether MO47 can prevent the formation of difficult-to-dissociate aggregates.

Acknowledgments

I would like to express my deepest gratitude to Dr Laurence Silpa and Professor Angela Russell, my supervisors, for their patient guidance, their constructive recommendations and for giving me this fascinating interdisciplinary research project. I would further like to thank my joint supervisor, Professor Sebastian Nijman. Special thanks are due to Dr Sally Cowley and Professor William James, who have given me a sense of belonging in their great laboratory; their constant supervision and astute advice has been invaluable for the completion of my work. I am incredibly grateful to Dr Hazel Roberts, Cathy Browne and Janes Vowles, for their considerable scientific support, their patience and their encouragement during my writing process. Nothing provides more happiness than combining your passions with learning from great people. Particularly, I would like to thank Cathy for her incredible effort in improving my English. My special thanks are extended to Dr Kenny Moore, Benjamin Dodsworth, Dr Julian Buchrieser and Dr Walther Haenseler, whose critique and scientific advice have been invaluable to me. I would like to express special thanks to Dr Alan Wainman, Dr Maryam Qurashi and Dr Andrew Jefferson for sharing their imaging expertise and helping my cells to put their best face forward.

I thank St. John's College for their support and community, making it an inspiring place to live and study. Special thanks are also due to Professor Christian Schultz from the University of Heidelberg for his infallible support and confidence in my plans. I want to emphasise the importance of my scholarship institutions *Studienstiftung des deutschen Volkes* and *Villigst*, whose intellectual guidance has shaped me, and provided considerable opportunities for my professional and personal development.

I am grateful to my friends Annette, Ed, Angelika, Kelli, Henry and Anna for creating a home for me in Oxford. To Annette, Ed and Angelika, thank you for bringing out the best in me, and for your unwavering confidence that *Jedem Anfang wohnt ein Zauber inne.* Outside of Oxford, I am thankful to Benny and Jemina, because you know me best and have often been my safe harbour. Finally, I would like to thank my lovely parents for their support, their encouragement and their confidence throughout my study and life.

Abbreviations

(-)-ILV	(-)-Indolactam V
[c]	Concentration
°C	Degree celsius
<	Is less than
>	Is more than
≤	Is less than or equal to
≥	Is more than or equal to
×	Times
≈	Approximately
®	Registered trademark
™	Trademark
ANOVA	ANalysis of VAriance
aPKC	Atypical protein kinase C
B2M	β-2 microglobulin
BMP	Bone morphogenetic protein
br	Biological replicates
CAM	Cell adhesion molecule
CD	Cluster of differentiation
cPKC	Conventional or classical protein kinase C
CRISPR	Clustered regularly inter-spaced short palindromic repeat
Da	Dalton
DMSO	Dimethyl sulfoxide
DNA	Deoxyribonucleic acid
DNase	Deoxyribonuclease
EB	Embryoid body
EDTA	Ethylenediaminetetraacetic acid
ELISA	Enzyme-Linked Immunosorbent Assay
EMT	Epithelial–mesenchymal transition
FACS	Fluorescence-activated cell sorting
FBS	Fetal bovine serum

FCS	Fetal calf serum
FSC	Forward scatter
g	Unit for relative centrifugal force
GAPDH	Glyceraldehyde 3-phosphate dehydrogenase
GFP	Green fluorescent protein
h	Hours
HDF	Human dermal fibroblasts
hES	Human embryonic stem cells
hESC	Human embryonic stem cell
Ig	Immunoglobulin
IL	Interleukin
iPSC	Induced pluripotent stem cell
kDA	Kilo dalton
Lamp1	Lysosomal-associated membrane protein 1
mAb	Monoclonal antibody
macpre	Macrophage precursor
MFI	Mean fluorescence intensity
mL	Millilitre
MoA	Mechanism of action
mRNA	Messenger RNA
NIM	Neural induction medium
nM	Nanomolar
NMM	Neural maintenance medium
nPKC	Novel protein kinase C
ns	Not significant
PBS	Phosphate-buffered saline
PCR	Polymerase chain reaction
PI	Propidium iodide
PKC	Protein kinase C
pMac	Yolk sac-derived macrophage
PS	Phosphatidylserine
qRT-PCR	Quantitative real-time PCR
RACK	Receptor for activated C kinase

RIPA	Radioimmunoprecipitation assay
ROCKi	Rho-kinase inhibitor
RT	Reverse transcription
SCF	Stem cell factor
SEM	Standard error of the mean
siRNA	Small interfering RNA
SSC	Side scatter
TBP	TATA-binding protein
TBS	Tris-buffered saline
tr	Technical replicates
VEGF	Vascular endothelial growth factor
μM	Micromolar
μm	Micrometer

Table of Contents

Abstract ..... **ii**

Acknowledgments ..... **iii**

Abbreviations ..... **iv**

Chapter 1: Introduction **1**

1.1 Induced pluripotent stem cells (iPSCs) 1

1.1.1 Characteristics of iPSCs 1

1.1.2 Applications and impact of iPSCs 2

1.1.3 iPSC culturing 3

1.2 Stemistry: small molecules to harness stem cell potential 9

1.2.1 Small molecules: definition, potential and caveats 9

1.2.2 The application of small molecules in stem cell biology 10

1.2.3 Rho-associated protein kinase inhibitors for iPSC culturing 10

1.3 Disruption of cell-cell adhesion for iPSC culturing 11

1.3.1 Targeting E-cadherin for contact-independence 11

1.3.2 A chemical screening to identify small molecules 13

1.3.3 (-)-Indolactam V: a protein kinase C activator 14

1.3.4 MO47: an optimised derivative of (-)-Indolactam V 16

1.4 Scope of this study 17

Chapter 2: Methods and Materials **19**

2.1 Cell culture 19

2.1.1 Cell lines 19

2.1.2 Human iPSC culture 19

2.1.3 HDF culture 21

2.1.4 Cell counts and cell viability 21

2.1.5 Generation of growth curves 22

2.2 Human iPSC differentiation 22

2.2.1 Embryoid body formation (spinning approach) 22

2.2.2 Directed differentiation of iPSCs to macrophages 25

2.2.3 Directed differentiation of iPSCs to cerebral cortex neurons 27

2.2.4 Thawing and freezing cells 30

2.3 Antibodies and dyes....31
2.4 Flow cytometry....33
2.5 Light microscopy....34
2.5.1 Brightfield and phase microscopy....34
2.5.2 Confocal microscopy....34
2.6 Genome-wide association studies (GWAS)....36
2.7 Quantitative real-time PCR (qRT-PCR)....36
2.7.1 RNA extraction....36
2.7.2 cDNA production by reverse transcription (RT)....37
2.7.3 Quantitative real-time PCR (qRT-PCR)....37
2.8 Enzyme-linked Immunosorbent Assay for soluble E-Cadherin....38
2.9 Caspase 3/7 Assay....38
2.10 Statistical analysis....39

Chapter 3: Studying phenotypes in 2D upon treatment with (-)-Indolactam V and MO47....40

3.1 Introduction....40
3.1.1 2D phenotypes and heterogeneity....40
3.1.2 Morphological criteria for contact-independent iPSC cultures in 2D....42
3.2 Inducing colony-independent iPSC culture in 2D....43
3.3 Reversibility of colony-independent phenotypes....45
3.4 Assessing the actin cytoskeleton upon treatment....47
3.5 Assessing focal adhesions upon treatment....51
3.6 Assessing area, perimeter and height of the cell nuclei upon treatment....55
3.7 Discussion and summary....57

Chapter 4: Elucidating the mechanisms of action of (-)-Indolactam V and MO47 62

4.1 Introduction....62
4.1.1 The importance of mechanism of action studies....62
4.1.2 E-cadherin and protein kinase C....63
4.2 Investigating protein kinase C....64
4.2.1 Protein kinase C is expressed in iPSC OX-1-18....65
4.2.2 Combined treatment of PKC activatiors and PKC inhibitors....67
4.3 Investigating E-cadherin....72
4.3.1 Assessing endocytosis and recycling of E-cadherin upon treatment....73
4.3.2 Assessing E-cadherin shedding upon treatment....80
4.3.3 Assessing the expression of cell surface E-cadherin....83
4.4 Assessing cytotoxicity upon treatment with (-)-Indolactam V....85

4.5 Summary and discussion 89

Chapter 5: Assessing iPSC characteristics after serial treatment with MO47 93

5.1 Introduction 93

5.2 Generating a stock of MO47 pretreated iPSCs 94

5.3 Assessing proliferation through KI-67 95

5.4 Assessing pluripotency 99

5.4.1 Assessing molecular pluripotency through core and state markers 99

5.4.2 Assessing functional pluripotency through differentiation *in vivo* 104

5.5 Summary and discussion 119

Chapter 6: Summary and final discussion 124

6.1 Summary of results 124

6.2 Implication and future challenges 125

6.3 Therapeutic implications 128

Chapter 1: Introduction

This thesis lies on the interface of stem cell biology and medicinal chemistry. It focuses on the technological development of 2D and 3D stem cell culturing. In this chapter, we introduce the concept of iPSCs, current culturing methods and challenges, and our proposed solution to these challenges via small molecules.

1.1 Induced pluripotent stem cells (iPSCs)

In 2006, Takahashi and Yamanaka revolutionised modern medicine and research with the discovery of the 'induction of pluripotent stem cells from mouse embryonic and adult fibroblast cultures by defined factors' (Takahashi *et al.*, 2006). Their momentous contribution illustrates how a set of defined transcription factors could induce a pluripotency state, close to that of human embryonic stem cells (Robinton *et al.*, 2012). The validation of the same principles in human somatic cells one year later (Takahashi *et al.*, 2007) and the reprogramming to induced pluripotent stem cells with new chemical or biological strategies has since sparked a renaissance in stem cell research (Shi *et al.*, 2017).

1.1.1 Characteristics of iPSCs

Human induced pluripotent stem cells (iPSCs) have the unique properties of indefinite self-renewal and the ability to differentiate into representatives of the three germ layers. In other words, they bear the potential to develop into all human cell types, except extra-embryonic tissues such as the placenta (Kimbrel *et al.*, 2015; Robinton *et al.*, 2012). In contrast to mouse iPSCs that resemble pre-implantation embryonic stem cells (naïve), human iPSCs correspond to post-implantation epiblast stem cells, and are therefore considered to be 'primed' (Nichols *et al.*, 2009; Weinberger *et al.*, 2016). Naïve and

primed stem cells display genetic and functional differences that have been reviewed extensively elsewhere, but is important to note that pluripotency states are highly dynamic (Li *et al.*, 2017; Weinberger *et al.*, 2016; Wu *et al.*, 2015b).

The advantages of iPSCs' indefinite self-renewal, genetic human origin, and accessibility, while circumventing the ethical limitations of human embryonic stem cells, offers substantial promises to research and medicine (Robinton *et al.*, 2012). Intriguingly, with the considerable progress of genetic engineering, iPSC technology is promising to become even more powerful (Hockemeyer *et al.*, 2016). Figure 1.1 describes the generation and potential application of iPSCs for various purposes.

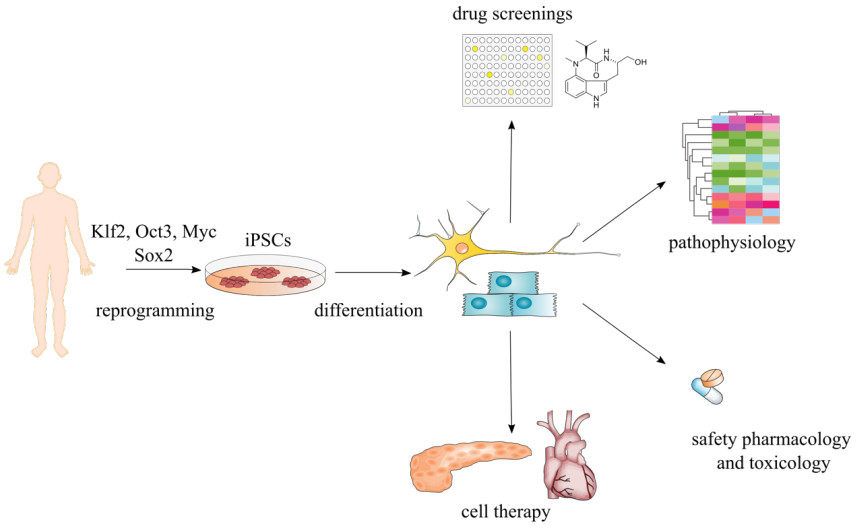

Figure 1.1 | Generation and application of induced pluripotent stem cells (iPSCs).

1.1.2 Applications and impact of iPSCs

iPSCs have an alluring potential for pathophysiological studies (Kim *et al.*, 2013; Passier *et al.*, 2016; Stepniewski *et al.*, 2015), safety pharmacology (Kandasamy *et al.*, 2015; Matsa *et al.*, 2016; Sirenko *et al.*, 2017), drug screenings (Grskovic *et al.*, 2011; Lee *et al.*, 2012), and regenerative medicine (Trounson *et al.*, 2016). Notably, iPSC technology holds tremendous promise for currently unmet clinical needs, and the first clinical trials

are attempting to bring iPSC therapy from bench to bedside (Kimbrel *et al.*, 2015). These therapeutic approaches include the treatment of age-related macular degeneration (Reardon *et al.*, 2014), spinal cord injuries (Assinck *et al.*, 2017), Parkinson's disease (Cyranoski, 2017; Kimbrel *et al.*, 2015), diabetes (Chen *et al.*, 2016; Rezania *et al.*, 2014), and heart disease (Chen *et al.*, 2016). Given the variety of different applications, the maintenance and expansion of iPSCs have become of great importance for the progress of the field.

1.1.3 iPSC culturing

The application of iPSC requires ease of use, efficiency, good manufacturing practice (GMP) compatibility and high expansion efficiency, without comprising pluripotency or increasing heterogeneity in the culture (Chen *et al.*, 2014; Lei *et al.*, 2013; Robinton *et al.*, 2012). Despite the breath-taking pace in manipulating and selecting iPSCs for precise cellular phenotypes, major challenges remain for improving culturing media, coating agents for 2D and the practices in 3D culturing (Ben-David *et al.*, 2013; Couture, 2010).

1.1.3.1 Culturing media

Human iPSCs are conventionally cultured in mTesR^{TM}1 medium, which contains fibroblast growth factor 2 (FGF-2), lithium chloride, γ-aminobutyric acid (GABA), TGF-β, and pipecolic acid (Chen *et al.*, 2014). Due to the serum albumin, the formulation of mTesR^{TM}1 is not xeno-free. Thus, E8, an optimised formulation of mTesR^{TM}1, which is free of β-mercaptoethanol and serum albumin, was developed (Chen *et al.*, 2014).

Media formulations are vital since primary cells such as iPSCs are highly sensitive to changing microenvironments and uncontrolled heterogeneity (Watt *et al.*, 2013). Consequently, media formulations with xenogeneic components, which increase the impurity of the iPSC culture, will need to be replaced by xeno-free media in the future

(Chen *et al.*, 2014; Couture, 2010). Notably, xenogeneic media cannot be used for the culturing of clinical-grade iPSCs (Chen *et al.*, 2014).

1.1.3.2 Current challenges in 2D culturing

Two-dimensional (2D) iPSC cultures consist of surface-adherent cell colonies with clearly-defined edges, arranged in monolayers (Figure 1.2). This allows iPSCs to be homogenously exposed to their medium, providing high reproducibility, and low rates of apoptosis and differentiation in the culture (Kempf *et al.*, 2016; Wakao *et al.*, 2012). However, the need for cell passaging is continuous, labour intensive and inefficient as there is considerable cell loss during each passage (Adil *et al.*, 2017). However, long-term serial passaging is associated with loss of pluripotency, and increase of genetic instability and abnormal karyotypes (Adil *et al.*, 2017).

2D colonies give rise to a lack of uniformity, which increases heterogeneity. This is due to iPSCs at different locations of the colonies displaying distinct growth properties. Cells in the centre of the colonies often experience overcompaction because of tightening of the cells, whereas cells at the edges experience a lack of external cues (International Stem Cell Banking, 2009; Kato *et al.*, 2016; Rosowski *et al.*, 2015). These growth properties explain why iPSCs at these locations are prone to differentiation or even apoptosis (Rosowski *et al.*, 2015).

Traditionally, iPSCs have been cultured on a population of fibroblasts called ‘feeders’. However, feeder cultures are impure and their effects on the iPSC culture are difficult to appreciate (Chen *et al.*, 2014). Feeder-free 2D culturing on matrices and coated layers, namely Matrigel™ or Geltrex™, circumvents the co-culturing of two different cell populations, and has become the method of choice in many laboratories (Chen *et al.*, 2014). Both gels are assortments of collagens (types I and IV), laminin, entactin, heparin

sulphate proteoglycan, matrix metalloproteinases, small molecules and growth factors in unknown proportions (Chen *et al.*, 2014; Hughes *et al.*, 2010). However, the poorly defined composition and a high degree of batch-to-batch variability of these coating agents poses major challenges (Hughes *et al.*, 2010). Importantly, Matrigel^{TM} and Geltrex^{TM} are composed of xenogeneic substrates extracted from Englebreth-Holm-Swarm sarcoma cells, and are therefore not compatible with clinical iPSCs standards (Chen *et al.*, 2014). Although there have been further advances for generating coating agents that are totally synthetic, the lack of quality control and universal standards in iPSC culturing still remains (Chen *et al.*, 2014). Therefore, establishing robust xeno-free coating agents is crucial for improving 2D culturing.

2D system are further limited by their spatial arrangements. The quantity of iPSCs needed for both clinical and industrial applications exceeds the current capacities of conventional 2D systems. For example, the number of iPSCs for cell therapy, including heart repair after myocardial infarctus or the application of insulin-producing β-cells for diabetes type I, is likely to exceed 2×10^9 cells (Zweigerdt *et al.*, 2011). For a drug screening with 1×10^6 compounds, approximately 1×10^{10} hSCs are required (Adil *et al.*, 2017). This is far beyond the logistical and economic capabilities of 2D systems.

Finally, monitoring cell parameters in 2D culture, including O_2, glucose rates, acidicity, proliferation and cell death, is practically infeasible (Kempf *et al.*, 2016). This is why 3D suspension cultures—that is amenable to scaleup and circumvents coating agents—has become crucial for the future of the field.

1.1.3.3 iPSC 3D culturing

3D cultures can be free-floating (e.g. suspension culture in bioreactors) or matrix-dependent (e.g. plated on microcarriers, encapsulated in hydrogels etc.) and are expected

to meet the high demand for cells needed for applications. Moreover, iPSC-derived organoids, which present a powerful model closer to the physiological conditions in the human body, require further progress of 3D cutluring systems (Fatehullah *et al.*, 2016). In particular, the combination of disease-specific iPSC lines and 3D technology enables the study of spatiotemporal cell-cell interactions (Shi *et al.*, 2017).

However, different 3D culturing systems have their own challenges (Figure 1.2). Firstly, the maintenance and differentiation practices in 3D systems are far less established than 2D platforms (Chen *et al.*, 2014). Secondly, an increase in cell damage due to shear forces has been observed for free-floating cultures in bioreactors (Chen *et al.*, 2014; Kempf *et al.*, 2016). Finally, passaging iPSCs as single cells (single-cell inoculation) or in clumps (clump inoculation) from 2D to 3D, generally results in the formation of heterogenous cell aggregates, even in stirred bioreactors (Kempf *et al.*, 2016). Cells in centre of these aggregates are generally underexposed to the medium, which results in variabilities of growth rates, apoptosis, differentiation and an eventual increase in heterogeneity (Chen *et al.*, 2014). Therefore, aggregates present a significant obstacle to culturing in 3D.

An elegant approach to reduce the size of cell agglomerates and counter the subsequent aggregation by gravity is the single-cell passaging into stirred bioreactors (Kempf *et al.*, 2016). I will refer to this 3D culturing model, when discussing future experiments and advantages of 3D systems over 2D systems in the results chapters. These bioreactor tanks integrate sampling for monitoring, allow iPSCs feeding through continuous perfusion instead of batch-feeding, and enable a homogenous suspension of cells, media and dissolved gases (Kropp *et al.*, 2016).

Despite this stirring technology, aggregates can not be fully dissociated by stirred bioreactors. To prevent these heterogenous agglomerates and reduce cell damage due to shear forces, various technologies have been developed to either control the size of the

aggregates or to circumvent them entirely. These include the application of microcarriers, micropatterning and hydrogel-encapsulation (Chen *et al.*, 2014; Kempf *et al.*, 2016). Despite their contribution to the field, these technologies have given rise to new caveats, including a lack of GMP compatibility, and difficulties in harvesting or monitoring of cells in these systems (Chen *et al.*, 2014).

Given the limitations of these approaches, chemical approaches, to disrupt large cell aggreagtes, as illustrated successfully in mouse iPSCs, offer an alternative solution to the field (Segal *et al.*, 2017; Soncin *et al.*, 2009). These chemical approaches come under the broader heading of stemistry (Figure 1.2).

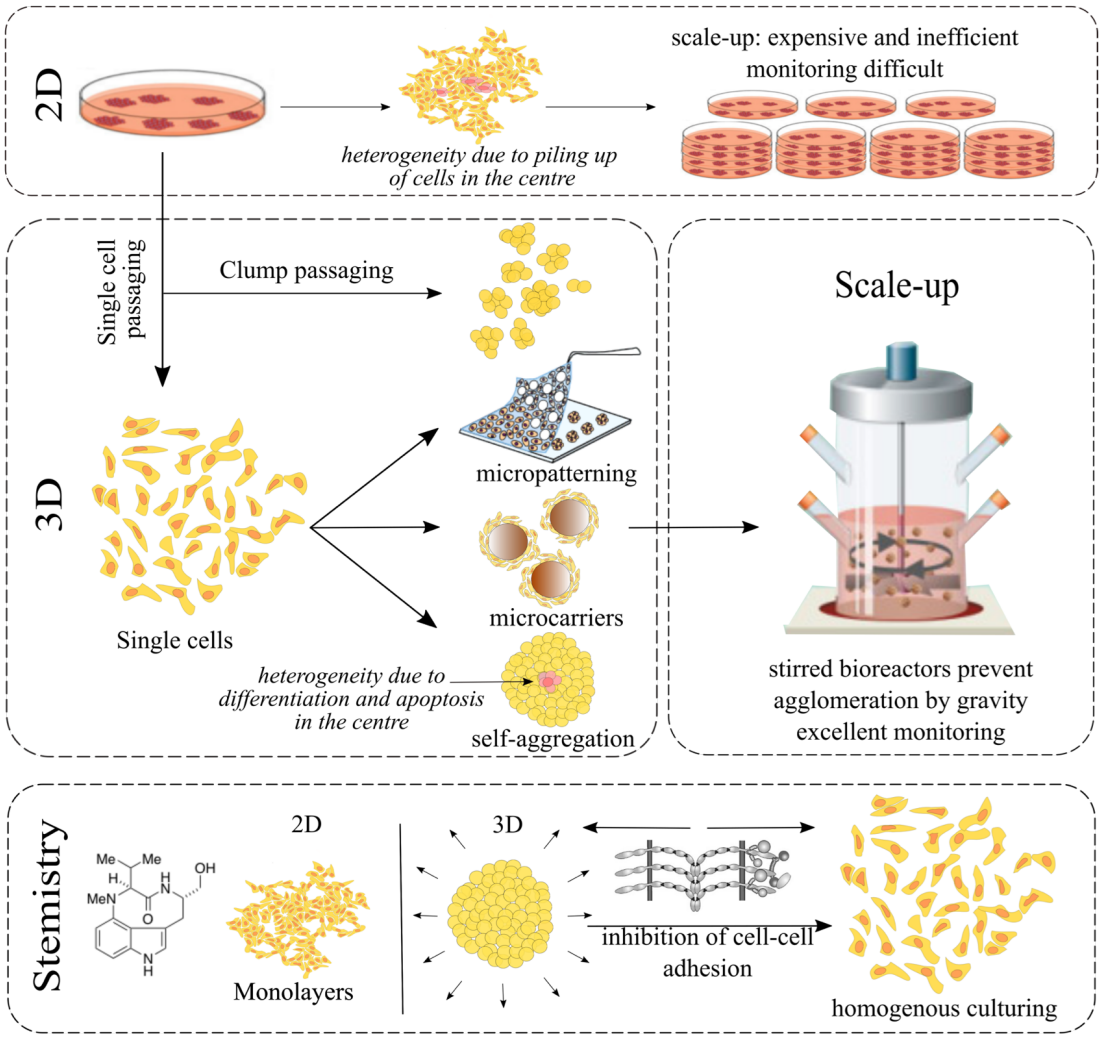

Figure 1.2 | Current strategies to overcome heterogeneity in 2D and 3D iPSC culturing.
iPSCs can either be cultured in 2D as monolayers or in suspension culture (3D). In 2D culture, the growth in iPSC colonies is characteristic. Cells in the centre of these colonies often undergo overcompaction, while cells at the edges are likely to experience a lack of external cues. In both conditions, cells are prone to differentiation or, when tightly packed, to apoptosis, which increases heterogeneity. Moreover, scaleup and monitoring in 2D is logistically challenging. Alternatively, iPSCs can be cultured in stirred bioreactors (3D). Cells in the centre of these aggregates are underexposed to the culturing medium, and are consequently prone to cell death and differentiation. Chemical approaches with small molecules are promising to overcome this lack of uniformity in 2D and 3D systems.

1.2 Stemistry: small molecules to harness stem cell potential

Simultaneous to the flourishing development of the genetic tools in stem cell biology, *stemistry* — the use of chemical strategies to manipulate stem cell fate — has seen its powerful emergence in medicinal chemistry (Davies *et al.*, 2015; Hendriks *et al.*, 2016). Importantly, the application of chemical strategies via small molecules has often provided new insights into the intricacies of signalling pathways in molecular biology (Arrowsmith *et al.*, 2015; Leeson, 2012; Li *et al.*, 2013b). Conversely, unravelling the mechanisms of action through biological studies has provided chemists with new potential targets for drug discovery (McFedries *et al.*, 2013).

1.2.1 Small molecules: definition, potential and caveats

Small molecules are purified organic entities defined by a chemical formula, specific physiochemical properties, and have, according to Lipinski *et al.* (2012), an ideal molecular weight <500 dalton (Da), and other properties, which allow cell permeability (Ganellin *et al.*, 2013; Leeson, 2012).

The advantages of small molecules include their capability to act on extra- and intracellular targets, and their high bioavailability upon oral application (Ganellin *et al.*, 2013; Veber *et al.*, 2002). Moreover, their ease of application presents a further advantage compared to complex techniques in genetic engineering (Zhang *et al.*, 2012). Small molecules further enable the temporally refined control of protein functions in terms of activation, inhibition and reversibility (Xu *et al.*, 2008). The possibility to tune concentrations allows inducing phenotypes dose-dependently; this presents a versatile tool to harness iPSC plasticity *ex vivo* and *in vivo* (Cao *et al.*, 2016; Li *et al.*, 2012b; Zhang *et al.*, 2012). The optimised combination with other small molecules offers another substantial advantage through synergistic effects, which could also be harnessed in the

context of chemical strategies for cell programming (Lin *et al.*, 2015; Yu *et al.*, 2014; Zhang *et al.*, 2012).

However, the versatility of small molecules can also be a disadvantage. An optimised small molecule design and profiling has always been essential for exquisite specificity, and this is difficult to achieve (Davies *et al.*, 2015; Frye, 2010). Off-target effects, biological *sequellae* such as cytotoxicity and undefined pharmacodynamic interactions pose major challenges to chemical approaches (Zhang *et al.*, 2012). Moreover, many small molecules, including kinase inhibitors, have been inadequately characterised in the past, which has subsequently resulted in the generation of poor data (Arrowsmith *et al.*, 2015; Davis *et al.*, 2011). Finally, phenotypic screens have identified attractive small molecules, but their mechanism of action often remains unknown. This can lead to erroneous conclusions about the phenotype-target relationship (Workman *et al.*, 2010).

1.2.2 The application of small molecules in stem cell biology

In stem cell biology, small molecules have already proven their potential to control and convert cell phenotypes in a precise and robust way (Li *et al.*, 2013a). This is increasingly harnessed for replacing expensive extrinsic factors that are necessary for iPSC culturing (Desbordes *et al.*, 2013; Li *et al.*, 2012b; Zhang *et al.*, 2012). Moreover, the translation of small molecules into medicine, including controlled stem cell reprogramming, homing, renewal and conversion, has become a powerful strategy to target tissue regeneration *in vivo* (Davies *et al.*, 2015; Langle *et al.*, 2014; Li *et al.*, 2013b; Liu *et al.*, 2016; Zhang *et al.*, 2012).

1.2.3 Rho-associated protein kinase inhibitors for iPSC culturing

The Rho-associated coiled-coil-containing protein kinase (ROCK) inhibitors Y-27632 and thiazovivin are pivotal examples of small molecules used for improving iPSC

culturing (Chen *et al.*, 2010; Ohgushi *et al.*, 2010; Watanabe *et al.*, 2007; Xu *et al.*, 2010). Rho-kinase inhibitors enhance the overall survival of iPSCs upon dissociation into single cells, and are nowadays considered to be indispensable tools for the scaleup of iPSC technology in 3D (Zhang *et al.*, 2012). Moreover, their discovery also provided valuable insights into the regulatory mechanisms of dissociation-induced vulnerability, and into the importance of cell-matrix and cell-cell adhesions for iPSC survival (Chen *et al.*, 2010; Xu *et al.*, 2010). Although Rho-kinase inhibitors have enhanced iPSCs survival rates after dissociation into single cells, they cannot prevent the formation of aggregates.

1.3 Disruption of cell-cell adhesion for iPSC culturing

The disruption of cell-cell adhesions via small molecules requires targeting of key adhesive molecules. Cell-cell adhesion is generally governed by three families, including cadherins at adherens junctions, claudins, ZO-1 and ZO-2 at tight junctions, and desmoglein and demsocollin at desmosomes (Cavallaro *et al.*, 2011; Gumbiner, 1996; Parsons *et al.*, 2010; van Roy *et al.*, 2008). It is important to note that all of these families play vital roles in physical adhesion, but also in cell polarity, tissue morphogenesis, differentiation, contact inhibition, cell growth and in essential signal transduction (Cavallaro *et al.*, 2011; Chen *et al.*, 2010; Gumbiner, 1996).

1.3.1 Targeting E-cadherin for contact-independence

E-cadherin is the prototype of all cell-cell adhesion molecules (CAMs) and a particularly interesting target for disrupting cell-cell adhesions in iPSCs (Figure 1.3). E-cadherin mediates Ca^{2+}-dependent homotypic cell interactions in epithelial and epithelial-like tissues, including iPSCs (Gumbiner, 2005; Li *et al.*, 2012a; Takeichi, 1977; van Roy *et al.*, 2008). Its structure consists of an endodomain composed of a juxtamembrane domain (JMD) and a β-catenin domain (BCD), a transmembrane domain, and an ectodomain of five tandem repeats (EC1-EC5) (van Roy *et al.*, 2008). Notably, its link to the actin

cytoskeleton is mediated via the intermediate proteins α-catenin, p120 and β-catenin (Figure 1.3).

Loss of E-cadherin and downregulation of the adhesive signature is associated with epithelial-mesenchymal transition (EMT) (Lamouille *et al.*, 2014). During this process, epithelial cells abrogate their apical-basal polarity and cell adhesion and upregulate gene signatures, which enhance the cells' motility, allowing them to develop an invasive phenotype (Eastham *et al.*, 2007; Lamouille *et al.*, 2014; Moreno-Bueno *et al.*, 2009). EMT is a vital process in cancer metastasis but can also be found under physiological conditions, including the development of human embryonic stem cells (Lamouille *et al.*, 2014; Moreno-Bueno *et al.*, 2009).

Notably, E-cadherin has been shown to govern core signalling regulatory pathways in stem cell survival and self-renewal (Li *et al.*, 2012a; Watanabe *et al.*, 2007; Xu *et al.*, 2010). By replacing Oct4, E-cadherin could even be used to fully reprogram mESCs (Redmer *et al.*, 2011). Therefore, it has become an interesting molecule for studying the intricacies of cell-cell adhesion and stem cell fate (Mani *et al.*, 2008; Segal *et al.*, 2017).

Encouragingly, the discovery of the crystal structure of ectodomains EC1 and EC2, which are critical for homotypic interactions with partners on neighbouring cells, has enabled the targeting of E-cadherin for inhibition (Nose, 1990; Overduin *et al.*, 1995). This discovery has already been harnessed to develop peptide inhibitors against E-cadherin in mouse ESCs (Parisini *et al.*, 2007; Segal *et al.*, 2017). It has been shown that small peptides, e.g. the trans-homodimerisation peptide CHAVC, could inhibit cell-cell adhesion in mouse iPSCs and ESCs, while maintaining essential E-cadherin signalling and cell viability (Segal *et al.*, 2017; Soncin *et al.*, 2009). However, this chemical approach through peptides could not be applied successfully in human iPSCs.

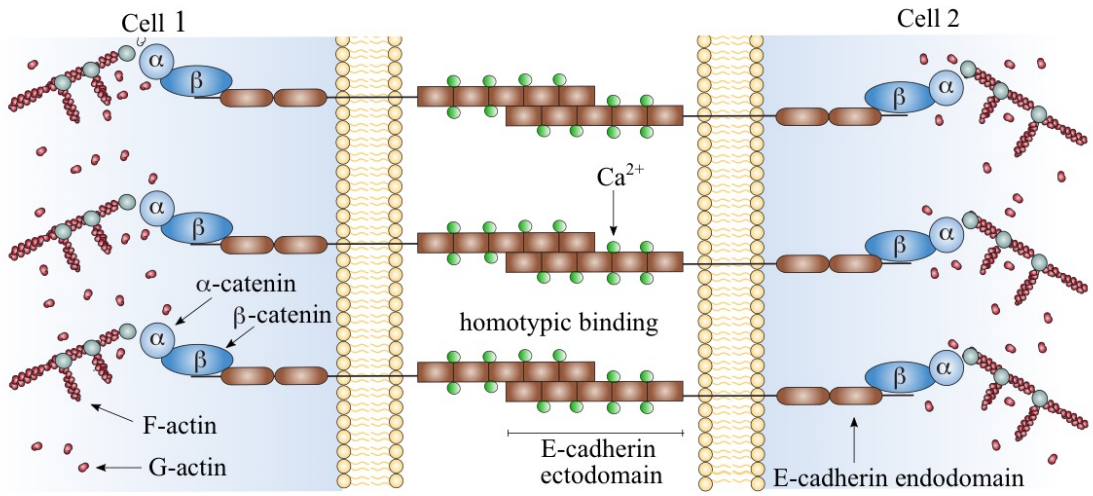

Figure 1.3 | E-cadherin mediated cell-cell adhesion.
Adapted from Hamon *et al.* (2006). Cell-cell adhesion is mediated by homotypic binding of E-cadherin molecules. The ectodomain of E-cadherin consists of 5 tandem repeats and binds calcium. The endodomain of E-cadherin is linked to the actin cytoskeleton (F-actin and G-actin) via the linking proteins α-catenin, β-catenin and p120 catenin.

1.3.2 A chemical screening to identify small molecules

Our group endeavoured to identify a small molecule that would simultaneously disrupt cell-cell adhesion in human iPSCs and stabilise E-cadherin signalling. To this end, our group performed an in-house chemical screening, which sought to identify phenotypes with high similarity to those treated with anti-E-cadherin antibody. Encouragingly, our group discovered (-)-Indolactam V (ILV) as a potential inhibitor of cell-cell adhesion in this screening. The chemical structure of (-)-Indolactam V is shown in Figure 1.4.

(-)-Indolactam V

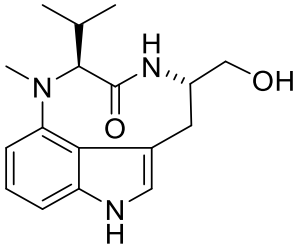

Figure 1.4 | Chemical structure of (-)-Indolactam V.

1.3.3 (-)-Indolactam V: a protein kinase C activator

A member of the teleocidin family of natural products, (-)-Indolactam V is known to have tumour-promoting activity (Griner *et al.*, 2007; Heikkila *et al.*, 1989). In stem cell research, (-)-Indolactam V has become a powerful chemical tool for the differentiation of iPSCs to pancreatic progenitors (Chen *et al.*, 2009b; Thatava *et al.*, 2011; Yang *et al.*, 2009).

(-)-Indolactam V is further classified as a member of protein kinase C (PKC) activators (Delaszlo *et al.*, 1986). PKCs comprise of a set of genes that encode for structurally related and almost ubiquitously expressed serine/threonin kinases, which act at the intersection of many signalling pathways (Steinberg, 2008). PKCs are located downstream of G-protein coupled receptors, followed by the stimulation of phospholipase C (PLC), the hydrolysis of 4,5-bisphosphaste (PIP2), and the generation of diacylglycerol (DAG).

Traditionally, PKCs have been divided into three lipid-sensitive enzyme subfamilies: conventional PKCs (α, βI, βII, γ), novel PKCs (δ, θ, η, ε) and atypical PKCs (ζ, ι/λ) (Newton, 2010; Steinberg, 2008).

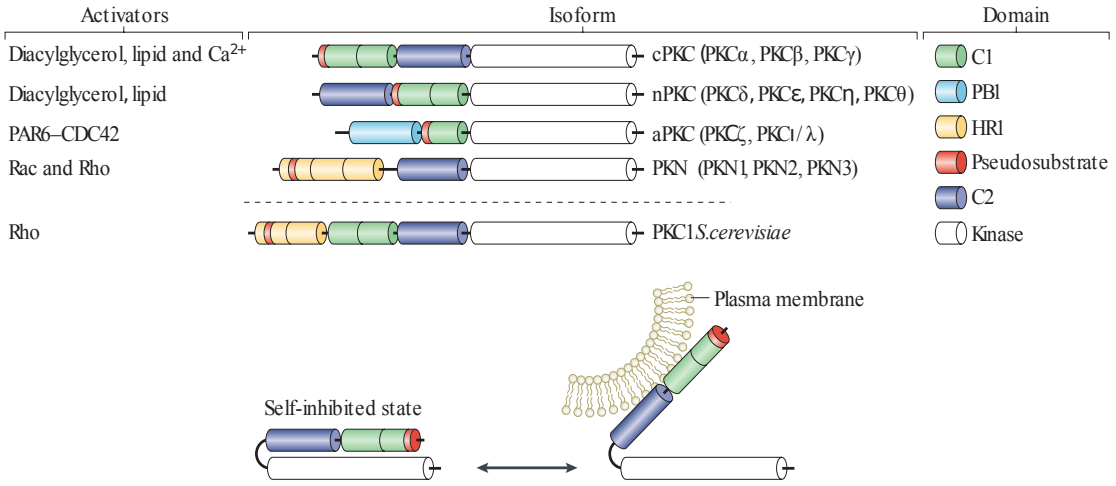

Figure 1.5 | Protein Kinase C (PKC) isoforms and their activators.
Adapted from Rosse *et al.* (2010). Different families of the PKC superfamily are displayed, including classical/conventional PKCs, novel PKCs, atypical PKCs and PKC-related kinases (PKN). This classification is based on differences in their structural properties, which also accounts for the affinity for different PKC substrates. In the inactivated state, the kinase activity is inhibited by an internal pseudosubstrate. Translocation and interaction with the plasma membrane resolves this internal inhibition.

This classification is based on variations in the cofactor-binding regulatory twin domains C1 (binding site for phorbol esters and DAG), and C2 (Ca^{2+}-binding) in the NH_2 terminus (Figure 1.5). Both DAG and intracellular Ca^{2+} have shown to be activators of the conventional PKCs (cPKCs) (Steinberg, 2008). In contrast, novel PKC (nPKC) isoforms lack the C2 domain and bind anionic phospholipids Ca^{2+}-independently (Steinberg, 2008). Thus, full nPKC activation can be achieved through DAG or phorbol esters like 12-myristate 13-acetate (PMA) alone. Atypical PKCs lack binding sites for DAG and intracellular Ca^{2+} (aPKCs) (Newton, 2010). PKCs highly depend upon spatial regulation through phosphorylation, scaffolds and molecular interactions (Igumenova, 2015; Steinberg, 2008). Their recruitment to the membrane, followed by second messenger phospholipid interations, is key in relaying an abundance of additional signals (Newton, 2001; Newton, 2009).

1.3.4 MO47: an optimised derivative of (-)-Indolactam V

Despite the powerful effect on phenotypes, (-)-Indolactam was shown to display strong pro-apoptotic effects on iPSCs (IC_{50} = 5μM, Appendix Chapter 1)[1]. A plausible reason for this is the activation of PKCδ, which subsequently accumulates in the nucleus and undergoes cleavage by caspase 3 (Brodie, 2003; Murriel *et al.*, 2004; Reyland, 2007).

Intriguingly, when the affinity of the chemical structure for PKC was abrogated through inverting a single stereogenic centre, the phenotypic effect also disappeared, suggesting a relation between PKC activation and the phenotype. As cytotoxicity of (-)-Indolactam V hampers application in 3D culturing of iPSCs, we sought a new small molecule candidate with protein kinase C as its downstream effector.

After identification of their targets, small molecules may be optimised in their chemical structure resulting in a new chemical with improved properties (Workman *et al.*, 2010). Thus, our group set out to synthesise several derivatives of (-)-Indolactam V, and tested whether they would display the same phenotype in the absence of pro-apoptotic stimuli. Encouragingly, our group identified a derivative of (-)-Indolactam V, MO47, which exhibited a highly similar phenotypic effect but allowed considerably higher cell viability (IC_{50} for apoptosis = 94μM, Appendix Chapter 1). In the chemical structure of MO47 the indole is substitued by a benzofuran bearing an alkyl chain. In addition, the stereogenic centre at C14 is inverted, and a methyl group is introduced as an additional substitute.

[1] This assay was performed by Dr Laurence Silpa, a post-doctoral associate in our group. The reference to this data will be relevant for the three results chapters in this thesis.

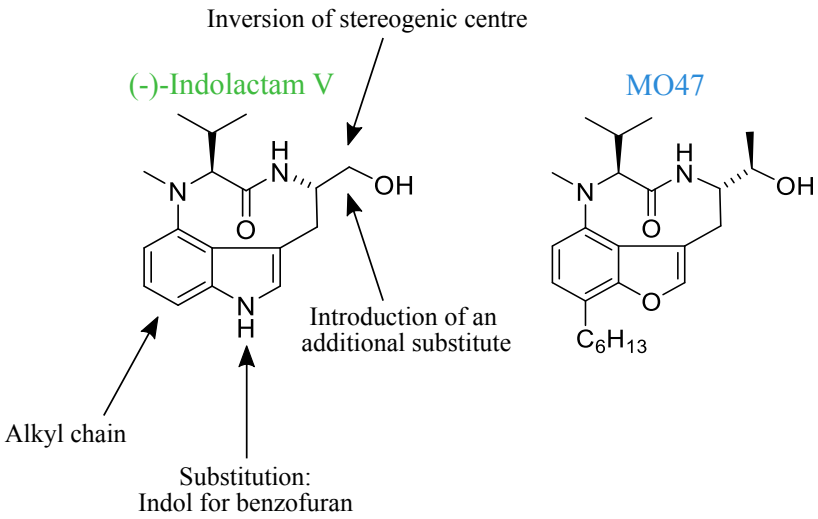

Figure 1.6 | Chemical structures of (-)-Indolactam V and MO47.
Four dissimilarities in the chemical structures account for the differences in protein kinase C isotype specificity.

In a previous study, MO47 displayed a 4-fold isoform affinity for PKCα over PKCδ, suggesting that different PKC isoform families might account for the phenotypic and the pro-apoptotic effect, respectively (Kozikowski *et al.*, 1995). Given this advantage of increased cell viability, MO47 has become more promising than (-)-Indolactam V to improve culturing conditions.

1.4 Scope of this study

This research project argues for a chemical approach to improve 2D and 3D culturing: the disruption of iPSCs colonies and cell-cell aggregates via two structurally related protein kinase C (PKC) activators, namely (-)-Indolactam V and MO47. The purposes of the research project are as follows:

(1) As a proof-of-principle, the phenotypic effects of (-)-Indolctam V and MO47 on iPSC morphology will be examined in 2D culture (Chapter 3).

(2) (-)-Indolactam V and MO47 are chemically related molecules with potentially different mechanisms of action. Considering the compounds as two distinct

chemical entities, we endeavour to elucidate their mechanisms of action with a particular focus on PKC and E-cadherin (Chapter 4).

(3) The application of small molecules for 2D and 3D iPSC cultures requires the reduction of heterogeneity without impairing key iPSC characteristics. Therefore, the main content of this thesis focuses on whether serial pretreatment with MO47 comprises the karyotype stability, the self-renewal, and molecular and functional pluripotency of iPSCs. To this end, pretreated iPSC will be subjected to spontaneous and directed differentiation to representatives of all three germ layers (Chapter 5).

This thesis is composed of six chapters. The following chapter, Chapter 2, is dedicated to the methods and materials used in this study. It is followed by three results chapters, Chapters 3, 4 and 5, which are detailed in objectives (1), (2) and (3), respectively. Chapter 6 concludes the results in this thesis and identifies further implications.

Chapter 2: Methods and Materials

2.1 Cell culture

2.1.1 Cell lines

This study was carried out with human dermal fibroblasts (HDF) and human iPSCs derived from the OX1-18 cell line. This previously published iPSC line was derived from human dermal fibroblasts by a skin biopsy from a male donor, aged 36, after informed consent (van Wilgenburg *et al.*, 2013). The reprogramming was performed using an adopted version of the originally published protocol by Takashi and Yamanka (Takahashi *et al.*, 2007; Takahashi *et al.*, 2006; van Wilgenburg *et al.*, 2013).

2.1.2 Human iPSC culture

2.1.2.1 iPSC culture (general)

Human iPSCs were cultured at 37°C and 5% CO_2 in feeder-free conditions. Cells were maintained in mTesR™1 (Stemcell Technologies, 85875), a complete, serum-free medium that contains recombinant human basic fibroblast growth factor and recombinant human transforming growth factor β. To reduce the risk of contamination 100 units/mL penicillin-streptomycin (Gibco™, 15140122) were added to the medium. Cells were generally passaged at 90-95% confluency using enzymatic dissociation. To lift the cells, the medium was aspirated entirely and cells were washed once in phosphate-buffer saline (Lonza, BE17-516F24) before incubating for 5 minutes in TrypLE Express (Gibco™, 12604013) at 37°C. Upon detachment, the plate was tapped, and the cells gently flushed to detach them further from the plate. Subsequently, the cell-TrypLE suspension was diluted 1:10 in PBS. After centrifugation at 400g for 5 minutes, cell pellets were flicked up, resuspended in prewarmed mTesR™1 supplemented with 10μM Rho-kinase inhibitor

Y-27632 (Abcam, ab120129). Cells were plated at a density of preferably 5×10^5 cells. Plating was performed onto 6-well plate (Greiner, 657160), which had been precoated with Matrigel™ at least 1h prior to plating (BD Biosciences, 354277) or Geltrex™ (Gibco™, A1413302). For culturing, a 100% medium change was performed daily.

2.1.2.2 iPSC culture with the small molecule MO47 (treated)

To generate a sufficient stock of MO47 pretreated iPSCs (experiments in chapter 5), a fresh cryovial of OX1-18 iPSCs was thawed and cells were plated at a density of 1×10^6/well. To allow the cells to recover from the thaw, they were then cultured for two passages in mTesR™1.

Treatment with 1μM MO47 or 0.1% DMSO (Sigma, D2650) was initiated during the plating after the first passage, and the same culturing practices as described above were applied. Prior to each feeding, mTesR™1 was supplemented with 0.1% DMSO (control) or 1μM MO47 (treated condition). A full medium change was performed daily, and cells were treated for a total of 3 passages. At each passage, iPSCs were plated at a density of 5×10^5 cells/well.

When reaching the third passage after 3 cycles of treatment, MO47 and DMSO treated iPSCs were frozen according to the procedure described below. After cryopreservation at -80°C for 48h, the cryovials were transferred to liquid nitrogen for long-term storage (see also chapter 5, Figure 5.1).

For the experiments described in chapter 5, MO47 and DMSO pretreated iPSCs were thawed simultaneously and plated at a density of 6.5×10^5 cells/well in mTesR™1 supplemented with Rho-kinase inhibitor Y-27632. Medium was changed daily, which allowed for a short compound wash-off period after the 3 cycles of treatment. Cells

reached confluency on day 5 after thawing (day 0), and were subsequently harvested for the relevant experiments.

2.1.2.2.1 (-)-Indolactam V and synthesis of MO47

The small molecule (-)-Indolactam V was purchased (Sigma, I0661) and had a purity of 99% according to the manufacturer. An authentic sample of MO47 was synthesised in our laboratory by Marcus Olivecrona according to the experimental procedure as suggested by Kozikowski *et al.* (1995). After purification by high performance liquid chromatography, a purity of 99% was measured.

2.1.3 HDF culture

HDFs were cultured at 37°C and 5% CO_2. Cells were passaged as described for iPSCs and maintained in T-25 flasks (Corning, 430639) with 6ml of HDF medium (Table 2.1). The medium was changed every 3rd to 4th day.

Table 2.1 | Human dermal fibroblast (HDF) medium preparation

	Final [c]	**Stock [c]**	**Catalogue number**	**Supplier**
Fibroblast medium				
Advanced DMEM	1×	1×	12491-015	Gibco™
GlutaMax™	1×	100×	35050	Gibco™
β-mercaptoethanol	100μM	100mM	21985023	Gibco™
Fetal calf serum (FCS/FBS)	0.1×	1×	F4135	Sigma

2.1.4 Cell counts and cell viability

To count cells and assess their viability, 19μL cell suspension mixed with 1μL of solution 13 (ChemoMetec, 910-3013, acridine-orange and DAPI) was loaded onto the chamber of an A8 counting slide (ChemoMetec, 942-0003). Non-viable cells were stained with DAPI, whereas viable cells where stained with acridine orange. Upon staining, cells were counted using the NucleoCounter NC-3000™ (ChemoMetec).

2.1.5 Generation of growth curves

To generate the growth curve presented in chapter 4.4, 1×10^5 iPSCs were plated in 500µL mTesR™1 onto a 24-well. Compound dilutions of (-)-Indolactam V were prepared by transferring half of the volume of the 4µM dilution to a 15mL falcon tube that contained the same volume of mTesR™1. This step was repeated until a concentration of 0.5µM (-)-Indolactam V was reached. After each 24h, the medium was changed and new dilutions prepared. At each time point, three wells of each condition were harvested. To this end, each well to be counted was washed with 500µL PBS and after aspiration 100µL TrypLE Express was added. The cells were then returned to the incubator for 8-10 minutes. Next, cells were examined under the microscope to assure their full detachment. 100µL PBS was added to each well and the remaining cell patches were gently washed off. The content of each well was then transferred to an Eppendorf tube and rinsed again with 100µL of PBS. Finally, the content of each well was counted twice using the technique described above.

2.2 Human iPSC differentiation

2.2.1 Embryoid body formation (spinning approach)

The spontaneous and directed differentiation to macrophages (Chapter 5.4.2.1 and 5.4.2.2) required the formation of embryoind bodies (EBs). The EB formation approach by spinning was chosen because of its high efficiency.

2.2.1.1 Embyroid bodies for the differentiation into macrophages

To generate spin-EBs, iPSCs were plated onto an AggreWells™ 800 plate (Stemcell Technologies, 27845). This enabled the formation of EBs that were consistent in size and shape, and contained approximately 12,500 cells (Chapter 5, Figure 5.6).

2.2.1.2 AggreWell™ plating

Near-confluent wells of a 6-well plate were washed once in PBS, and iPSCs lifted by enzymatic dissociation, suspended and centrifuged as described above. After centrifugation, iPSCs were resuspended at a concentration of 4×10^6 cells/mL in mTesR™1 supplemented with 10μM Rho-kinase inhibitor. Before plating, each well of the AggreWells™ plate was rinsed with 500μL of Aggrewell Rinsing Solution (Stemcell Technologies, 07010). To remove air bubbles, the plate was centrifuged at 2000g for 5 minutes. Next, the rinsing solution was aspirated and the well was rinsed again with 2mL PBS. After removal of PBS, 1mL of mTesR™1 was pipetted into each well. 1mL of cell suspension was then added to make up to a total volume of 2mL per well. Subsequently, the cell suspension was gently mixed using a Gilson p1000 and the plate was centrifuged at 100g for 3 minutes. Before returning the cells to the incubator, each well was examined under the microscope to ensure that cells were equally distributed among the microwells.

2.2.1.3 EB feeding

The following day, a 75% medium change with the relevant prewarmed EB medium was performed. To this end, 1mL medium was aspirated using a Gilson p1000. Next, 1mL of new medium was gently added, dripping down the side of each well to avoid the EBs to be dislodged. This step was repeated once, and feeding repeated daily for the following three days.

2.2.1.4 EB harvesting

On day 4 after plating, EBs were harvested and transferred to T175 cell culture flasks (Corning, 431466). To dislodge the EBs from the microwells, the medium in each well was pipetted up and down several times using a 5mL serological pipette. The entire content of each well was then transferred onto an prewetted 40μM cell strainer (BD Biosciences, 352340) that was inverted and placed on a 50mL falcon tube. Next, EBs were washed onto the inverted cell strainer using 5mL PBS to repeatedly wash out each well of the AggreWells™ plate. Once all EBs had been transferred onto the cell strainer membrane, the latter was turned over onto a new 50mL falcon tube. To detach the EBs from the strainer membrane, 4mL of the relevant medium was pipetted onto the strainer. The EBs for each condition were then split into half and plated either in a T175 cell culture flask for the macrophage differentiation or a 60mm petri dish (Corning, 3295) for the TaqMan hPSC ScorecardTM Panel assay.

2.2.1.5 Analysis of spontaneous differentiation using the TaqMan hPSC Scorecard™ Panel

To form EBs (Chapter 5.4.2.1), the manufaturer's protocol described in the user guide for the TaqMan hPSC Scorecard™ Panel (Applied Biosystems™, A15870) was adapted, and EBs generated according to the EB-spin formation protocol as outlined above. Importantly, no growth factors were added to the EB medium (Table 2.2). Between day 1 and 3, a 75% medium change was performed daily. On day 4, EBs of each condition were harvested in a total of 10mL EB medium and plated onto two 60mm tissue cultured-treated dishes coated with 2mL Geltrex™ matrix. This allowed the cells to attach rapidly and grow out from the EBs. Between day 4 and 14, a 75% medium change was performed every other day.

Table 2.2 | TaqMan hPSC Scorecard™ Panel, medium preparation

	Final [c]	Stock [c]	Catalogue number	Supplier
EB Scorecard™ medium				
DMEM/F12	80%	1×	12634-010	Gibco™
GlutaMax™	1×	100×	35050	Gibco™
β-mercaptoethanol	100µM	100mM	21985023	Gibco™
KnockOut™ Serum Replacement	20%	1×	F4135	Gibco™
MEM Non-essential Amino Acids Solution	1×	10mM	11140050	Gibco™

2.2.1.5.1 Harvesting EBs from adherent culture

On day 14, each cell culture dish was harvested. The culture medium was removed and cells were gently washed in 5mL PBS for 2 minutes. Subsequently, 700µl RLT buffer (Qiagen) was pipetted onto each plate. RLT was supplemented with 1% of pure β-mercaptoethanol (Sigma, M6250) to reduce RNase activity. Upon cell lysis, a cell scraper (Sarstedt, 831830) was used to collect the remaining cell content. After careful homogenisation by using a Gilson p1000, the total of 700µl slurry was transferred in aliquots of 350µl onto two QIAGEN shredder membranes (Qiagen, 79654), and stored at -80°C.

2.2.2 Directed differentiation of iPSCs to macrophages

2.2.2.1 Directed differentiation to macrophage precursors via EBs

Two different media were formulated for the generation of macrophages (Chapter 5.4.2.2). The macrophage precursor (macpre) medium consisted of hematopoietic, serum-free X-VIVO™-15 medium supplemented with IL-3 and M-CSF (Table 2.3). IL-3, a hematopoietic growth factor that is involved in the direction of multipotent hematopoietic stem cells into myeloid progenitor cells (Yang *et al.*, 1986). M-CSF, also known as CSF-1, is a vital stimulating factor for the differentiation into mononuclear phagocytic cells (Stanley *et al.*, 1994).

EBs were harvested as described above and collected from the cell strainer in 4mL macpre medium. Subsequently, 36mL of the macpre medium was added to make up a total volume of 40mL, which was then split into two and transferred to T175 cell culture flaks.

In the following 4 weeks, 10mL fresh macpre medium was added weekly to the flasks. After 5 weeks, a total of 40mL macrophage precursors was harvested, counted, and pelleted as described above.

2.2.2.2 Macrophage maturation (pMac)

To differentiate macrophage precursors to macrophages (pMac, Figure 5.9), the pelleted macrophage precursors were resuspended in macrophage medium (Table 2.3). The plating was performed onto a tissue-cultured coated 6-well plate at a density of 1.5×10^6 in 2mL medium per well. After 4 days, an additional volume of 2mL macrophage medium was added to each well. This allowed floating cells to attach further within the following 4 days. 8 days after plating, cells were imaged as described below, and after a total of 14 days of maturation, cells were collected for flow cytometry analysis.

Table 2.3 | Medium preparation for the directed differentiation to macrophages

	Final [c]	Stock [c]	Catalogue number	Supplier
EB medium				
mTesR™1	1:1		85875	Stemcell Tech.
BMP-4	50ng/mL	10µg/mL	PHC9534	Gibco™
VEGF	50ng/mL	10µg/mL	PHC9394	Gibco™
SCF	20ng/mL	10µg/mL	130-093-991	Miltenyi
Macrophage precursor medium				
X-VIVO™ 15	1×	1×	BE04-418F	Lonza
GlutaMax™	1mM	100×	35050061	Gibco™
β-mercaptoethanol	100µM	100mM	21985023	Gibco™
IL-3	25ng/mL	50µg/mL	PHC0034	Invitrogen
M-CSF	100ng/mL	100µg/mL	PHC9504	Invitrogen
Penicillin-streptomycin	100U/mL	10,000U/mL	15140122	Gibco™
Macrophage medium				
X-VIVO™ 15	1×	1×	BE04-418F	Lonza
GlutaMax™	1mM	100×	35050061	Gibco™
β-mercaptoethanol	100µM	100mM	21985023	Gibco™
M-CSF	100ng/mL	10µg/mL	PHC9504	Invitrogen
Penicillin-streptomycin	100U/mL	10,000U/mL	15140122	Gibco™

2.2.3 Directed differentiation of iPSCs to cerebral cortex neurons

iPSCs were differentiated to cerebral cortex neurons (Chapter 5.4.2.3, Figure 5.12). following the previously established protocol by Shi *et al.* (2012a). For this purpose, iPSCs that had been pretreated with MO47 or DMSO were thawed and cultured as described above. On day 5 after thawing, cells were plated at a density of 4×10^6/well onto a 6-well plate precoated with Geltrex™. Subsequently, neural induction was initiated by a medium change to neural induction medium (NIM, day 1) (Table 2.4). A full medium change of 2mL NIM was performed daily. Upon formation of a neuroepithelial sheet on day 11, cells were passaged either with dispase II or with EDTA.

For dispase II passaging, 200µL of dispase II (Gibco™, 17105041) were added to the 2mL of medium in each well, and incubated for 30 minutes at 37ºC. Next, the lifted clumps of the neuroepithelial sheet were transferred to 10mL of NIM in a 15mL falcon tube. When the cells had settled, the medium was aspirated and the wash repeated with 10mL of NIM.

For EDTA passaging, each well was washed once in 2mL of 0.5mM EDTA (Invitrogen™, AM9260G) solution and then incubated in 1mL for 4-6 minutes. Next, EDTA was carefully aspirated and the cells were gently washed off the plate by gentle flushing using a Gilson p1000. Subsequently, cells were washed in 5mL of NIM.

After the washing, iPSCs were plated in 2mL of NIM onto a 6-well plate that had been precoated with laminin (10ug/mL in PBS; Sigma, L2020). Cells that had not settled down the following day were directly transferred onto new wells that had previously been precoated with 20µg/mL laminin. This allowed rescue of these cells, and increased the efficiency of attachment, especially after dispase II passaging. In wells in which the cells had settled down, a medium change to neural maintenance medium (NMM) was performed (Table 2.4). On days 12 to 15, the neural maintenance medium was supplemented with 20ng/mL fibroblast growth factor (R&D systems, 233-FB-025). Thereafter, a full medium change was performed every other day.

On day 18, newly formed rosettes were passaged either with dispase II or manually. For the latter, rectangles containing rosettes were cut with a needle, and in case of large size, scored into multiple rectangles. Subsequently, the cell sheets were lifted manually, collected with a Gilson p200 and transferred in 2mL of NMM onto a new well that had been precoated with 20µg/mL laminin. Between day 18 and 25, a full medium change was performed every other day.

On day 25, cells were washed once in 2mL PBS and incubated in 0.5mL StemPro™ Accutase™ Cell Dissociation Reagent (Gibco™, A111050) for 7 minutes. Subsequently, they were flushed off the plate using a 5mL serological pipette and the Accutase™ cell suspension was diluted 1:10 in neurobasal medium (21103049, Gibco™). Next, cells were centrifuged at 200g for 3 minutes. Upon pelleting, cells were resuspended at a concentration of 2.5×10^5 cells/mL in NMM, and 2mL cell suspension of each condition was plated onto a new well that had previously been precoated with 20ng laminin/mL. Subsequently, the medium was changed every other day.

Table 2.4 | Medium preparation for directed differentiation to cerebral cortex neurons

	Final [c]	**Stock [c]**	**Catalogue number**	**Supplier**
Neural Induction Medium				
N2 + B27 medium	1:1			
SB431542	10μM	10mM	1614	Tocris
Dorsomorphin	1μM	1mM	3093	Tocris
Neural Maintenance Medium	Consisting of 1:1 N2 + B27 medium			
N2 medium				
Advanced DMEM/F12	1×	1×	12634-010	Gibco™
N2 supplement	1×	100×	17502048	Gibco™
Insulin	5μg/mL	10μg/mL	91077C	Sigma
GlutaMax™	1mM	100mM	35050061	Gibco™
β-mercaptoethanol	100μM	100mM	21985023	Gibco™
Penicillin-streptomycin	50U/mL	5000U/mL	15140122	Gibco™
B27 medium				
Neurobasal medium	1×	1×	21103049	Gibco™
B27 supplement	1×	100×	17504044	Gibco™
GlutaMax™	1mM	100mM	35050061	Gibco™
Penicillin-streptomycin	50U/mL	5000U/mL	15140122	Gibco™
Coating agents				
Laminin (in PBS)	10-20ng/mL		L2020	Sigma
Geltrex™ (in KODMEM)	1:100	1×	A1569601	Gibco™

2.2.4 Thawing and freezing cells

For cryopreservation, cells were harvested as described above and resuspended in the relevant culturing medium. The cell suspension was then aliquoted into cryovials (Starlab, E3090-6222), mixed 1:1 with freezing medium (Table 2.5), transferred into precooled freezing containers (Mr. Frosty™, Thermo Fisher Scientific) and stored at -80˚C for a maximum of 48h before storage in liquid nitrogen.

Table 2.5 | Freezing medium preparation

	Final [c]	Stock [c]	Catalogue number	Supplier
2× iPSC freezing medium				
DMSO	20%	1×	D2650	Sigma
Knockout DMEM	20%	1×	10829-018	Gibco™
Fetal calf serum (FCS/FBS)	60%	1×	16141-079	Gibco™
Mixed 1:1 with mTeSR™1			85875	Stemcell Technologies
2× HDF freezing medium				
DMSO	20%	1×	D2650	Sigma
Fetal calf serum (FCS/FBS)	80%	1×	10829-018	Gibco™
Mixed 1:1 with HDF medium				
2× Neural freezing medium				
DMSO	20%	1×	D2650	Sigma
Neural maintenance medium	80%	1×	10829-018	Gibco™
Mixed 1:1 neural maintenance medium				

For thawing cells, cryovials where placed in a 37°C water bath until only a small amount of the ice remained. Subsequently, the cell suspension was immediately diluted 1:10 in PBS, centrifuged at 400g for 5 minutes, and the pellet resuspended in prewarmed medium.

2.3 Antibodies and dyes

Table 2.6 | Primary antibodies

	Host	Isotype, conjugate fluorophore	Supplier/catalogue number	[c]
Flow cytometry				
Anti-CD44	Mouse	IgG_1	Life Tech.	1:40
Anti-SSEA3	Rat	IgM, Alexa Fluor 488	Biolegend, 330306	1:80
Anti-SSEA4	Mouse	IgG_3, APC	R&D, FAB1435A	1:20
Anti-Tra1-60	Mouse	IgM, PE	Biolegend, B118883	1:10
Anti-Nanog	Anti-	IgG, 647	Cell Signaling, 5448S	1:10
Anti-E-cadherin	Mouse	IgG_{2a}, SHE78-7	Invitrogen, 13-5700	1:200
Anti-E-cadherin	Mouse	IgG_1	BD Pharmingen, 56289	1:200
Anti-KI-67	Mouse	IgG_1	Merck, MAB4190	1:400
Anti-CD11b	Mouse	IgG_1, APC	Biolegend, 301309	1:25
Anti-CD14	Mouse	IgG_1, PE	ImmunoTools, 21620144	1:25
Anti-CD45	Mouse	IgG_1, APC	ImmuniTools, 21270456	1:25
Confocal microscopy				
Anti-Rab-5	Rabbit	IgG	Cell Signaling, 3547	1:200
Anti-Rab-7	Rabbit	IgG	Cell Signaling, 2094S	1:200
Anti-Lamp-1	Rabbit	IgG	Cell Signaling, 3243S	1:200
Anti-Rab-9	Rabbit	IgG	Cell Signaling, 5133S	1:200
Anti-Rab-10	Rabbit	IgG	Cell Signaling, 4262S	1:100
Anti-Rab-11	Rabbit	IgG	Cell Signaling, 3539S	1:200
Anti-E-cadherin	Mouse	IgG_{2a}, SHE78-7	Invitrogen, 13-5700	1:1000
Anti-Pax-6	Rabbit	IgG (polyclonal)	Covance, PRB-278P	1:300
Anti-Tuj1/Tubulin β3	Mouse	IgG2a	Covance, MMS-435P	1:200

Table 2.7 | Secondary antibodies, isotype controls and dyes

	Host	Isotype, species, conjugate /fluorophore	Supplier/ catalogue number	[c]
Flow cytometry				
Isotype control	Mouse	IgG_1	Biolegend, 400107	1:50
Isotype control	Rat	IgM, Alexa Fluor 488	Biolegend, 400811	1:100
Isotype control	Mouse	IgG_3, APC	R&D, IC007A	1:20
Isotype control	Mouse	IgM	Biolegend, 401617	1:10
Isotype control	Rabbit	IgG, Alexa Fluor 647	Cell Signaling, 2985S	1:10
Secondary antibody	Donkey	IgG, anti-mouse, Alexa Fluor 647	Invitrogen, A-31571	1:1000
Secondary antibody	Goat	IgM, anti-mouse, Alexa 488	Invitrogen, A-21042	1:1000
Secondary antibody	Goat	IgG_{2a}, anti-mouse, Alexa 647	Invitrogen, A-21241	1:1000
Secondary antibody	Goat	IgG, anti-rabbit, Alexa Fluor 647	Invitrogen, A-21244	1:1000
Confocal microscopy				
Secondary antibody	Donkey	IgG, anti-mouse, Alexa Fluor 647	Invitrogen, A-31571	1:1000
Secondary antibody	Goat	IgM, anti-mouse, Alexa 488	Invitrogen, A-21042	1:1000
Secondary antibody	Goat	IgG_{2a}, anti-mouse, Alexa 647	Invitrogen, A-21241	1:1000
Secondary antibody	Goat	IgG, anti-rabbit, Alexa Fluor 647	Invitrogen, A-21244	1:1000
Secondary antibody	Donkey	IgG, anti-mouse, Alexa Fluor 647	Invitrogen, A-31571	1:1000
Dyes				
Hoechst 33342		361	ThermoScientific, 62249	1:10,000
CytoPainter Phalloidin-iFluor		488	Abcam, ab176753	1:1000
CellMask Plasma Membrane Stain		649	Invitrogen,	1:1000
Propidium iodide		535	Abcam, Annexin-V-FITC kit, Ab14085	1:20
Annexin-V-FITC		FITC	Abcam, Annexin-V-FITC kit, Ab14085	1:20

2.4 Flow cytometry

Flow cytometry is a laser- or impedance-based analysis for cell sorting, cell isolation, and the detection of cell surface molecules. Moreover, it allows for the profiling of cellular particularities such as size, granularity, cell cycle stage, and DNA content (Etzrodt *et al.*, 2014). For this study, the detection of cell surface markers, the profiling of size and granularity, the identification of DNA content, and the distinction between healthy and apoptotic cells have played a vital role.

For immunohistochemistry (Figures 4.7, 5.2, 5.4 5.11), cells were washed in PBS and harvested using enzymatic dissociation as described above. After centrifugation, cells were resuspended in FACS buffer consisting of PBS, 10 µg/mL human IgG, 1% FBS. To avoid the internalisation of cell surface markers, which would decrease fluorescence intensity, FACS buffer was precooled at 4°C and further supplemented with 0.1% azide. Cells were either stained for 30-45 minutes prior to fixation in FACS buffer (preferably at 4°C) or after fixation (10 minutes in 2% paraformaldehyde-FACS buffer). After fixation, cells were washed once in FACS buffer. Depending on the localisation of the immunohistochemistry target, the fixed cells were then permeabilised in pure methanol at -20°C for at least 30 minutes. Cells were stored up to 4 weeks in FACS buffer at 4°C or in methanol at -20°C.

Antibodies were diluted in FACS buffer and mixed with cell suspension in 96-well V-bottomed plate or 1.5mL Eppendorf tubes. Staining was performed in a total of 50 or 100µl FACS buffer supplemented with the appropriate antibody concentrations (Table 2.6). After each antibody staining, cells were washed twice in FACS buffer. If staining was performed with unconjugated antibodies, a staining with a secondary antibody followed for 30-45 minutes at 4°C (Table 2.7). The flow cytometry analysis was

performed on FACS Calibur (Becton Dickinson), and data analysis carried out with the software FlowJo.

For the Annexin-V-PI assay (Chapter 4.4, Figure 4.8), iPSCs were plated at a density of 1×10^5 cells/well onto a 24-well plate, and treated for 24h, 48h and 72h with (-)-Indolactam V or 0.1% DMSO. Prior to each medium change, the plate was centrifuged at 400g so that detached or apoptotic cells would not be aspirated during the medium change. When harvesting, the supernatant of each sample was transferred to 1.5mL Eppendorf tubes and centrifuged at 400g for 5 minutes. Next, the iPSCs on the plate were washed with 500µL Hanks' Balanced Salt Solution (HBSS, Gibco™, 14170112), and lifted using enzymatic dissociation. Subsequently, the pellet of the supernatant and the enzymatically dissociated cells were mixed so that previously the entire cell population could be analysed. Subsequently, each condition was stained with 5µL propidium iodide and 5µL Annexin-V-FITC in 100µl staining buffer (Annexin-V-FITC kit, Ab14085) for 15 minutes at room temperature. Prior to analysis using flow cytometry, 200µL of binding buffer were added to each sample. Compensation was performed using the software FlowJo.

2.5 Light microscopy

2.5.1 Brightfield and phase contrast microscopy

Light microscopy is key in assessing cell viability, confluency, and morphological changes of treated and untreated cells in 2D culturing. For this study, phase contrast images were taken using the EVOS XL Core Imaging System (ThermoFisher).

2.5.2 Confocal microscopy

Confocal microscopy is a laser-based scanning technique in which a focused laser beam is used to excite fluorophores at a single point on the sample plane (Thorn, 2016). Prior to imaging (Figures 3.3, 3.5, 4.4, 4.5, 5.3, 5.5, 5.14), cells were cultured open µ-slides

(Ibidi, 80827). Each of these slides contains 8 wells and was precoated with 200µL of the relevant coating agent. Cells were plated at preferable densities of 1-1.5×10^5 cells, and cultured in volumes ranging from 200-400µl/well. Plating was performed in total volume of 400µl well to allow the cells to be evenly spread. For fixation, 200µL of 2% PFA-PBS was added and cells incubated for 10 minutes at room temperature. If necessary, cells were permeablised and blocked in 200µl PBS/1% BSA/0.3% Triton™ X-100 at 4°C overnight or for 45 minutes at room temperature.

For confocal microscopy of cortical neuronal progenitors (Chapter 5.4.2.3, Figure 5.14), rosettes were manually passaged on day 18 in 400µl of NMM onto a precoated µ-slide and grown until day 25. Next, cells were washed in 300µL PBS and fixed for 10 minutes in 2% PFA at room temperature. After one wash in 300µL PBS, cells were permeabilised and blocked in PBS/Triton X-100/1% donkey serum/1% goat serum at 4°C overnight.

Confocal microscopy images were analysed with ImageJ/Fiji for pictures in 2D (X,Y) and 3D (z-stacks; X,Y, Z). Changes in contrast or brightness were equally applied to all images. For quantification, measurements of the nuclei area, the nuclei perimeter, the phalloidin signal (Chapter 3.4, Figure 3.4 B) and the cell density (nuclei/area, Chapter 3.4, Figure 3.4 A) were determined in a previously optimised automated approach using the software CellProfiler. To determine the density of the nuclei and the phalloidin signal for the DMSO conditions, the original image was cropped into excerpts which only displayed colonies; areas between the colonies were not included as counts in these cell-free areas would have reduced the density measure artificially (Chapter 3.4, Figure 3.3). The analysis for the treated conditions was performed in areas which were fully covered by cells (no free areas, for a further illustration of the selected pictures see Figure 3.3). The height of the nuclei was measured on z-stacks in a single-blind assay using the

software ImageJ/Fiji. To this end, each z-stack was cropped into five 2D excerpts (orthogonal view, YZ), and the measurements were performed by a postdoctoral associate in our laboratory.

2.6 Genome-wide association studies (GWAS)

DNA was extracted from cell pellets that had previously been stored at -80°C, using the DNeasy Mini Kit (Qiagen, 69504) according to the manufacturer's protocol. DNA yields were measured loading 1.5µL of extracted DNA onto the NanoDrop™ 2000c spectrophotometer (Thermo Scientific™). The optical density of each sample was subsequently verified for its purity (A 260/280 ratio ≅ 1.8), and 1000ng of extracted DNA were loaded per Eppendorf tube. The extracted DNA was then sent for analysis using the Infinium OmniExpress-24 v1.2 Kit (Illumina).

2.7 Quantitative real-time PCR (qRT-PCR)

2.7.1 RNA extraction

RNA was either extracted from cell pellets that had previously been stored at -80°C, or from cell slurry. For lysis, 350µL RLT buffer supplemented with 1% pure β-mercaptoethanol were added and the cell slurry was transferred onto a QIAshredder spin column (Qiagen). Subsequently, cell lysates were spun on the QIashredder column and RNA extracted using the RNeasy kit (Qiagen) according to the manufacturer's protocol. An optional on-column DNase treatment for 15 minutes was performed. RNA yields were measured by loading 1.5µL of extracted RNA onto the NanoDrop™ 2000c spectrophotometer. The optical density of each sample was subsequently verified for its purity (A 260/280 ratio ≅ 2).

2.7.2 cDNA production by reverse transcription (RT)

cDNA was produced by using either the Ambion RETROScript™ Kit (Invitrogen, AM1710) or the High Capacity cDNA Reverse Transcription Kit (Applied Biosystems™, 4368814), and in both cases a total of 1µg RNA/sample was loaded for the cDNA reaction. For the TaqMan hPSC Scorecard™ Panel, cDNA was produced using the High Capacity cDNA Reverse Transcription Kit according to the manufacturer's protocol.

2.7.3 Quantitative real-time PCR (qRT-PCR)

qRT-PCR was either performed using a SYBR® Green- (Applied Biosystems, 4309155) or a TaqMan®-based approach. To this end, the previously generated cDNA was diluted and prepared according to Table 2.8 and Table 2.9. The primers for PKC isoforms and E-cadherin were adopted from Awadelkarim *et al.* (2012) and Labernadie *et al.* (2017) and ordered from Sigma. Prior to all experiments, the efficiencies of the endogenous control (TBP) and the primer pairs were tested (Appendices, Figures IV.1 and IV.2).

Table 2.8 | SYBR® Green sample preparation

	Primer mix (5µM each)	2× SYBR® Select MM	Nuclease-free H_20	Total volume
SYBR® Green reaction				
Volume/sample	0.5µL	12.5µL	10µL	23µL
+				
2 µL template cDNA (20µL cDNA reaction diluted 1:5 in H_20)				25µL

Table 2.9 | TaqMan® sample preparation

	TaqMan® primer	TaqMan® Gene Expression MM	Nuclease-free H_20	Total volume
TaqMan® reaction				
Volume/sample	1µL	10µL	7.2µL	18.2
+				
1.8 µL template cDNA (20µL cDNA reaction diluted 1:10 in H_20)				25µL

The total volume of master mix and cDNA was loaded onto a MicroAmp™ Optical 96-Well Reaction Plate (Applied Biosystems, N8010560), and the qRT-PCR reaction run on the StepOnePLus™ Real-Time PCR System (Applied Biosystems, 4376598). Analysis of relative gene expression levels was performed according to the ΔΔCT approach (Livak *et al.*, 2001).

2.8 Enzyme-linked Immunosorbent Assay for soluble E-Cadherin

For ELISA (Chapter 4.3.2, Figure 4.6), cells were plated over night at a density of 1×10^6 cells onto precoated wells of a 6 well format. The following morning, the medium was changed and the appropriate concentration of (-)-Indolactam V (1μM), MO47 (1μM) or EDTA (50μM) was added to 1mL mTesR™1 per well. After 24h of treatment, the supernatant was transferred to Eppendorf tubes, and centrifuged at 400g for 5 minutes. Subsequently, the supernatant was transferred to new Eppendorf tubes in order to filter out floating cells and debris that would have falsely increased the amount of soluble E-cadherin in the supernatant. Afterwards, they transferred onto wet ice, and analysed using the Human E-cadherin ELISA Kit (Invitrogen™, 991700) according to the manufacturer's protocol. To quantify the concentration of soluble E-Cadherin, a standard curve including concentrations ranging from 2.7μg to 0.084μg was generated in parallel. The absorbance was measured at 450nm, using the Every SpectraMax® M plate reader (Molecular Devices).

2.9 Caspase 3/7 Assay

Apoptosis IC_{50} values were determined using the Caspase-Glo® 3/7 Assay (Promega, G8090) according to the manufacturer's protocol.[2] A previous experiment for the

[2] This assay was performed by Dr Laurence Silpa, a post-doctoral associate in our laboratory.

determination of the cell density revealed an optimal linear range of the assay at 10.000 cells/well in a 96 well format (Appendices, Figure III).

2.10 Statistical analysis

The statistical analysis in this study was performed using the software GraphPad Prism. For the comparison of the treated to the control conditions, two-tailed t test, one-way ANOVA with Dunnett's multiple comparisons test or two-way ANOVA with Holm-Šídák's multiple comparisons were performed. Replicates are presented as mean ± SEM. Biological triplicates (cells seeded, cultured and treated in independent wells) and technical replicates (identical sample used for replicates) are indicated as 'br' or 'tr', respectively. Statistical significance is marked as ns ($P > 0.05$), * ($P \leq 0.05$), ** ($P \leq 0.01$), *** ($P \leq 0.001$) and **** ($P \leq 0.0001$).

Chapter 3: Studying 2D phenotypes induced by (-)-Indolactam V and MO47

3.1 Introduction

2D and 3D cultures pose similar challenges, namely heterogeneity resulting in a susceptibility towards differentiation, G_0 arrest and apoptosis (Cahan *et al.*, 2013; Wu *et al.*, 2015a). While the formation of aggregates in 3D remains a roadblock in scaleup approaches, iPSC colonies in 2D are, due to their variability in size, shape and compaction, by nature heterogeneous (Kato *et al.*, 2016; Rosowski *et al.*, 2015).

As an initial proof-of-principle study, the work in this chapter focuses on morphological phenotypes upon treatment with (-)-Indolactam V and MO47. We chose to perform this initial morphological study in 2D, since the conditions in 2D are more robust, enable better monitoring of morphological phenotypes over time, and can easily be harnessed for follow-up experiments.

3.1.1 2D phenotypes and heterogeneity

iPSCs can morphologically be defined by their cobblestone shape with large nuclei containing large nucleoli and an overall sparse cytoplasm (Cahan *et al.*, 2013; Robinton *et al.*, 2012). Standard 2D iPSC and ESC cultures display monolayers defined by compact colonies with defined borders (Healy *et al.*, 2015; Kato *et al.*, 2016; Lowry *et al.*, 2008).[3]

[3] The morphology of iPSCs has been shown to be identical to hESCs. Therefore, this chapter refers to both stem cell types. For further reference see Takahashi K, Tanabe K, Ohnuki M, Narita M, Ichisaka T, Tomoda K*, et al.* (2007). Induction of pluripotent stem cells from adult human fibroblasts by defined factors. Cell 131**:** 861-872. Healy L, Ruban L, & SpringerLink (Online service) (2015) *Atlas of Human Pluripotent Stem Cells in Culture*. Springer US : Imprint: Springer,. Boston, MA. Available from Full text from SpringerLink http://dx.doi.org/10.1007/978-1-4899-7507-2.
, Lowry WE, Richter L, Yachechko R, Pyle AD, Tchieu J, Sridharan R*, et al.* (2008). Generation of human induced pluripotent stem cells from dermal fibroblasts. Proc Natl Acad Sci U S A 105**:** 2883-2888.

In these colonies, E-cadherin and the actin cytoskeleton play vital roles in cell motility (Davidson *et al.*, 2016), environmental sensing (Geiger *et al.*, 2009) and cell-cell interaction (Geiger *et al.*, 2009). Notably, the importance of the actin cytoskeleton for the survival and maintenance of hESCs and iPSCs was laid bare through the discovery of Rho-kinase inhibitor (Chen *et al.*, 2010; Ohgushi *et al.*, 2010). The dissociation-associated cell death stimulated by hypercontraction of stress fibres could, henceforth, be targeted for improving culturing conditions (Xu *et al.*, 2010).

iPSCs require a compact colony formation and are epithelialised through E-cadherin-mediated adherens junctions (Ohgushi *et al.*, 2010; Singh *et al.*, 2013; Soncin *et al.*, 2009). Although iPSCs colonies are tightly packed in an epithelial-like pattern, the adhesion strength between the cells remains low to allow further plasticity for the expansion of the colonies (Chan *et al.*, 2009; Singh *et al.*, 2013).

The expansion of iPSC colonies follows a polarised pattern in which cells that are mainly at the edges of the colony expand, while the centres mainly increase in compaction (Healy *et al.*, 2015). This has two major implications. Firstly, cells at the edges are prone to a lack of external cues and are more inclined to differentiation (Rosowski *et al.*, 2015). Secondly, iPSCs thickening and piling up in the centre lengthen their state in G_1 and are susceptible to G_0 arrest (Wu *et al.*, 2015a). The subsequent overcompaction exerts cellular stress and induces cells that commit to differentiation. One frequent example in this context is the formation of neuronal rosettes (Healy *et al.*, 2015). Moreover, overcompaction and tightening of focal adhesions prevents the cells from spreading out again and forming homogenous monolayers (Healy *et al.*, 2015). This morphological variability is accompanied by a heterogeneous expression of pluripotency markers across the population (Chan *et al.*, 2009; Wakao *et al.*, 2012). With each colony further varying

in size and shape, 2D systems provide heterogeneous conditions, which present an ideally suited model for the study of morphological heterogeneity (Kato *et al.*, 2016).

3.1.2 Establishing morphological criteria for 2D iPSC culture

In order to evaluate the morphological phenotypes in this study, a series of morphological criteria that were hypothesised to enable more homogenous culturing conditions in 2D (and potentially in 3D as an ultimate goal) shall be established: (1) disruption of iPSC colonies with clear edges; (2) equal distribution of iPSCs across the adherent monolayer; (3) decrease in cell density and compaction; (4) reversibility and reproducibility of the phenotypic effect; (5) remodelling processes of the actin cytoskeleton; (6) abrogation of an epithelial-like phenotype; (7) disruption of E-cadherin-mediated cell-adhesion; (8) survival of single cells at low densities.

Based on these desired properties, this chapter hypothesises that a chemical approach through (-)-Indolactam V and MO47 induces a colony-independent, more homogenous phenotype in 2D, which can potentially be harnessed for 3D culturing.

3.2 Inducing colony-independent iPSC culture in 2D

As a first proof-of-principle study, iPSC phenotypes were examined upon treatment with (-)-Indolactam V and MO47. iPSCs were plated at a density of 1×10^6cells/well onto a 6-well plate. On the following day, iPSCs were treated for 3h, 12h, and 24h prior to imaging with 1μM (-)-Indolactam V, 1μM MO47 or 0.1% DMSO (control and vehicle for all conditions). These temporal intervals were chosen to assess immediate effects and their progression until this progressive phenotype reached its full expression at 24h. Treating the cells at different times but imaging them at the same time point further allowed assessment of these different phenotypes at equal cell density, provided that cell proliferation was not impaired. Figure 3.1 A and Figure 3.1 B show the effect of (-)-Indolactam V and MO47 over time. The morphology change after 3h indicates the induction of a new phenotype. The iPSC colonies are less compact and appear to diverge. The phenotypes at 12h are much stronger and appear to reach their full expression at 24h, especially for MO47 treated cells. A colony-based phenotype can neither be identified at 12h or 24h after treatment.

In summary, these data indicate that iPSCs exhibit a strong, almost immediate morphological change upon treatment with (-)-Indolactam V or MO47. This morphological phenotype is characterised by a progressive spreading of iPSCs and results in the abrogation of dense colonies with clearly-defined edges.

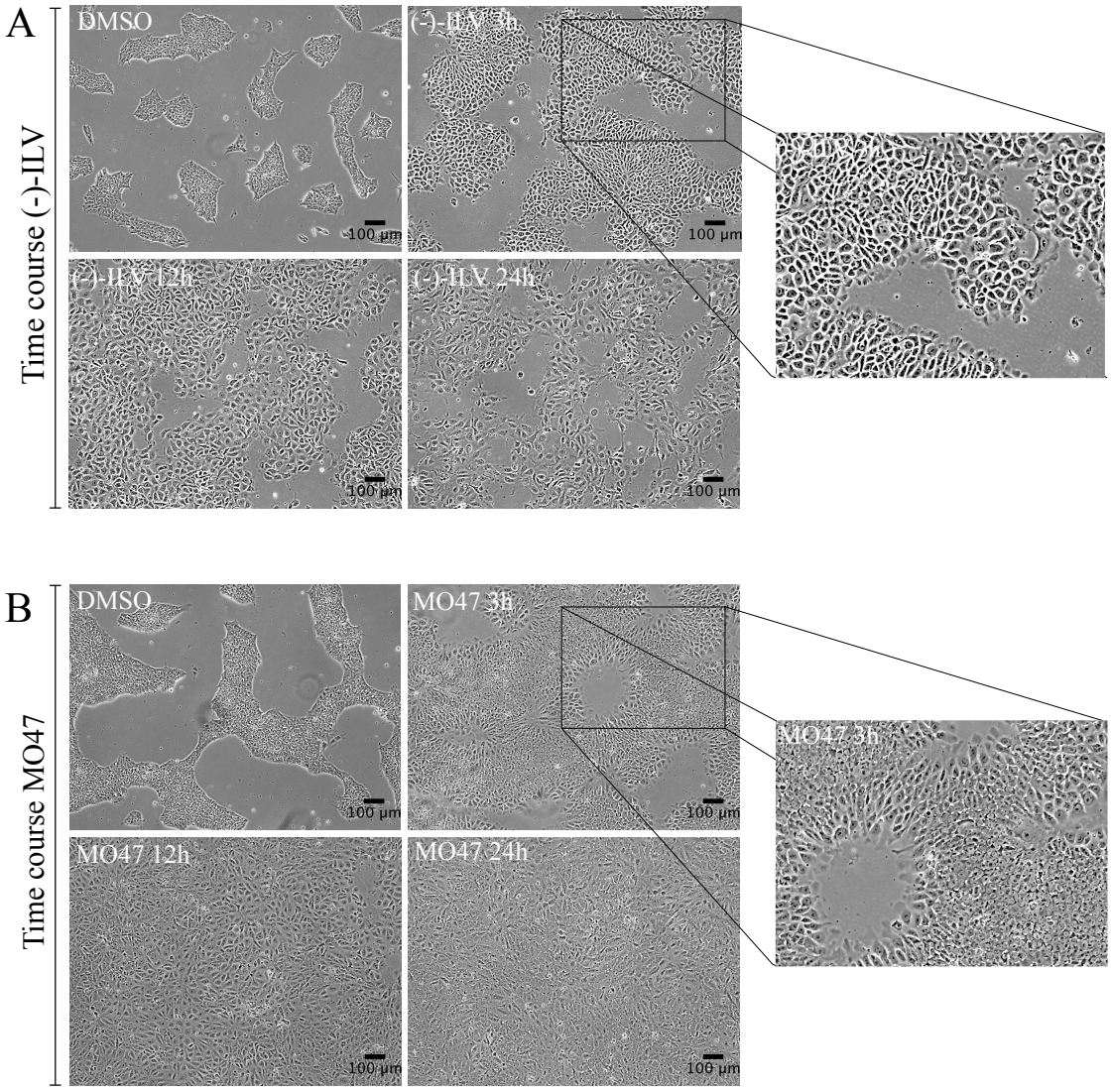

Figure 3.1 | Colony-independent iPSC cultures can be induced using (-)-Indolactam V and MO47.

Shown are images of iPSCs treated with 1µM (-)-Indolactam V **(A)** or MO47 **(B)** at 3h, 12h and 24h prior to imaging. Note the almost immediate deformation of the colonies identified at 3h after treatment (magnified excerpts). Populations treated with MO47 for 3h display a distinct membrane blebbing with protrusions indicating cell movement. The control phenotype (DMSO), in contrast, is marked by compact colonies with clearly defined edges. Phase contrast; magnification = 100×; scale bars = 100 µM.

3.3 Reversibility of colony-independent phenotypes

To further characterise the effect of (-)-Indolactam V and MO47 on iPSC cultures, we endeavoured to assess whether morphological alterations would persist after treatment. We hypothesised that the effect was inducible and reversible in presence or absence of the compounds, accordingly. For this purpose, iPSCs were plated and cultured in mTesR™1, which contained Rho-kinase inhibitor. After 24h, the medium was changed—which also removed Rho-kinase inhibitor—and iPSCs were cultured in mTesR™1 supplemented with 1μM (-)-Indolactam V or MO47 for 24h. Finally, the compounds were washed off by a medium change and culturing in mTesR™1 without the compounds was continued for 24h. At each medium change the conditions were imaged using phase contrast. Figure 3.2 shows the expression of three different phenotypes in a serial approach. After plating in medium with Rho-kinase inhibitor, iPSCs display an elongated, spread morphology with missing colony-association. After subsequent treatment with 1μM (-)-Indolactam V or MO47 for 24h, colony-based iPSCs are still absent and exhibit spread phenotypes. Finally, the colony-based morphology is restored 24h wash-off period.

In summary, these results show that the morphological effects on iPSCs upon treatment with (-)-Indolactam V and MO47 are reversible and still enable a regular colony formation 24h after compound removal.

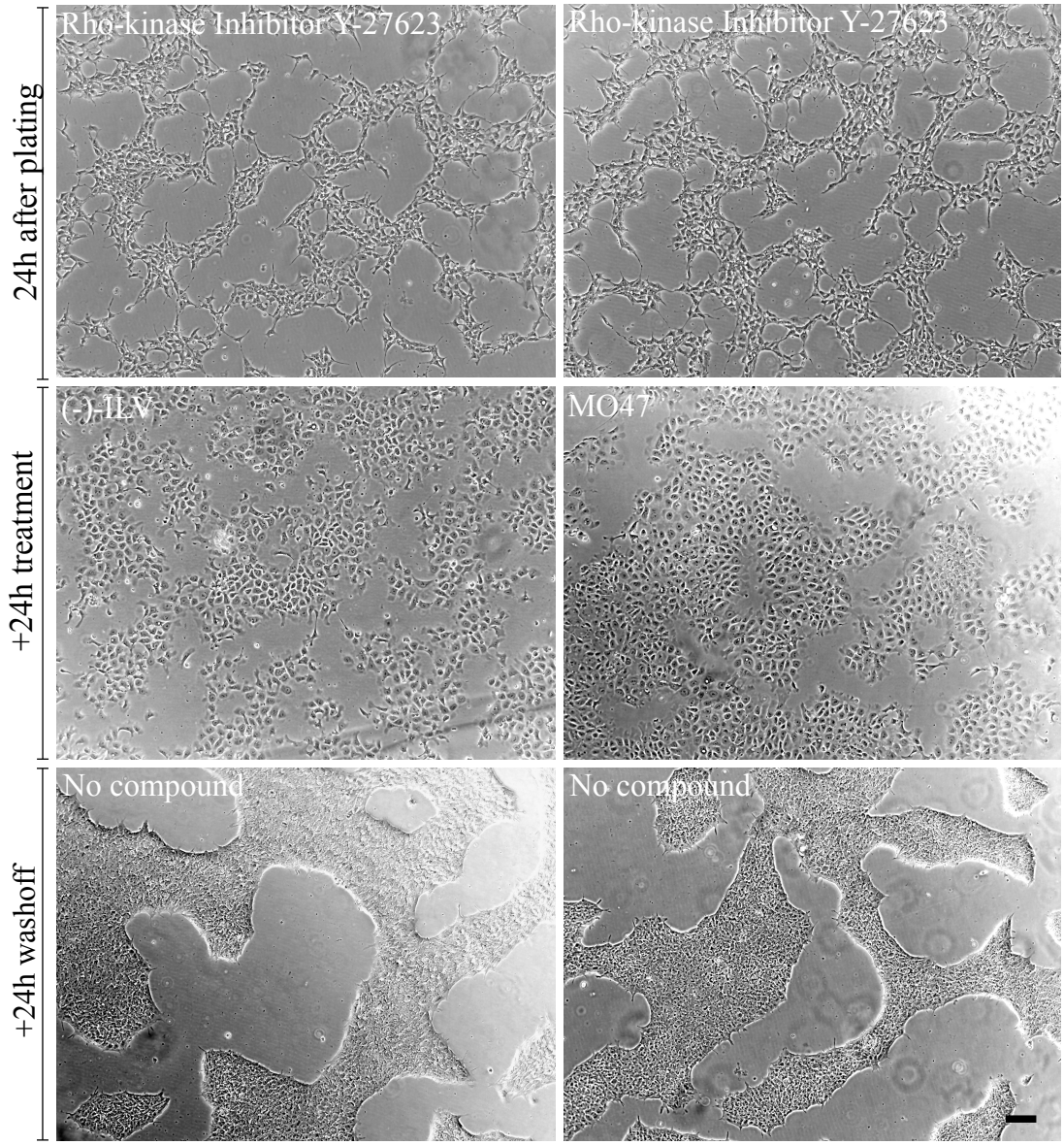

Figure 3.2 | Reversibility of the phenotypic effect induced by (-)-Indolactam V and MO47.

iPSCs were plated with Rho-kinase inhibitor Y-27623 (upper panel) and then treated with (-)-Indolactam V (left, middle panel) and MO47 (right, middle panel) for 24h. To assess the reversibility of the phenotypic effects, the compounds were washed off in both conditions. After 24h the formation of compact colonies with clearly-defined edges can be observed (lower panel). Phase contrast; magnification = 100×; scale bar = 100μm.

3.4 Assessing the actin cytoskeleton upon treatment

It has recently been reported that iPSC colonies in 2D are characterised by a strong actin fence that encircles individual colonies and mainly consists of ventral stress fibres (Narva *et al.*, 2017; Naumanen *et al.*, 2008). Importantly, this actin girdle exerts mechanical effects and acts like a tension band, thereby impinging on colony compaction, pluripotency and polar spindle arrangements during mitosis (Narva *et al.*, 2017).

We hypothesised that one prerequisite for the emergence of the previously observed phenotypes was the remodelling of the actin cytoskeleton (Davidson *et al.*, 2016; Mullins *et al.*, 1998). To characterise potential rearrangements of globular and filamentous actin, iPSCs were plated onto a μ-slide. After the cells had attached, the medium was changed and Rho-kinase inhibitor washed-off for 12h prior to treatment. This allowed reduction of the chemical influences on the cytoskeleton by Rho-kinase inhibitor. Subsequently, iPSCs were treated with 1μM (-)-Indolactam V and MO47 for 24h, fixed, permeabilised and stained with Phalloidin-iFluor 488, a dye that specifically stains filamentous actin. To highlight the global arrangeme nt of individual cells, the nuclei were stained with Hoechst.

Figure 3.3 shows the standard colony-based iPSC phenotype (upper panel) and colony-independent, homogenous monolayers upon treatment with either 1μM (-)-Indolactam V (middle panel) or MO47 (lower panel). The quantified data for the images in Figure 3.3 are presented in Figure 3.4. Compared to DMSO, treatment with (-)-Indolactam V and MO47 induced a 3.48-fold and 2.69-fold reduction of the cell density (nuclei/area), respectively (Figure 3.4 A).

Untreated conditions are marked by an actin fence consisting of ventral stress fibres (Figure 3.3, upper panel, white arrows). Treated conditions exhibit a global mesh of stress

fibres across the monolayer (this can be identified even better on Figure 3.5). This is corroborated by the finding that iPSCs treated with (-)-Indolactam V and MO47 exhibit a 5.87-fold and a 3.29-fold (tr) higher signal for actin (as stained by Phalloidin-iFluor 488) compared to DMSO, respectively (Figure 3.4 B).

Taken together, these data indicate that upon treatment with (-)-Indolactam V and MO47 the typical iPSC colony morphology disappears. iPSCs are spread, and marked by a decrease in cell density and the remodelling of the actin cytoskeleton.

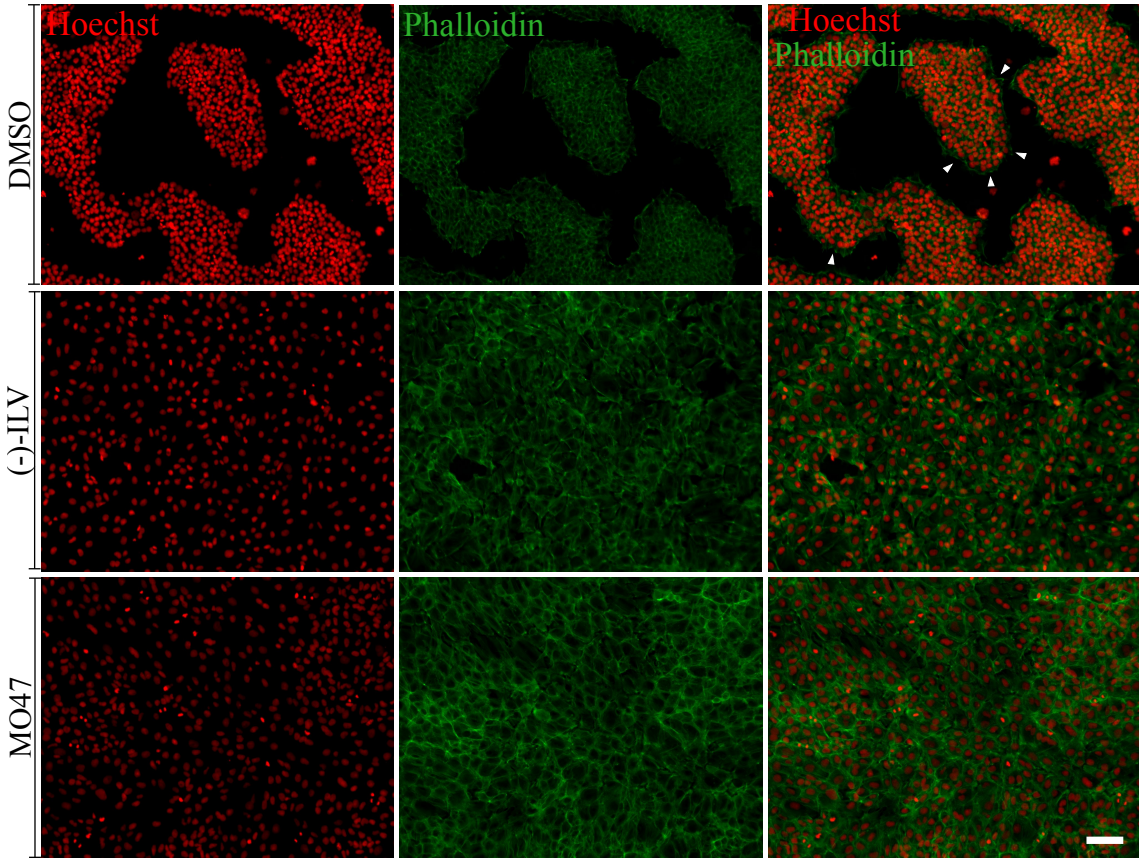

Figure 3.3 | Remodelling of the actin cytoskeleton upon treatment with (-)-Indolactam V and MO47.

iPSCs were plated onto a µ-slide, treated for 24h with 1µM (-)-Indolactam V (middle panel) or MO47 (lower panel) and stained with Hoechst (red) and Phalloidin-iFluor 488 (green). Note the clear actin fence (white arrows, upper panel) surrounding the edges of compacting colonies in the standard condition (DMSO). This fence is replaced by a mesh of actin fibres and the dense colonies give way to a homogenous cell spread as indicated by the nuclei. LED illuminated fluorescent microscopy; magnification = 100×; scale bar = 100µm.

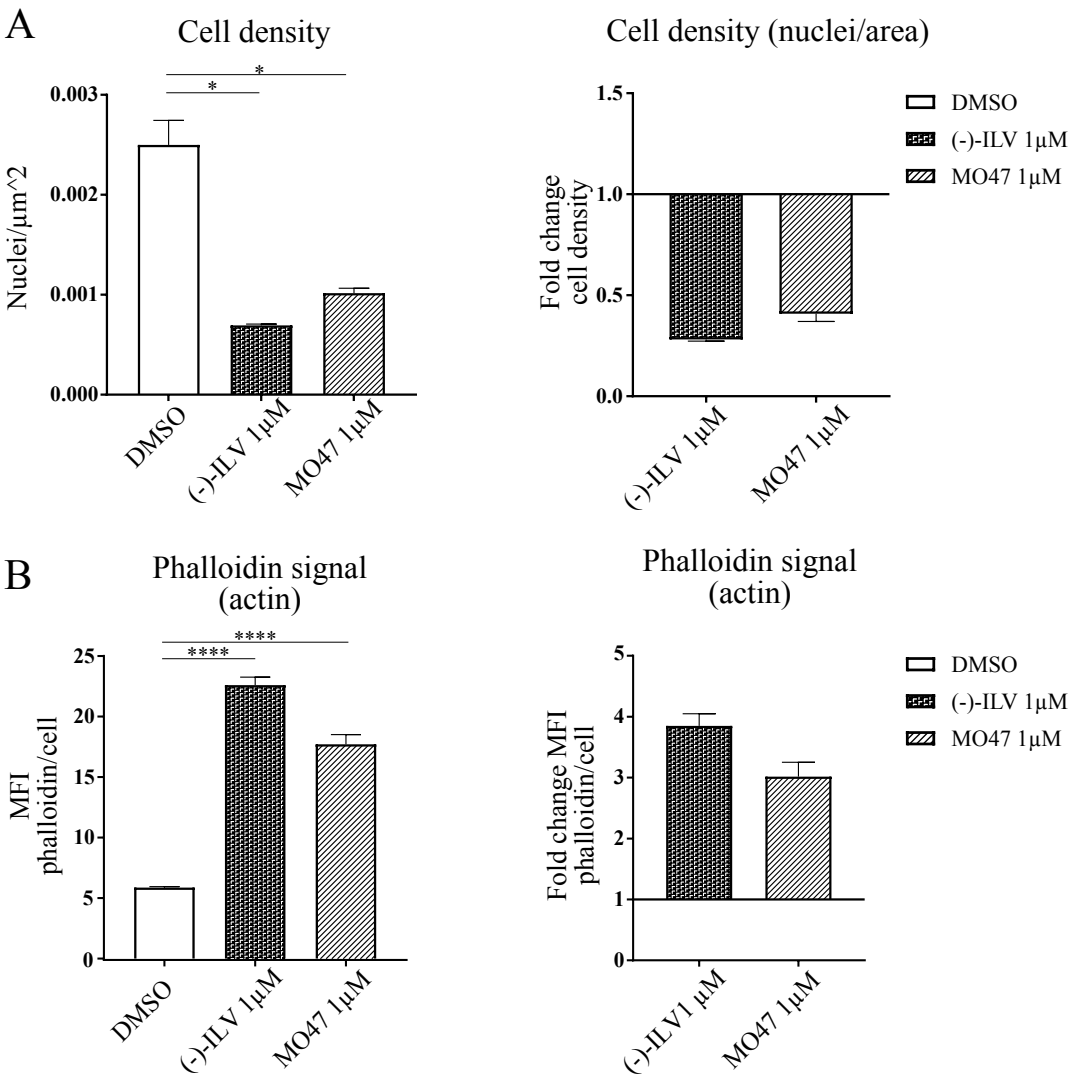

Figure 3.4 | Phenotypic effects of (-)-ILV and MO47 on the cell density and the actin cytoskeleton.

The quantified data for the images presented in Figure 3.3 are shown. iPSCs were treated for 24h with 1µM (-)-ILV and MO47. **(A)** Comparison of the cell density (nuclei/area) of (-)-Indolactam V (mean±SEM: 0.00070±0.000012; n=4) and MO47 (mean±SEM: 0.001045±0.000046; n=4) treated iPSCs shows a significant (tr) difference to control conditions (mean±SEM: 0.002499±0.000246; n=3). **(B)** Quantification of the mean fluorescence intensity for the actin cytoskeleton (stained by phalloidin) reveals a significant (tr) increase of actin fibres in the treated conditions ((-)-ILV mean±SEM: 22.44 ±0.53; n=4; MO47 mean±SEM: 17.32 ±0.68; n=4; DMSO mean±SEM: 5.87±0.08; n=4). One-way ANOVA, Dunnett's multiple comparisons test; ns ($P > 0.05$), * ($P \leq 0.05$), ** ($P \leq 0.01$), *** ($P \leq 0.001$) and **** ($P \leq 0.0001$).

3.5 Assessing focal adhesions upon treatment

E-cadherin plays a pivotal role in the formation and integrity of epithelial and epithelial-like tissues such as iPSCs (Li *et al.*, 2012a; van Roy *et al.*, 2008). Being the chief mediator of colony compaction and directly linked to the actin cytoskeleton, E-cadherin is key to understanding the adhesive signature in iPSCs (Kato *et al.*, 2016; Singh *et al.*, 2013; Wakao *et al.*, 2012).

We hypothesised that the remodelling of the actin cytoskeleton would also result in a rearrangement of focal adhesions. Therefore, iPSCs were plated at a density of 1×10^5 cells on a μ-slide. After the cells had settled on the plate, the medium was changed so that the Rho-kinase inhibitor could be washed off for 8 hours. Subsequently, iPSCs were treated with DMSO (0.1%), 1μM (-)-Indolactam V and 1μM MO47 for 3h, 6h and 24h prior to fixation. Next, immunohistochemistry was performed using Hoechst (blue), Phalloidin-iFluor 488 (green) and an anti-E-cadherin mAb follow by a secondary Ab (red).

Figure 3.5 presents the 3 different colour channels for 3 different treatment (DMSO, (-)-Indolactam V and MO47) at 3h, 6h and 24h. At all three time points, the nuclei appear to be less dense, especially for iPSCs treated with (-)-Indolactam V for 24h. The emergence of stress fibres and the reorganisation of the actin cytoskeleton in the treated conditions appear to be progressive and are especially visible for iPSCs treated with (-)-Indolactam V for 24h. Importantly, for (-)-Indolactam V at 24h, the focal adhesions appear to be rearranged and the E-cadherin signal is blurred, which might be indicative of the cell spreading. A different trend can be observed for MO47; despite a clear rearrangement after 6h, a distinct E-cadherin signal still encircles the cytoplasm at 24h. The nuclei appear to be more prominent upon treatment with (-)-Indolactam V and MO47.

Overall, these data show that (-)-Indolactam V and MO47 induce strong phenotypes that are characterised by prominent stress fibres and remodelling processes of E-cadherin mediated cell-cell adhesion

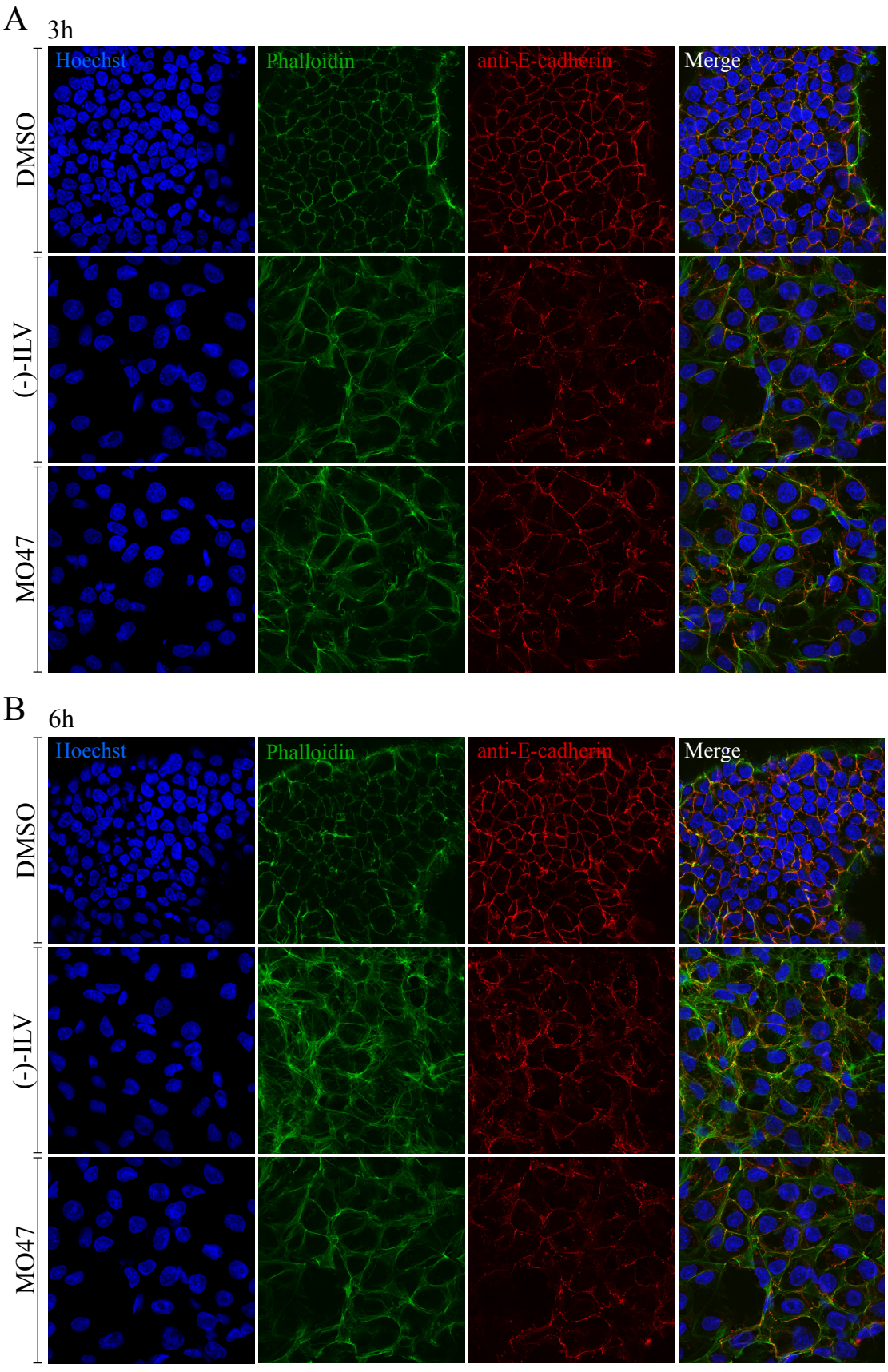
A
3h
Hoechst
Phalloidin
anti-E-cadherin
Merge
DMSO
(-)-ILV
MO47
B
6h
Hoechst
Phalloidin
anti-E-cadherin
Merge
DMSO
(-)-ILV
MO47

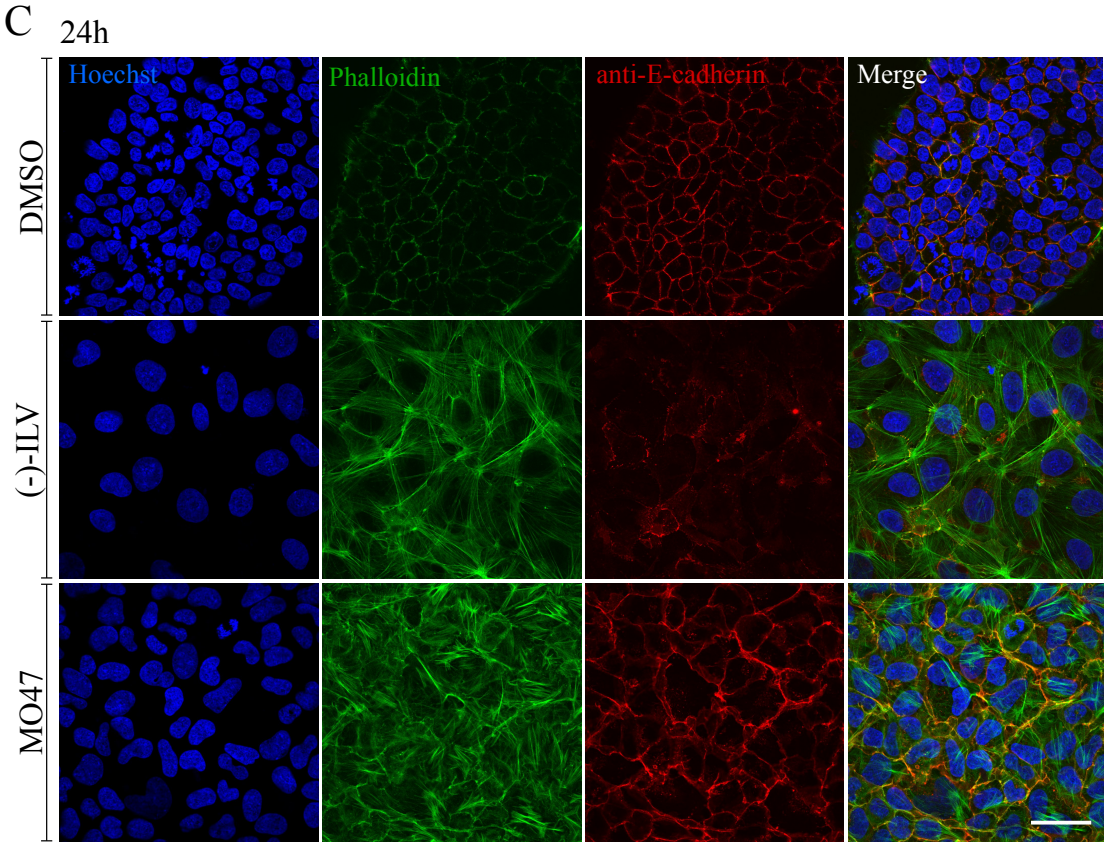

Figure 3.5 | Time course treatment with (-)-Indolactam V and MO47.
iPSCs were plated onto a µ-slide and treated with 1µM (-)-Indolactam V (middle panel) or MO47 (lower panel) for 3h **(A)**, 6h **(B)** and 24h **(C)**. All conditions were stained with Hoechst, Phalloidin-iFluor 488 and anti-E-cadherin mAb for confocal microscopy. In all three conditions, the nuclei in the treated conditions appear less dense and the E-cadherin signal is reorganised. Control conditions are marked by an actin fence surrounding the colonies, whereas treatment with (-)-Indolactam V and MO47 induces a progressive increase of actin stress fibres and colony disruption. Confocal microscopy; magnification = 600×; scale bar = 100µm.

3.6 Determining area, perimeter and height of the cell nuclei upon treatment

As treatment with (-)-Indolactam V and MO47 induced membrane blebbing and spreading, we hypothesised that the remodelling processes of the cytoskeleton induced a flatter phenotype with nuclei that were larger in area but smaller in height.

To determine the area, the perimeter and the height of the nuclei (as surrogate for the cytoplasm), iPSCs were plated at a density of 1×10^5 cells on a μ-slide. On the following day, cells were treated with DMSO (0.1%), 1 μM (-)-Indolactam V and 1 μM MO47 for 24h, fixed and stained with Hoechst (blue) for confocal microscopy. To determine the area and the perimeter of the nuclei, three images of different locations in each condition were taken. The images were further taken in planes, in which the nuclei displayed their largest area. For quantification, the images were analysed by the software CellProfiler. To determine the height of the cells, z-stacks were imaged for all three conditions.

Figure 3.6 shows that MO47 treated iPSCs have a significantly (tr) flatter nucleus with a larger mean area (mean±SEM: 243.94±10.01; n=3), larger mean perimeter (mean±SEM: 66.74±2.16; n=3) but smaller mean height (mean±SEM: 2.79±0.22; n=3) than the DMSO control (means±SEM for area, perimeter, height: 138.29±6.09; 52.55±1.38; 7.20±0.43; n=3). These phenotypic changes can also be observed for (-)-Indolactam V (means±SEM for area, perimeter, height: 338.24±58.24; 72.59±5.34; 4.99±0.47; n=3), whereas only the decrease in the height is significant.

In summary, these quantified results are in accordance with the induction of spread, flattened phenotypes upon treatment with (-)-Indolactam V and MO47.

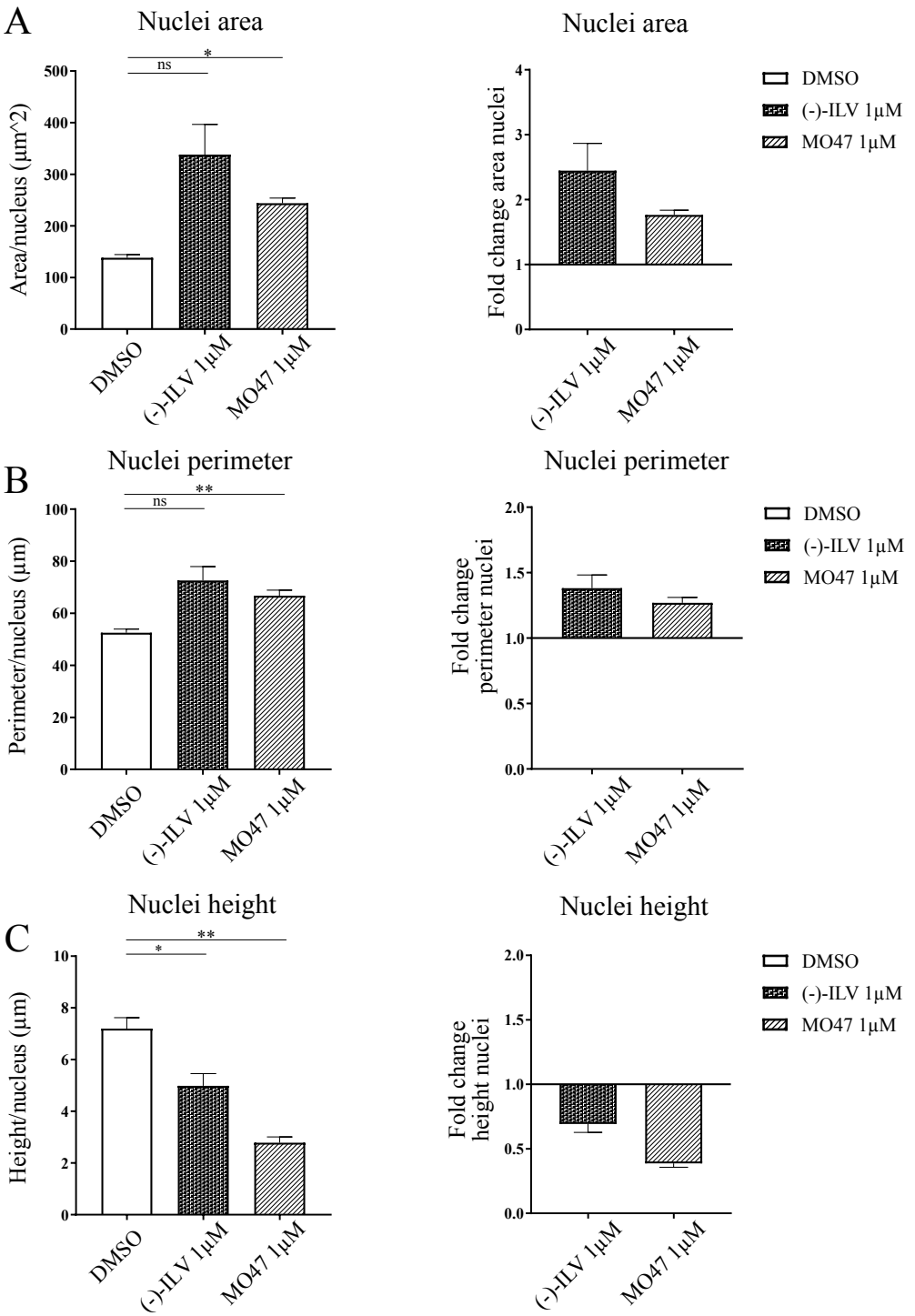

Figure 3.6 | Effects of (-)-ILV and MO47 on nucleus area, perimeter and height.
iPSCs were plated onto a µ-slide, treated with 1 µM (-)-Indolactam V, MO47 or DMSO for 24h, fixed and stained with Hoechst. In all three conditions, the nuclei area, perimeter and height were determined on confocal microscopy images. **(A)** iPSCs treated with MO47 have a significantly (tr) flatter nucleus with a larger area (mean±SEM: 243.94±10.01; n=3), **(B)** larger perimeter (mean±SEM: 66.74±2.16; n=3) and **(C)** smaller height (mean±SEM: 2.79±0.22; n=3). Changes of these properties can also be observed for (-)-Indolactam V (mean±SEM for area, perimeter, height: 338.24±58.24; 72.59±5.34; 4.99±0.47; n=3) but are only significant for the changes in the nucleus height (mean±SEM for area, perimeter, height: 138.29±6.09; 52.55±1.38; 7.20±0.43; n=3). One-way ANOVA, Dunnett's multiple comparisons test; ns ($P > 0.05$), * ($P \leq 0.05$), ** ($P \leq 0.01$), *** ($P \leq 0.001$) and **** ($P \leq 0.0001$).

3.7 Discussion and summary

In this chapter, the induction of morphological phenotypes in iPSCs upon treatment with (-)-Indolactam V and MO47 was assessed in 2D culturing. We hypothesised that both compounds induced more homogenous morphological phenotypes in 2D, and that these phenotypes could potentially be harnessed for 3D culturing. To evaluate the phenotypic effects, we established 8 criteria, which shall be discussed in the following.

Firstly, as a proof-of-principle study, iPSC morphologies were analysed 3h, 12h and 24h after addition of the compounds (-)-Indolactam V and MO47. Encouragingly, treatment resulted almost immediately in the induction of a new phenotype. Dense colonies with clearly-defined edges were abrogated (criterion 1), which was corroborated by the absence of the colony-typical actin fence in both treated conditions. In contrast to the DMSO condition, which was marked by colonies varying in size and shape, a homogenously spread populations emerged upon 24h treatment with (-)-Indolactam V and MO47 (criterion 2). Importantly, the homogenous distribution of cells was accompanied by a decrease of cell density, which was significant for MO47 but not for (-)-Indolactam V (criterion 3).

The spreading of the cells appeared to be stronger for (-)-Indolactam V; after 3h the colonies were already disrupted, whereas, in the MO47 treated condition, iPSCs exhibited a considerable membrane blebbing at this stage. Moreover, the decrease in cell density was more conspicous for (-)-Indolactam V than for MO47. A plausible explanation for these differences is the strong pro-apoptotic effect of (-)-Indolactam V (IC_{50} = 5μM, Appendix Chapter 1). Thus, impaired proliferation and increased cell death are likely to account for less cells per area in the (-)-Indolactam V treated condition.

Given the emergence of these spread phenotypes, it is conceivable that treatment with (-)-Indolactam V or MO47 could prevent the overcompaction in the centre of the colonies, and enable more uniformity in terms of cell growth. However, it is difficult to base conclusions merely on morphological criteria. Therefore, it remains open whether the compounds would overall reduce the heterogeneity in 2D culture. Notably, it has been shown that the heterogeneity in 2D culture can also be measured through other phenotypic criteria. Importantly, iPSCs at the edge of the colonies have been shown to expression different levels of pluripotency markers compared to the cells in the centre (Chan *et al.*, 2009; Kato *et al.*, 2016). Therefore, it is worth pursuing whether an increased homogeneity in morphology also corresponds to a reduction of heterogeneity in the expression of pluripotency markers.

Small molecules have the unique advantage of enabling temporally defined control and reversibility of phenotypes (Xu *et al.*, 2008). These properties could also be harnessed in this study as removal of the compounds resulted in the restoration of colony-based phenotype (criterion 4). The reversibility of the phenotypic effect is especially important for the application in iPSCs, where the original cell state, after successful scaleup, needs to be restored for further processing. Previous work in our lab (data not shown) indicates that the alternation of induction and reduction of the phenotypic effect could even be repeated for several times, so that compound addition and removal would result in a 'yoyo-like' effect. Moreover, in a pilot project for live cell imaging, the restoration of the colony-based morphology appeared to be slower for (-)-Indolactam V than for MO47 and varied according to the cell density.

The reorganisation of the actin cytoskeleton was another conspicuous element of the phenotypes induced upon treatment with (-)-Indolactam V and MO47 (criterion 5) (Svitkina *et al.*, 1999). The staining with fluorescent-conjugated phalloidin staining

generally presents a robust technique to detect rearrangements of filamentous actin (Knowles *et al.*, 1992; Svitkina *et al.*, 1999). It is likely that the membrane protrusions and the cell spreading were mediated by nascent actin fibres and Arp2/3 complexes. In confocal microscopy, (-)-Indolactam V and MO47 treated iPSCs exhibited a prominent mesh of actin fibres that was linked at one (dorsal stress fibres) or even two ends (ventral stress fibres) to focal adhesions (Naumanen *et al.*, 2008). Interestingly, these branched fibres are generally associated with the formation of lamellipodia and might equally be indicative of increased cell motility (Naumanen *et al.*, 2008). These observations on the confocal images could further be corroborated by a significant increase of phalloidin signal in the treated conditions. A quantification approach via confocal microscopy appeared to be more reliable in our case, since the enzymatic dissociation into single-cells for flow cytometry and other assays would have altered the organisation of filamentous actin. Despite the coherence between the quantified data and the observations on the images, it is difficult to reach a conclusion on the function of these prominent stress fibres. Clearly, the generation of a GFP-actin cell line for live cell imaging would allow to understand the remodelling dynamics of the actin cytoskeleton better.

The results in this chapter further underscored the remarkable plasticity of iPSCs. Upon treatment, the epithelial-like morphology of iPSCs was completely altered (criterion 6), and a significant flattening of the nuclei, a loss of the cylindrical form, cell spreading and a conspicuous remodelling of the cytoskeleton was induced. For MO47, E-cadherin remained locally concentrated on the cell membrane. In contrast, for (-)-Indolactam V, the E-cadherin signal became increasingly blurred, suggesting that the cell-surface protein was dispersed rather than locally concentrated in this phenotype. These morphological rearrangements remind of the morphological process observed during epithelial-mesenchymal transition (EMT) (Hay, 1995; Lamouille *et al.*, 2014; Moreno-

Bueno *et al.*, 2009). Intriguingly, EMT has been shown to promote motility via the dissociation of compact tissues into single cells; increased motility and disruption of cell-cell adhesion through loss of E-cadherin also play a pivotal role in ESCs during early development (Eastham *et al.*, 2007; Lamouille *et al.*, 2014). Clearly, despite these morphological similarities, EMT is a highly complex process and draws upon a plethora of regulatory processes, including the upregulation of mesenchymal as well as the downregulation of epithelial gene signatures (Lamouille *et al.*, 2014; Moreno-Bueno *et al.*, 2009). The work described in this chapter is mainly based on morphological observations. Thus, the notion of a chemically induced EMT-like process is not sufficiently characterised here, but the analysis of characteristic gene signatures deserves further attention.

Finally, the induction of contact-independence cannot be confirmed since focal adhesions were still present in both conditions (criterion 7). A further assay to test the potential of (-)-Indolactam V and MO47 for their application in disrupting cell-cell adhesion would have been the enzymatic dissociation and subsequent seeding as single cells (criterion 8). The maintenance of single cells is especially crucial for any application in 3D, where cell aggregates constitute a roadblock for more homogenous culturing conditions. This lack of data presents a considerable caveat to this study and is due to unavailability of MO47 that occurred at an early stage of this project, and persisted until the submission of this work.

Furthermore, given the shortages of MO47, the results of this chapter are entirely based on the iPSC line OX1-18. To confirm that the morphological observations are inherent to pluripotent stem cells treated with these compounds and not a feature particular to this single cell line, it will be necessary to extend these studies over multiple lines. Notably, it has been shown that iPSCs cell lines harbour a high degree of genetic heterogeneity

accounting for line-to-line variabilities in epigenome, transcriptome, proteome, and even the cell morphology (Kilpinen *et al.*, 2017; Narsinh *et al.*, 2011).

In summary, (-)-Indolactam V and MO47 induce strong, reproducible and reversible phenotypes in 2D culture. Although the disruption of cell-cell adhesion into a contact-independent iPSC culture cannot be confirmed, both compounds induce colony-disrupted phenotypes with a disc-like morphology and a conspicuous mesh of stress fibres, suggesting increased cell motility. It is intriguing whether this altered phenotype can be harnessed for 2D and 3D culturing. Clearly, the induction of these strong phenotypes gives rise to further studies of the mechanism of action (chapter 4) and the maintenance of pluripotency potential upon treatment (chapter 5).

Chapter 4: Elucidating the mechanisms of action of (-)-Indolactam V and MO47

4.1 Introduction

Small molecules are versatile tools and their properties, which include dose-dependency, ease of use, reversibility and rapid action offer substantial promise for the manipulation of stem cell fate (Davies *et al.*, 2015; Zhang *et al.*, 2012). Notably, their application in research and medicine for controlled stem cell reprogramming, controlling, homing, renewal and conversion has become a powerful strategy for iPSC technology (Davies *et al.*, 2015; Li *et al.*, 2013b; Liu *et al.*, 2016; Zhang *et al.*, 2012).

However, this potential for a variety of different applications also explains why the structural optimisation of small molecules remains key for exquisite specificity (Davies *et al.*, 2015). (-)-Indolactam V, for example, assessed in this study for its potential to induce a beneficial phenotype for 2D and 3D culturing, also presents a useful tool in the differentiation of iPSCs towards the pancreatic lineage (Chen *et al.*, 2009b). This is why the thorough characterisation of small molecules in terms of their mechanism of action (MoA), their promiscuity and their biological *sequellae* is of paramount importance in this context (Arrowsmith *et al.*, 2015; Davies *et al.*, 2015; Frye, 2010; Li *et al.*, 2013a; Workman *et al.*, 2010).

4.1.1 The importance of mechanism of action studies

Mechanism of action studies — as illustrated by the discovery of new core regulatory signalling pathways in the context of Rho-kinase inhibitors — harbour tremendous value for both biological and chemical studies (Bunnage *et al.*, 2015; Watanabe *et al.*, 2007; Xu *et al.*, 2010). While new insights into the intricacies of signalling pathways helps to understand molecular biology better, unravelling the mechanisms of action also provides

chemists with new potential targets for drug discovery (McFedries *et al.*, 2013). Phenotypic screens allow identification of new drug candidates on the cellular context but offer little insight into pharmacological mechanistics (Schenone *et al.*, 2013). Notably, well-characterised mechanisms of action are pivotal to avoid erroneous conclusions in terms of the target-phenotype relationship (Bunnage *et al.*, 2015).

4.1.2 E-cadherin and protein kinase C

In our case, the small molecules (-)-Indolactam V and MO47 were already characterised as PKC activators, and the effects on PKC isoforms were hypothesised to be linked to the induction of a new phenotype (Hirota *et al.*, 1987; Kozikowski, 1994). Since the literature highlights many cases of inadequately or insufficiently characterised chemical probes, the mechanisms of actions of both PKC agonists required further investigation in this project (Arrowsmith *et al.*, 2015; Baell *et al.*, 2014; Workman *et al.*, 2010).

The work in this chapter aims to assess the mechanism of action of (-)-Indolactam V and MO47 as two distinct chemical entities. Based on our chemical screen, we hypothesised that the phenotypic effect was due to a link between PKC and E-cadherin. In addition to these functional signalling pathway studies, we endeavoured to characterise toxicity.

4.2 Investigating protein kinase C

PKC encompasses a group of signal-transducing molecules that act at the crossroad of many signalling pathways (Steinberg, 2008). Despite their structural similarities, PKC isoforms are a heterogeneous group of molecules, varying in function and effector affinity (Dempsey *et al.*, 2000; Steinberg, 2008). Indeed, differences in the structural properties of (-)-Indolactam V and MO47 have shown to govern their isoform specificity; while (-)-Indolactam V displays little if any PKC specificity, MO47 exhibits a higher affinity to cPKCs (Kozikowski *et al.*, 1995). Thus, it is of paramount importance to investigate PKC activators for all PKC isoforms.

4.2.1 Protein kinase C is expressed in iPSC OX-1-18

In addition to functional differences, PKCs have been shown to exhibit tissue-specific expression (Dempsey *et al.*, 2000; Qvit *et al.*, 2014; Steinberg, 2008). We hypothesised that the tissue-specific expression of PKC isoforms in iPSCs would also account for tissue-to-tissue variability in the mechanism of action.

To determine the expression of PKCs in iPSCs, we chose a suitable reference gene for stringent normalisation (endogenous control), the transcription factor TATA box-binding protein TBP (Kim *et al.*, 2004; Zhang *et al.*, 2005) (Appendix Chapter 4). This nuclear marker promised to be more robust than a cytoplasmic endogenous control, since treatment with (-)-Indolactam V and MO47 altered cytoskeletal organisation. Next, we validated the primer efficiency of PKC isoform primers adopted from Awadelkarim *et al.* (2012) (Appendix Chapter 4).

Subsequently, iPSCs were treated for 72h with 1μM (-)-Indolactam V or MO47 and mRNA levels were determined using qRT-PCR. Figure 4.1 shows the mean relative expression level ± SEM of conventional, novel and atypical PKC isoforms normalised to the endogenous control TBP in untreated and treated iPSCs. PKC δ, ι and ζ are more highly expressed than other isoforms. There is a significant difference in the expression of PKC γ (**), PKC δ (*), PKC η (*), PKC θ (***) between (-)-Indolactam V treated and untreated conditions.

In summary, these data indicate that conventional (α, β, and γ), novel (δ, ε, η and θ) and atypical (ι and ζ) PKC isoforms are expressed in the iPSC line OX1-18 and that this expression is not significantly altered upon treatment with MO47 for 72h.

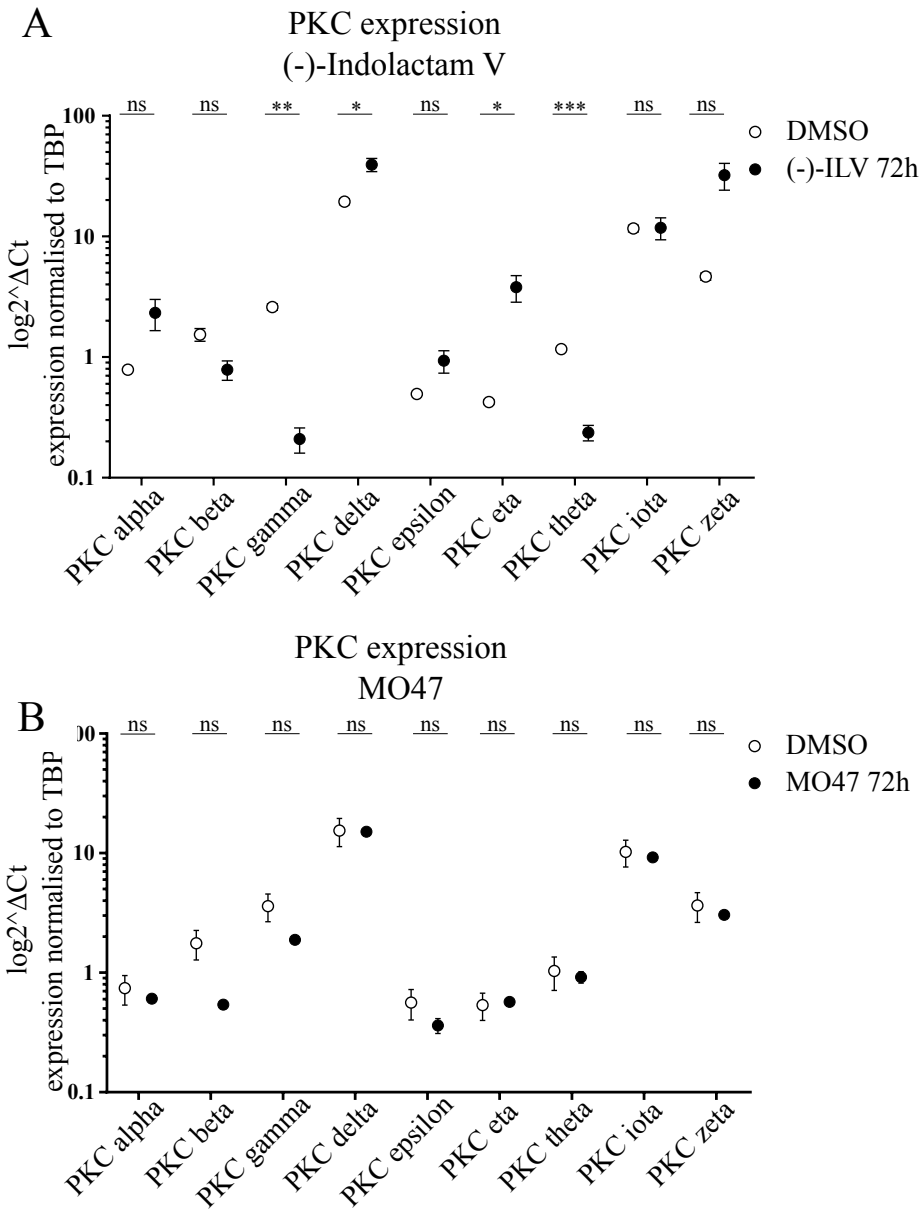

Figure 4.1 | PKC isoforms are expressed in the iPSC line OX-18 upon treatment with (-)-Indolactam V and MO47.

qRT-PCR was performed to determine the relative expression levels of PKC isoforms normalised to TBP. iPSCs were treated for 72h with (-)-Indolactam V **(A)** or MO47 **(B)**. All PKC isoforms are expressed in treated and untreated samples. There was a significant difference between treated and untreated conditions for PKC gamma (mean±SEM for DMSO and ILV: 2.60±0.16, n=3; 0.21±0.05, n=2), PKC delta (mean±SEM: 19.44±1.08, n=3; 39.37±3.88, n=2), PKC eta (mean±SEM: 0.42±0.02, n=3; 3.80±0.70, n=2) and theta (mean±SEM: 1.17±0.03, n=3; 0.24±0.03; n=2) in iPSCs treated with (-)-Indolactam V.

Symbols represent the mean relative expression ± SEM (br) normalised to the endogenous control TBP. For (-)-Indolactam V, the mean±SEM is composed of two samples as one sample was excluded due to insufficient mRNA yields. In case of very small SEMs, the error bars are not displayed. Two-tailed t test, ns ($P > 0.05$), * ($P \leq 0.05$), ** ($P \leq 0.01$), *** ($P \leq 0.001$) and **** ($P \leq 0.0001$).

4.2.2 Combined treatment of PKC activatiors and PKC inhibitors

Given the heterogeneity within the PKC family, elucidating isoform-specific mechanism of action requires the application of isozyme-specific pharmacological and genetic tools (Mochly-Rosen *et al.*, 2012). Importantly, the failure of many therapeutic approaches in the context of PKC has underscored the importance of identifiying isoform-specific downstream signalling (Dowling *et al.*, 2015; Mochly-Rosen *et al.*, 2012).

Having confirmed the expression of PKCs in our model, we concluded that the induced morphological changes could, in theory, be mediated by any of these expressed isoforms. We hypothesised that combining PKC activators with specific inhibitors of PKC isoforms could elucidate the relevance of these isoforms for the phenotypic effect.

The indolocarbazoles Gö6976 and the bisindolylmaleimide Gö6983 belong to the family of PKC inhibitors and have been shown to inhibit PKC isoforms at nanomolar concentrations (Martiny-Baron *et al.*, 1993; Wu-Zhang *et al.*, 2013). While Gö6976 has been reported to be a specific inhibitor of the conventional PKC isoforms α and β, Gö6983 acts as pan-PKC inhibitor with more affinity for conventional and novel isoforms compared with atypical isoforms (Martiny-Baron *et al.*, 1993; Wu-Zhang *et al.*, 2013).

To test the potential disruption of the morphological phenotype upon treatment with one of these inhibitors, iPSCs were plated at a density of 1×10^5 cells/well onto a 24-well plate and subjected to combinatorial treatment with varying concentrations of (-)-Indolactam V (1.0 and 0.5μM) and Gö6976 or Gö6983 (1.0, 2.5 and 5μM).

Figure 4.2 shows the matrices for combinatorial treatment with (-)-Indolactam V and the two Gö inhibitors. The cPKC inhibitor Go6976 had no effect on (-)-Indolactam V-induced morphology. In contrast, treatment with Gö6983 at 1.0, 2.5 and 5μM disrupts the phenotypic effect of (-)-Indolactam V. In the absence of the inhibitors, the spread

phenotypic effect as described in chapter 3 is characteristic (positive control). At 2.5 and 5.0μM of Gö6976 appears to have major adverse effects on the viability of iPSCs.

Overall, these data suggest that the phenotypic effect of (-)-Indolactam V on iPSCs can be disrupted by the pan-PKC inhibitor Gö6983, whilst inhibition of PKC α and β through Gö6976 shows no effect on the spread phenotype.

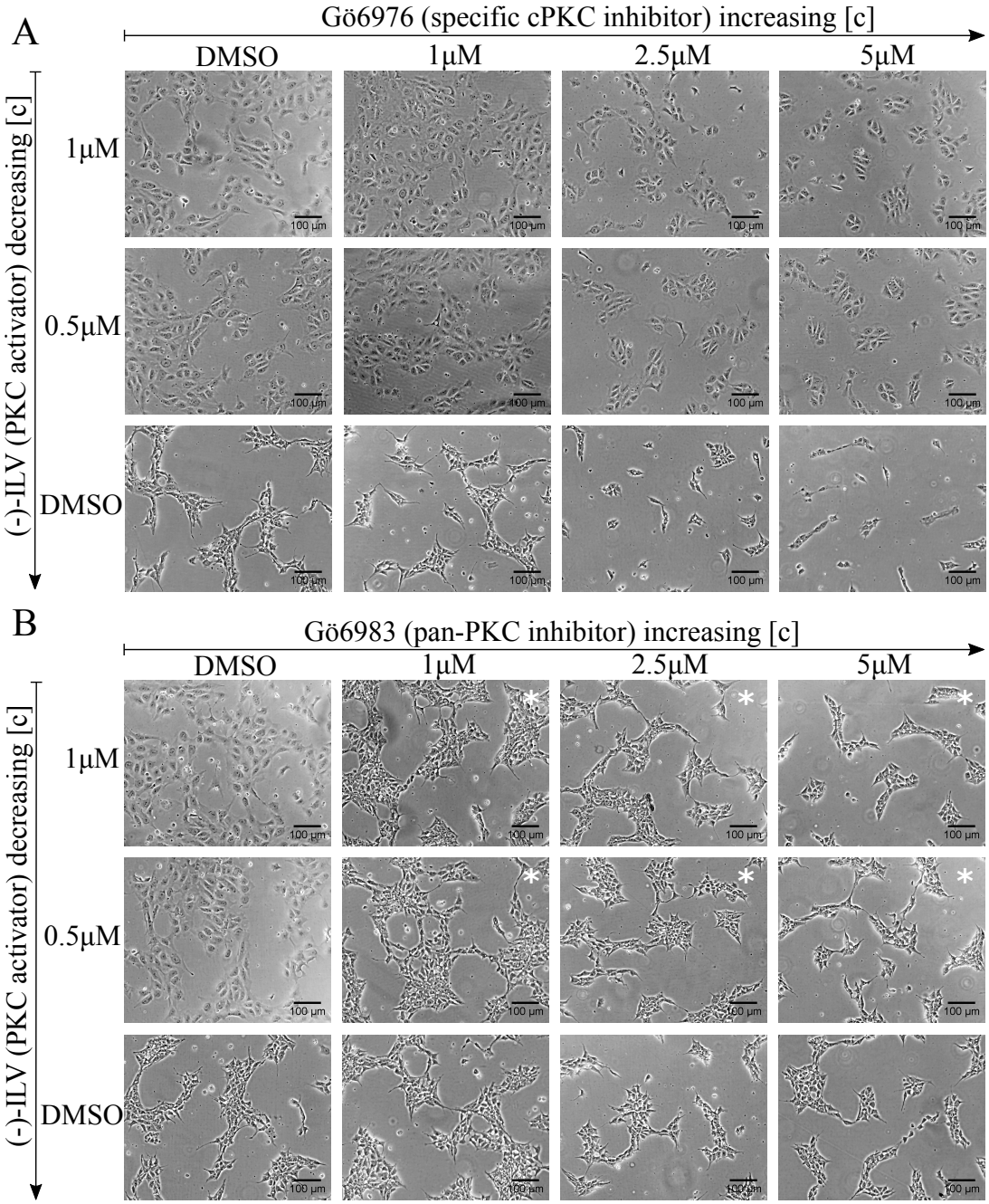

Figure 4.2 | Combinatorial treatment of (-)-Indolactam V and the PKC inhibitors Gö6976 and Gö6983.

iPSCs were treated with the PKC activator (-)-Indolactam V (0.5 and 1.0µM) and the PKC inhibitors Gö6976 **(A)** or Gö6983 **(B)** at different concentrations (1.0, 2.5 and 5.0µM) at the same time. Different phenotypes are displayed in matrices for both inhibitors. Conditions in which the phenotype is disrupted in presence of the PKC activators and the PKC inhibitors are marked with a white asterisk. iPSCs treated with (-)-Indolactam V exhibit a spread phenotype (positive control). In absence of both compounds (DMSO), iPSCs are characterised by their typical elongated form due to Rho-kinase inhibitor (negative control). Phase contrast, magnification = 100×, scale bars = 100µm.

We decided to further explore whether the combinatorial treatment of Gö6976 and Gö6983 with MO47 and (-)-Indolactan V would have similar effects and whether the induced morphological changes could also be disrupted when they had previously been induced for 24h. Therefore, iPSCs were plated at a density of 1×10^5 cells/well onto a 24-well plate and treated with 1μM (-)-Indolactam V or 1μM MO47 for 24h. The following day, the medium was changed and treatment at 1μM continued either in a combinatorial approach with the PKC inhibitors Gö6976 and Gö6983 (both 1μM) or with the PKC activators alone.

Figure 4.3 A shows the co-treatment of (-)-Indolactam V with Gö6976 and Gö6983, and confirms the phenotypes observed in Figure 4.2. The phenotypic effect is also abrogated, when combinatorial treatment is performed with Gö6983 and MO47 (Figure 4.3 B).

In summary, these data show that the phenotypic effects of (-)-Indolactam V and MO47 can be disrupted by combined treatment with the pan-PKC inhibitor Gö6983 even if the morphological phenotype has previously been induced for 24h.

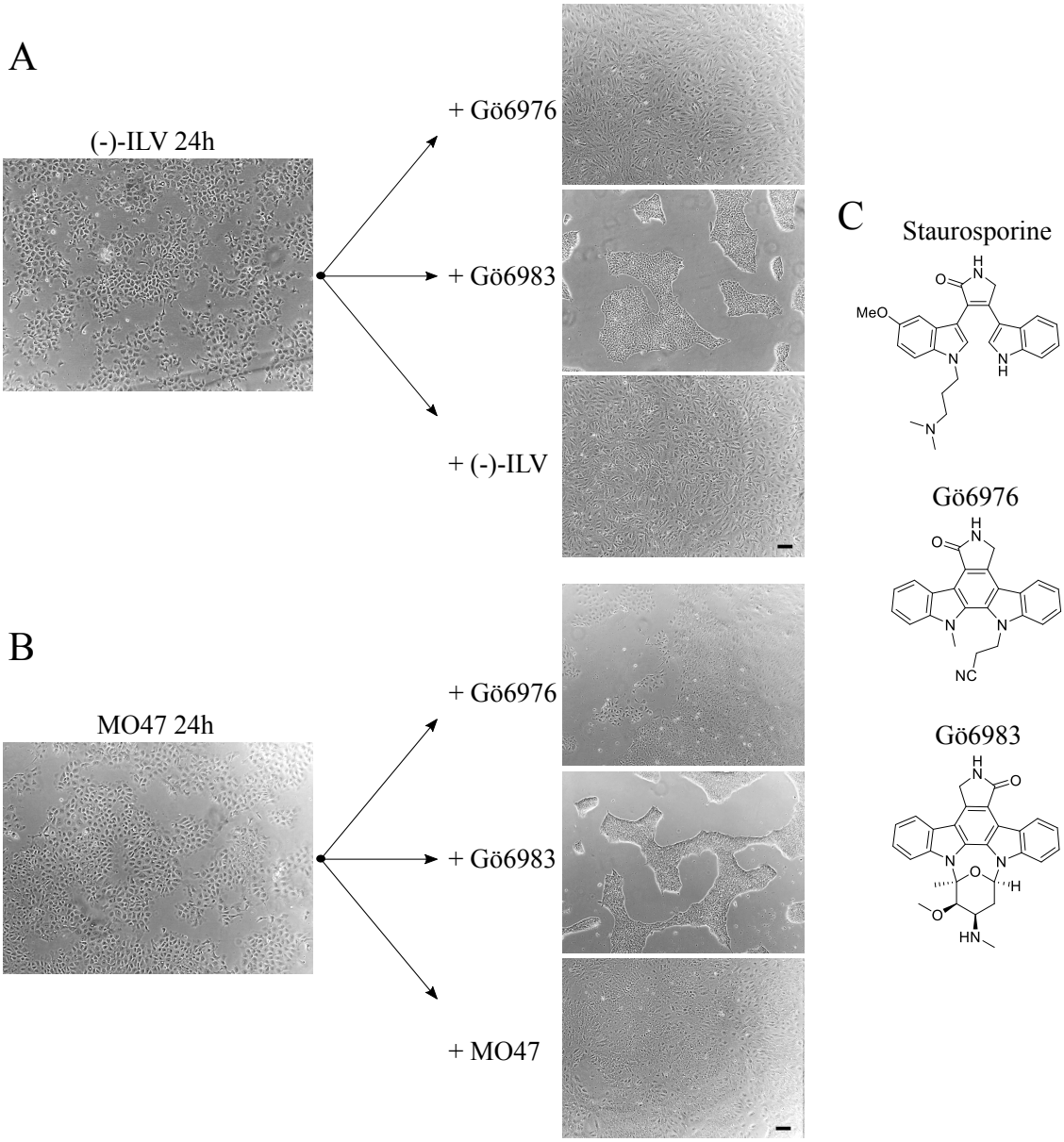

Figure 4.3 | Combinatorial treatment of (-)-Indolactam V and MO47 with the PKC inhibitors Gö6976 and Gö6983.

iPSCs were treated with the 1µM of the PKC activators (-)-Indolactam V **(A)** and MO47 **(B)**. After 24h, the medium was changed and the treatment was continued either in a combinatorial approach with the PKC inhibitors Gö6976 and Gö6783 (both 1µM) or with the PKC activators alone (positive control). iPSCs treated with PKC activators ((-)-Indolactam V, MO47) and the PKC inhibitor Gö6983 display a colony-based morphology. Co-treatment with Gö6976 does not abrogate the spread phenotype. Phase contrast; magnification = 100×; scale bars = 100µm. **(C)** Chemical structures of sterosporine, Gö6976 and Gö6983.

4.3 Investigating E-cadherin

Conventional and novel PKC isoforms play pivotal roles in the regulation and mediation of cell-cell adhesion and motility (Anilkumar, 2003; Igumenova, 2015; Mochly-Rosen, 1995). Notably, PKCs are involved in the remodelling of the actin cytoskeleton (Anilkumar, 2003), general membrane trafficking of surface proteins (Alvi *et al.*, 2007) and in the endocytosis and the recycling of E-cadherin (Alvi *et al.*, 2007; Kitajima *et al.*, 1999; Kyuno *et al.*, 2013). Moreover, PKCδ was reported to be involved in suppressive effects on E-cadherin, thereby inducing an epithelial-mesenchymal transition-lile process and a scattered phenotype (Chen *et al.*, 2009a). Intriguingly, treatment with the two PKC activators (-)-Indolactam V and MO47 resulted in a spread, flattened phenotype, which was accompanied by a rearrangement of E-cadherin on the cell membrane.

Given the spread morphology upon treatment with (-)-Indolactam V and MO47, we hypothesised that these phenotypic changes might be due to changes in the organisation of focal adhesions mediated by E-cadherin. To examine whether the induced phenotypes correlated with changes in the E-cadherin expression, we explored three scenarios: (1) The loss of E-cadherin from the membrane due to endocytosis and potential recycling, (2) an increase of E-cadherin shedding and (3) the preservation of E-cadherin on the cell membrane.

4.3.1 Assessing endocytosis and recycling of E-cadherin

E-cadherin expression on the cell surface is partly regulated by internalisation into the cytoplasm via clathrin-dependent and clathrin-independent mechanisms (Akhtar *et al.*, 2001; Niessen *et al.*, 2011). Upon endocytosis, E-cadherin molecules are processed in a sequence of membrane-associated early endosomes and are eventually either redirected to the membrane, stored in unique compartments or degraded in lysosomes (Ivanov *et al.*, 2004). Lysosomal targeting of E-cadherin — which also occurs during EMT — involves passage through compartments that are rich in the markers Rab5, Rab7 and Lamp1, and their specific inhibition impairs E-cadherin trafficking. (Palacios *et al.*, 2005; van Roy *et al.*, 2008).

Rab5 and Rab7 belong to the Ras superfamily of small GTPases that are involved in clathrin-mediated endocytosis and accompany trafficking from donor to acceptor compartments (Kumari *et al.*, 2010; Simons *et al.*, 1993). While Rab5 is vital for the initiation of early endosomes, Rab 7 is located downstream of Rab5 and mediates the transition from early to late endosomes and can also be found in lysosomes (Bucci *et al.*, 2000; Feng *et al.*, 1995; Simons *et al.*, 1993; Zeigerer *et al.*, 2012). Lysosome-associated membrane protein 1 (Lamp1) is most abundant on lysosomes and encompasses various functions such as transport of degradation products and lysosomal acidification (Saftig *et al.*, 2009).

In contrast, Rab9, Rab10 and Rab11 are involved in retrograde protein trafficking and can therefore be used as markers for recycled E-cadherin. Rab9 acts as a mediator in trafficking of late endosomes and the trans-Golgi machinery (Lombardi *et al.*, 1993). Rab10 is specifically localised at the endoplasmic reticulum and a major regulator of its function (English *et al.*, 2013; Galvez *et al.*, 2012). Rab11 is integral part of the endosome recycling compartment with various functions and is also in the shuttling of cell

membrane proteins back to the plasma membrane (Grosshans *et al.*, 2006; Kelly *et al.*, 2012).

Given the localisation of Rabs and Lamp1 in different compartments of the endosomal degradation and recycling pathway, they are ideally suited to track the fate of endocytosed proteins. We hypothesised that the localisation of internalised E-cadherin and endocytosis or recycling markers could determine the fate of internalised E-cadherin.

To this end, iPSCs were plated at a density of 1×10^5 cells/well onto an μ-slide and treated the following day with 1μM (-)-Indolactam V and MO47 for 24h. Subsequently, iPSCs were fixed, permeabilised and stained with Hoechst, anti-E-cadherin and mAbs against Rab5, Rab7, Lamp1, Rab9, Rab10 and Rab11 followed by secondary Abs. All conditions were imaged using confocal microscopy.

Figure 4.4 shows the confocal images plotted for iPSCs treated with DMSO, (-)-Indolactam V and MO47 in individual and merged channels. Co-localised signal of E-cadherin and endocytosis markers appears yellow in the merged plot. Rab5 and E-cadherin show no co-localisation, but accumulation of intracellular signal (white arrows) in the E-cadherin channel can be identified in iPSCs treated with MO47 (Figure 4.4A). Rab7 signal appears to follow a similar trend and only partially co-localises with E-cadherin in iPSCs treated with MO47 (Figure 4.4B). For Lamp1, partial co-localisation of the signals can be observed in all three conditions but does not seem to follow a clear pattern. Moreover, Lamp1 binds to the actin cytoskeleton in iPSCs treated with (-)-Indolactam V, suggesting increased trafficking along the actin cytoskeleton.

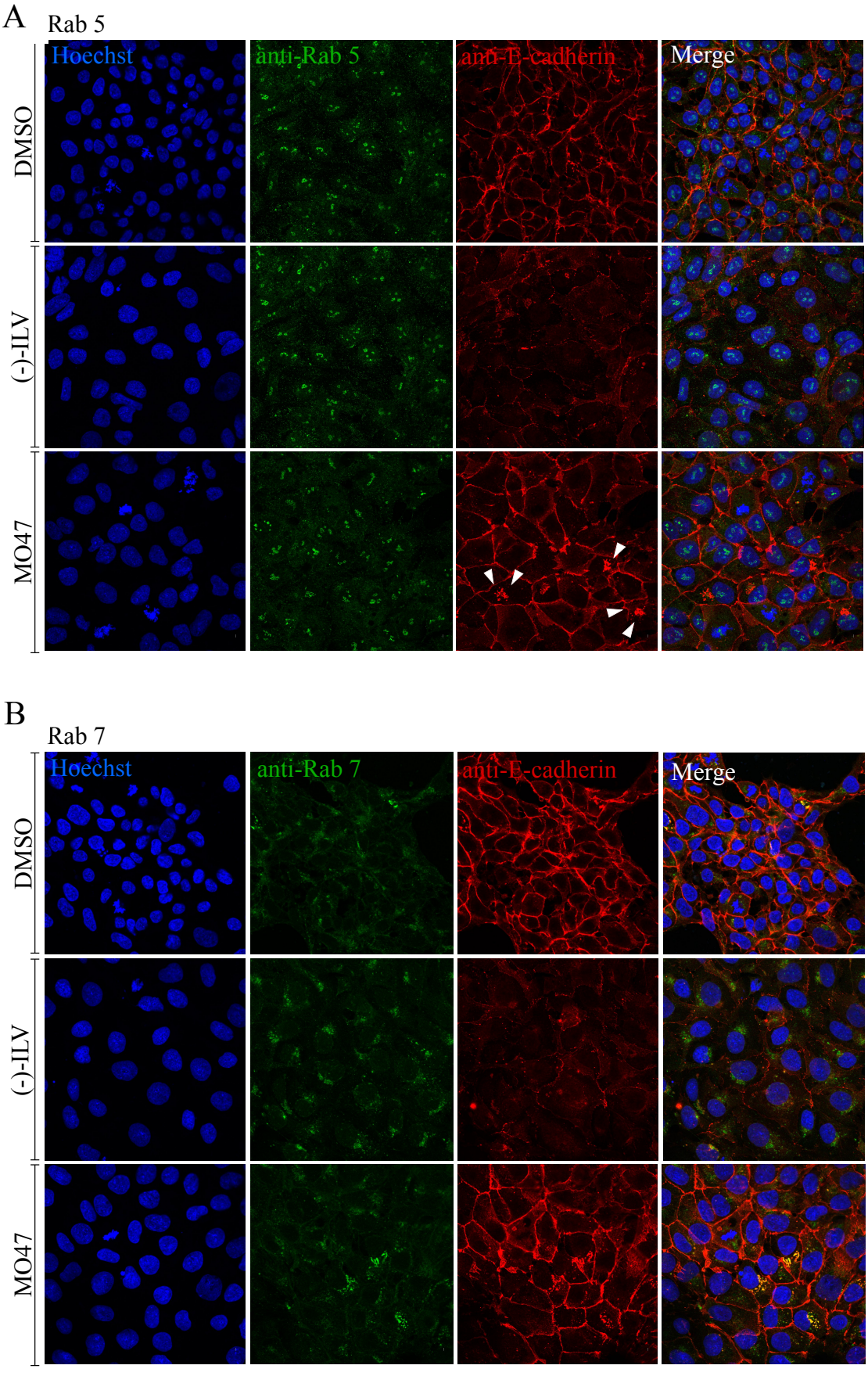
A
Rab 5
Hoechst
anti-Rab 5
anti-E-cadherin
Merge
DMSO
(-)-ILV
MO47
B
Rab 7
Hoechst
anti-Rab 7
anti-E-cadherin
Merge
DMSO
(-)-ILV
MO47

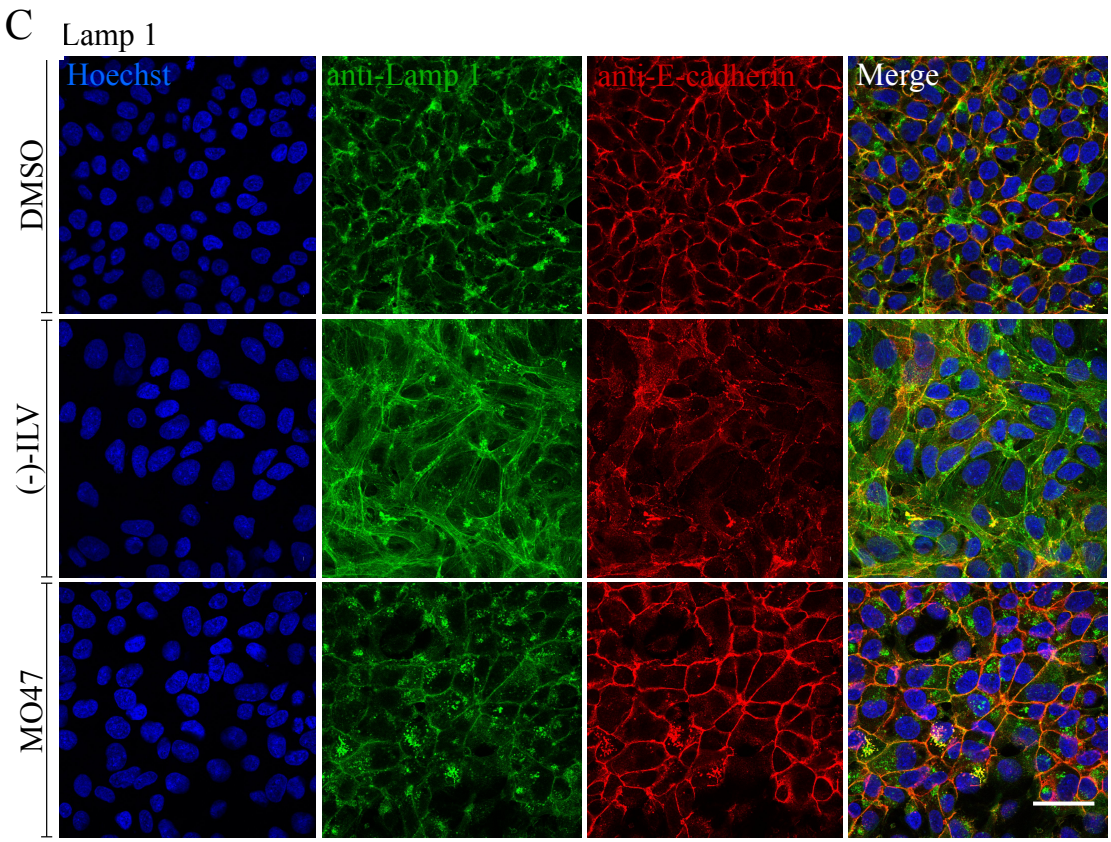

Figure 4.4 | Assessing the co-localisation of internalised E-cadherin and the endocytosis markers Rab5, Rab7 and Lamp1.

After treatment with 1µM (-)-Indolactam V and MO47 for 24h, iPSCs were fixed, permeabilised and stained with Hoechst, anti-E-cadherin mAb and mAbs against the endocytosis markers Rab5 (**A**), Rab7 **(B)** and Lamp1 **(C)**. Subsequently, all conditions were imaged using confocal microscopy. Different channels are plotted individually (Hoechst (blue), endocytosis markers (green), E-cadherin (red)) or in a combined plot (merge). Co-localising signals of E-cadherin and endocytosis markers appear yellow in the merged plot. White arrows indicate intracellular E-cadherin signal. Confocal microscopy; magnification = 600×; scale bar = 50µm.

Figure 4.5 displays iPSCs treated with the same conditions, but confocal microscopy was performed after immunohistochemistry with mAbs against Rab9 (A), Rab10 (B) and Rab11 (C). Neither of the three markers appears to co-localise in a coherent pattern with E-cadherin (yellow signal). For staining with anti-Rab9 mAb, almost no signal can be identified in all three conditions. The same trend appears to apply for Rab10, except for non-specific signal in the DMSO control. For Rab11, the signal appears to be stronger for DMSO than for (-)-Indolactam V and MO47 treated iPSCs but the degree of co-localisation of both signals is poor.

Overall, these data indicate that E-cadherin does not clearly accumulate in the cytoplasm nor consistently co-localises with endocytosis and recycling makers upon treatment with (-)-Indolactam V and MO47.

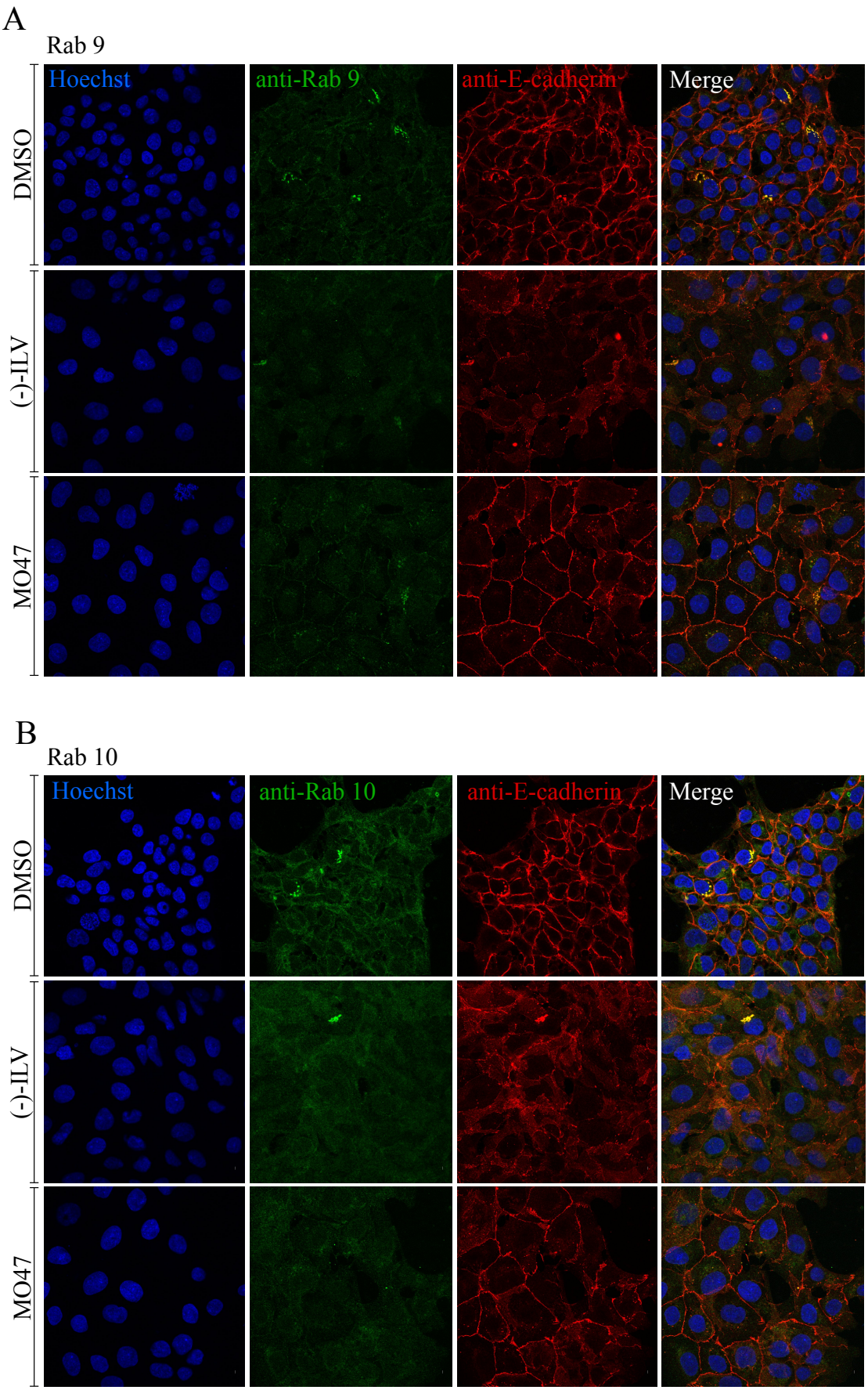
A
Rab 9
Hoechst
anti-Rab 9
anti-E-cadherin
Merge
DMSO
(-)-ILV
MO47
B
Rab 10
Hoechst
anti-Rab 10
anti-E-cadherin
Merge
DMSO
(-)-ILV
MO47

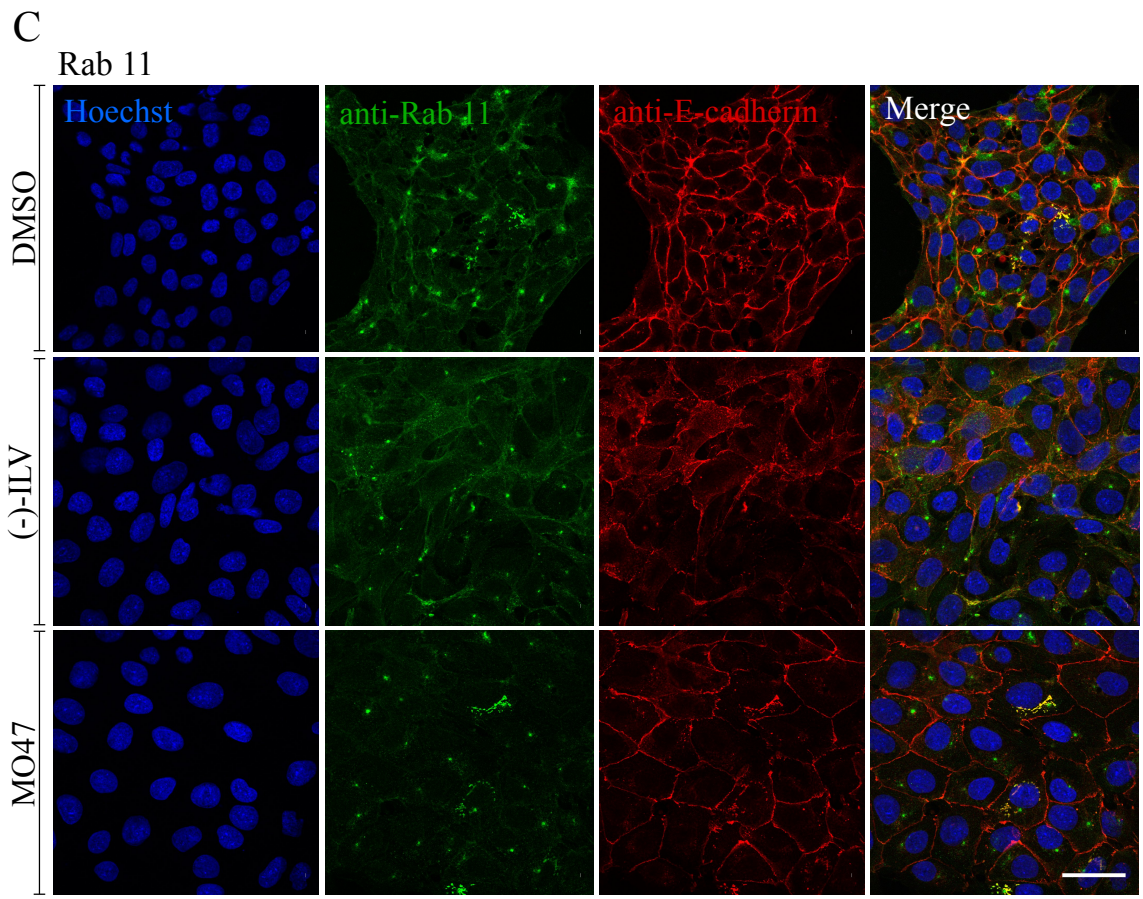

Figure 4.5 | Assessing the co-localisation of internalised E-cadherin and the recycling markers Rab9, Rab10 and Rab11.

After treatment with 1µM (-)-Indolactam V and MO47 for 24h, iPSCs were fixed, permeabilised and stained with Hoechst, anti-E-cadherin mAb and mAbs against the recycling markers Rab 9 (**A**) and Rab10 **(B)** and Rab11 **(C)**. Subsequently, the three conditions DMSO (control), (-)-Indolactam V and MO47 were imaged with confocal microscopy. Different channels are plotted individually (Hoechst (blue), recycling markers (green), E-cadherin (red)) or in a combined plot (merge). Co-localising signals of E-cadherin and endocytosis markers appear yellow in the merged plot. Confocal microscopy, magnification = 600×, scale bar = 50µm.

4.3.2 Assessing E-cadherin shedding

Since no endocytosis or recycling marker consistently co-localised with intracellular E-cadherin upon treatment with (-)-Indolactam V and MO47, ectodomain cleavage of E-cadherin was explored.

In addition to endocytosis, the tightly-regulated expression of E-cadherin is also mediated by E-cadherin cleavage, and can be observed in iPSCs (Rosner *et al.*, 2016; van Roy *et al.*, 2008). Notably, E-cadherin cleavage occurs during apoptosis, cell-cell dissociation, calcium dyshomeostasis and upon treatment with tumor-promoting stimuli (Niessen *et al.*, 2011; Steinhusen *et al.*, 2001; van Roy *et al.*, 2008). Cleavage of the E-cadherin molecule can either be mediated by a PS1/g-secretase at the endodomain or by metalloproteinases (MMPs) at the membrane-ectodomain interface (van Roy *et al.*, 2008). The most prominent MMP in this context is ADAM10, a transmembrane protease that is highly expressed in epithelial tissues (Maretzky *et al.*, 2005).

We hypothesised that potential cleavage of E-cadherin mediated by MPPs would increase the amount of shed E-cadherin in the supernatant, which could subsequently be detected using ELISA. To test E-cadherin shedding effects, iPSCs were plated at a density of 2×10^6 cells/well onto a 6-well plate, and treated the following day with 1μM (-)-Indolactam V and MO47 for 24h. Subsequently, the supernatant was analysed in technical triplicates using ELISA. Absolute values for E-cadherin were obtained by normalisation to a standard curve.

Treatment with (-)-Indolactam V shows a significant increase (tr) in the amount of soluble E-cadherin in the supernatant. The increase of soluble E-cadherin in the supernatant of iPSCs treated with MO47 is not significant.

In summary, these data indicate that treatment with (-)-Indolactam V results in increased amounts of soluble E-cadherin in the supernatant.

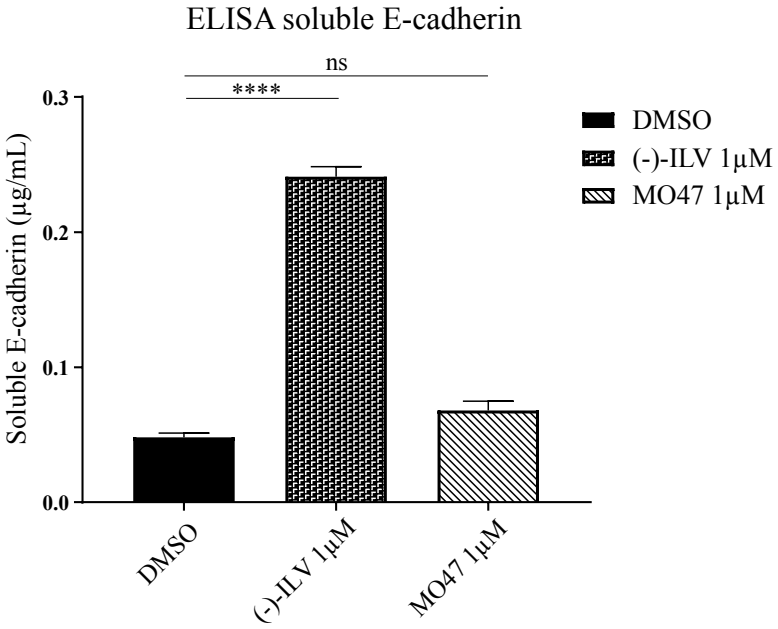

Figure 4.6 | Analysing soluble E-cadherin in the supernatant of iPSCs upon treatment with (-)-Indolactam V and MO47.

iPSCs were treated with 1µM (-)-Indolactam V and MO47 for 24h and the supernatant of each condition was analysed using ELISA. Absolute values for soluble E-cadherin in the supernatant were obtained by normalisation to a standard curve. The amount of soluble E-cadherin in the supernatant of (-)-Indolactam V treated iPSCs (mean±SEM: 0.2410±0.0075; n=3) is significantly (tr) higher than in the supernatant of the DMSO control (mean±SEM: 0.0481±0.0031; n=3), whereas for MO47 (mean±SEM: 0.0680±0.0067; n=3) the increase of soluble E-cadherin is not significant. One-way ANOVA, Dunnett's multiple comparisons test, ns ($P > 0.05$), * ($P \leq 0.05$), ** ($P \leq 0.01$), *** ($P \leq 0.001$) and **** ($P \leq 0.0001$).

4.3.3 Assessing the expression of cell surface E-cadherin

Finally, the third scenario was explored: the preservation of E-cadherin on the cell surface. Expression levels of E-cadherin in (-)-Indolactam V and MO47 treated iPSCs were analysed using flow cytometry.

To this end, iPSCs were plated at a density of 1×10^5 cells/well onto a 24-well plate, treated for 3h,12h and 24h with 1μM (-)-Indolactam V and harvested simultaneously. Live cell staining was performed using anti-E-cadherin mAb followed by incubation with a secondary Ab and flow cytometry.

Figure 4.7 B shows the expression of cell surface E-cadherin for each condition. In the control conditon, E-cadherin is clearly expressed and is characterised by a clear signal shift compared to the technical control (secondary Ab only). The signal for E-cadherin in the (-)-Indolactam V treated conditions is as high as for the DMSO control, or even higher for 12h and 24h treatment. Phase contrast images confirm phenotypic changes in all treated conditions (Figure 4.7 A).

Taken together, these data suggest that E-cadherin is preserved on the cell surface of iPSCs upon treatment with (-)-Indolactam V.

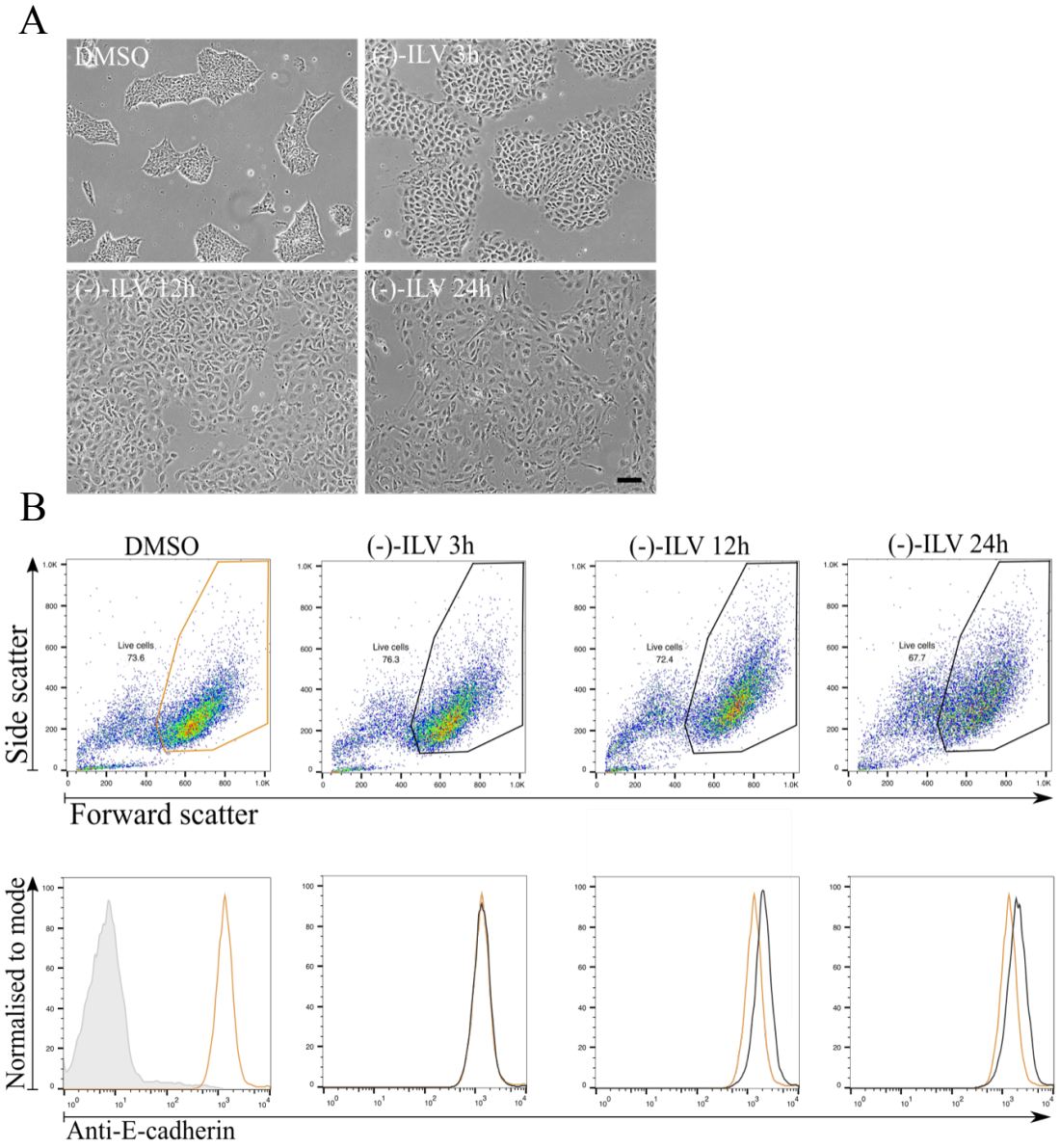

Figure 4.7 | Analysing the expression of cell surface E-cadherin upon treatment with (-)-Indolactam V using flow cytometry.

iPSCs were treated with 1μM (-)-Indolactam V for 3h, 12h and 24h and imaged before harvesting. **(A)** The phenotypic effect can be observed in all treated conditions. Phase contrast, magnification = 100×, scale bar = 100μm. **(B)** For flow cytometry, live iPSCs were stained with anti-E-cadherin mAb followed by a secondary antibody. **(B, upper panel)** The same gate to select for live cells was applied to each condition. **(B, lower panel)** The DMSO control (orange histogram) is compared to a technical control (secondary antibody only, shaded grey). Every treated condition (black histograms) is compared to the DMSO control (orange histogram). Treated and untreated iPSCs display similar expression levels of cell surface E-cadherin.

4.4 Assessing cytotoxicity upon treatment with (-)-Indolactam V

Previous work in our laboratory suggested that MO47 conferred an advantage over (-)-Indolactam V via its reduced cytotoxicity in iPSCs. Notably, as shown in Figure 4.7 B, upper panel, (-)-Indolactam V treatment shifts iPSCs towards a heterogeneous population with decreased size. A potential explanation for the emergence of this second population, especially visible at 24h, is the induction of pro-apoptotic effects of (-)-Indolactam V. We hypothesised that these adverse effects on cell viability could be best characterised by generating a growth curve and performing an Annexin-V-PI assay with treated iPSCs.[4]

Annexin-V is a cellular protein and displays a strong affinity to phosphatidylserine (PS) (Logue *et al.*, 2009). In healthy cells, PS is constitutively translocated to the inner leaflet of the cell membrane via translocases and scramblases (Logue *et al.*, 2009; Martin *et al.*, 1995). In apoptotic cells, PS is invariably translocated to the outer leaflet, functioning as early marker of apoptotic cells prior to cell permeabilisation and nuclear condensation (Koopman *et al.*, 1994; Logue *et al.*, 2009). Together with propidium iodide, a dye for permeabilised cells, Annexin-V has become a powerful quantitative approach to assess cell viability.

To test the effect of (-)-Indolactam V on cell viability, iPSCs were plated in triplicates at a density of 1×10^5 cells/well onto a 24-well plate and treated for 24h, 48h and 72h with 1μM (-)-Indolactam V. Upon collection of all conditions, live cell staining with FITC-conjugated Annexin-V and PI was performed, followed by analysis with flow cytometry. For the generation of a growth curve, treatment was continued until 96h.

Figure 4.8 A-D shows the analysis of (-)-Indolactam V treated iPSCs using flow cytometry. The morphological changes are characteristic in all treated conditions (A).

[4] It was originally planned to test (-)-Indolactam V and MO47 together in both assays. Due to shortages of the compound MO47, merely the effects of (-)-Indolactam V could be assessed.

Upon treatment, iPSC populations shift progressively from the quadrant of healthy cells (Q4) to early apoptotic (Q3) and late apoptotic cells (Q2) (Figure 4.8B). The decrease of healthy cells in treated iPSCs is highly significant (br, $p<0.0001$) and the increase in early apoptotic cells is especially prominent at 72h (mean±SEM: 16.57±1.05; n=3) when compared to 48h (mean±SEM: 6.61±0.11; n=3). The growth curve corroborates the progression of cytotoxicity over time (Figure 4.8 E). After 48h the proliferation in treated iPSCs is significantly (br, $p<0.0001$) impaired compared to control conditions

In summary, this data show that treatment with (-)-Indolactam V is dose-dependently toxic over time.

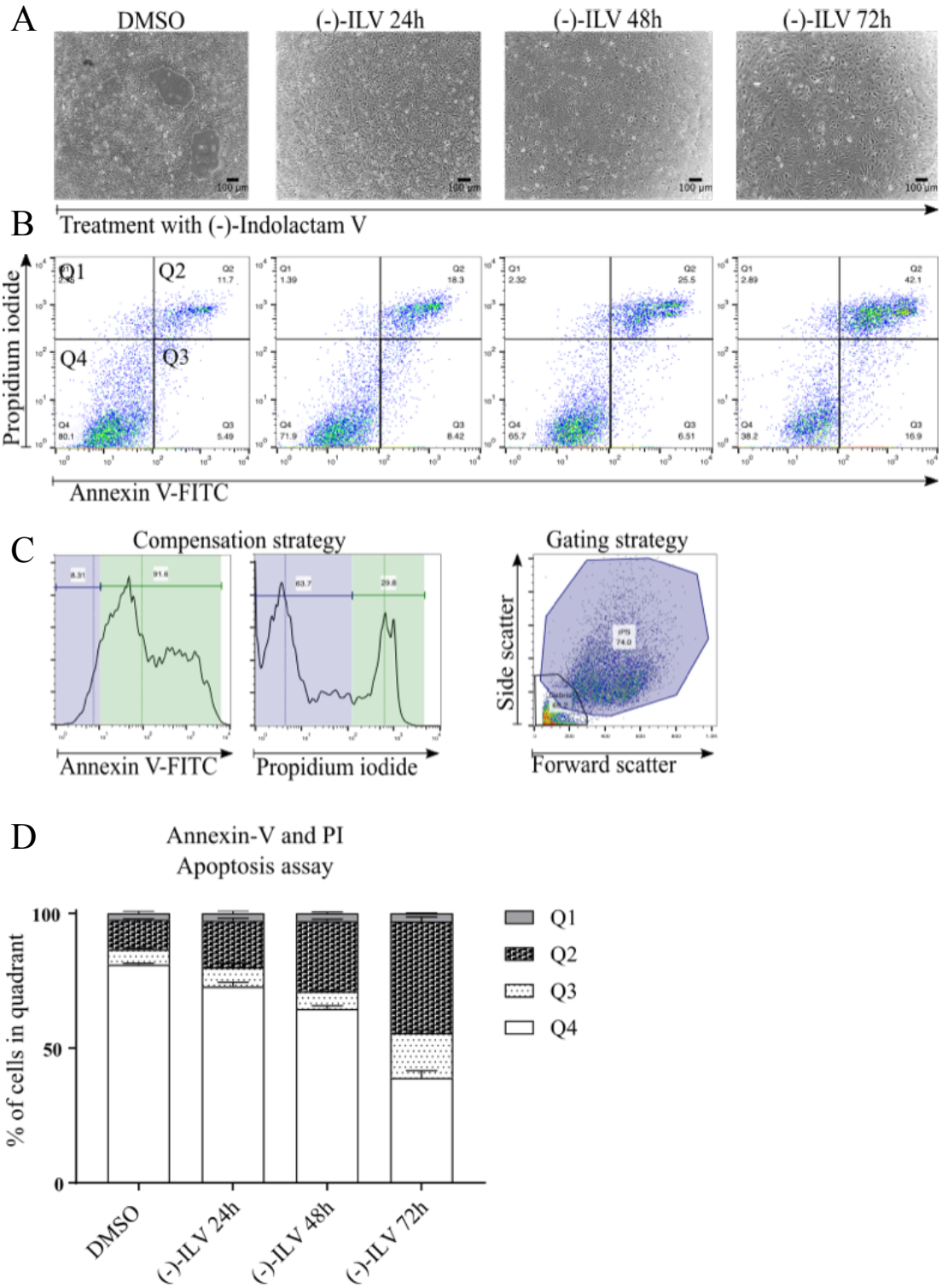
A
DMSO
(-)-ILV 24h
(-)-ILV 48h
(-)-ILV 72h
B
Treatment with (-)-Indolactam V
Propidium iodide
Q1
Q2
Q4
Q3
Annexin V-FITC
C
Compensation strategy
Annexin V-FITC
Propidium iodide
Gating strategy
Side scatter
Forward scatter
D
Annexin-V and PI
Apoptosis assay
% of cells in quadrant
100
50
0
Q1
Q2
Q3
Q4
DMSO
(-)-ILV 24h
(-)-ILV 48h
(-)-ILV 72h

E

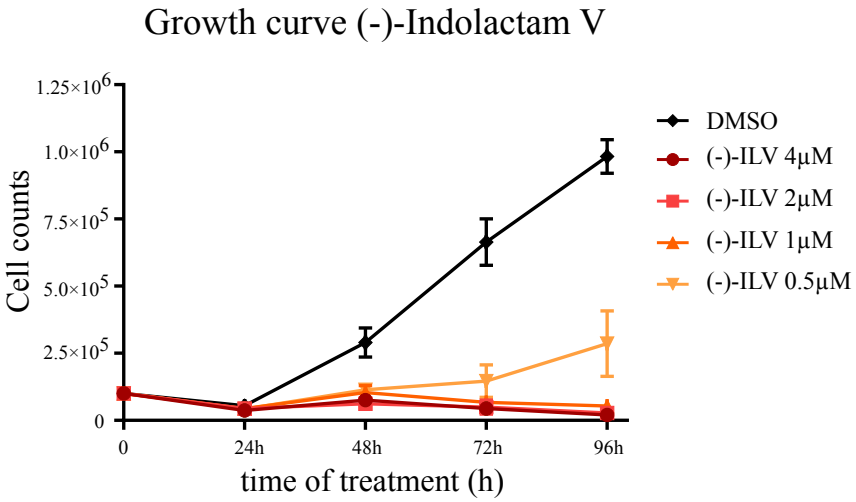

Figure 4.8 | Analysing the cytotoxic effects of (-)-Indolactam V using an Annexin-V-PI assay and a growth curve.

iPSCs were treated with 1µM (-)-Indolactam V for 24h, 48h and 72h (the growth curve was continued until 96h). **(A)** The phenotypic effect can be observed in all treated conditions, with a apparent decrease of cell density at 72h. Phase contrast, magnification = 100×, scale bar = 100µm **(B)** All conditions were stained with Annexin-V and PI and analysed using flow cytometry. Double negative populations (Q4) are healthy, single positive populations for Annexin-V are have entered early apoptosis (Q3), double positive populations have entered late apoptosis and undergo necrosis (Q2). **(C)** Populations in (B) were previously compensated in the PI channel to avoid false positive signals due to spill over from the FITC-Annexin-V channel. During the gating process, debris is excluded. **(D)** The mean percentage ± SEM of each populations in Q1-Q4 is plotted in stacked bars. Each subcolumn represents the mean percentage of cells ± SEM in each of the quadrant gates. All subcolumns together represent the iPSCs in one condition. Mean±SEM for Q1, Q2, Q3 and Q4 for all four conditions: DMSO (2.34±0.89; 11.13±0.30; 5.56±0.45; 80.97±0.47; n=3); (-)-ILV 24h (2.74±0.99; 17.47±0.88; 6.96±1.62; 72.83±1.57; n=3); (-)-ILV 48h (2.82±0.54; 26.07±0.67; 6.61±0.11; 64.50±1.15; n=3); (-)-ILV 72h (2.97±0.09; 41.53±1.67; 16.57±1.05; 38.93±2.68; n=3). Differences in Q1 for all conditions and in Q3 for DMSO, (-)-ILV 24h and (-)-ILV 48h are not significant. All other differences in each quadrant are highly significant (****). Two-way ANOVA; Holm-Sidak's multiple comparison test.

(E) Growth curve of iPSCs treated with (-)-Indolactam V. At each time point, iPSCs were counted in triplicates. Each curve consists of the mean absolute cell number for each count ± SEM. The curves for treated iPSCs are coloured (brighter colours indicate lower concentrations of the compound); the control condition (DMSO) is plotted on a black. Counts for treated iPSCs at 48h and later are significantly (br) lower (****) for all conditions compared to untreated iPSCs (DMSO). No significant differences exist between the counts for all conditions at 0h (plating) and 24h. Two-way ANOVA with multiple comparisons, Dunnett's multiple comparisons test, ns ($P > 0.05$), * ($P \leq 0.05$), ** ($P \leq 0.01$), *** ($P \leq 0.001$) and **** ($P \leq 0.0001$).

4.5 Summary and discussion

The work presented in this chapter aimed to elucidate the mechanisms of action of (-)-Indolactam V and its derivative MO47 as two distinct chemical entities. Taken together, the data do not provide enough evidence to confirm our initial hypothesis whereby the phenotypic effects were due to a link between PKC and E-cadherin. Although chemical inhibition of PKC isoforms with a pan-PKC inhibitor resulted in the disruption of the phenotypes, the role of E-cadherin in the induction of these phenotypes remains unresolved.

In a first step, the role of individual PKC isoforms was investigated. The mRNA expression of all conventional, novel and atypical isoforms could be confirmed for treated and untreated iPSCs, and variations from isoform to isoform were robust in both data sets. Highly expressed PKC isoforms, such as PKCδ, are more likely to be enhanced by non-specific PKC activators. Since (-)-Indolactam V displays less affinity to atypical but similar affinity to conventional and novel isoforms, PKCδ is a potential target for activation by (-)-Indolactam V. Importantly, PKCδ has been shown to mediate major pro-apoptotic effects via caspase-3 (Brodie, 2003; Goerke, 2002; Reyland, 2007; Zhu *et al.*, 2010). Therefore, the enhanced activity of PKCδ by (-)-Indolactam V might explain the induction of strong apoptotic effects. Since MO47 exhibits a higher affinity to cPKCs, differences in isoform specificity might account for differences in cytotoxic effects. Pro-apoptotic effects might also explain the significant differences in the expression of the PKC isoforms γ, δ, θ, η and ε upon treatment with (-)-Indolactam V. Furthermore, the level of mRNA expression of isoforms was not significantly altered upon treatment with MO47. This is in line with the literatures as PKCs do not participate in homoeostatic feedback loops, whereby the activation on the protein level results in its transcriptional downregulation (Newton, 2001). Pro-apoptotic effects of (-)-Indo Instead, PKCs are

generally regulated by subcellular localisation, and upon activation translocate to the cell membrane where they bind to isoform specific anchoring proteins called 'receptors for activated c-kinase' (RACKs) (Igumenova, 2015; Mochly-Rosen, 1995; Newton, 2001). Thus, a powerful tool to identify isoforms that are relevant for the mechanism of action of (-)-Indolactam V and MO47 might be the creation of isoform-specific PKC-GFP cell lines. This would allow to detect isoform-specific enrichment at the cell membrane upon treatment.

To narrow down potential candidates for the mechanisms of action, it was assessed whether the phenotypic effect could be abrogated by combinatorial treatment of PKC activators with PKC inhibitors. Encouragingly, the phenotypic effect was disrupted when treating iPSCs with Gö6983, a pan-PKC inhibitor, and a PKC activator at the same time. In contrast, Gö6976, an inhibitor of PKCs α and β, did not neutralise the morphological phenotype, suggesting that the phenotypic effect was potentially mediated by novel PKC isoforms. It is important to note that the promiscuity of staurosporine-related chemicals such as Gö6976 and Gö6983 presents a considerable caveat in the interpretation of these findings. Although a low degree of promiscuity has been reported for Gö6976 and Gö6983 in as far as they have been analysed (Anastassiadis et al., 2011), staurosporine itself has been proven to inhibit more than 80% of the kinome (Arrowsmith *et al.*, 2015; Davis *et al.*, 2011; Workman *et al.*, 2010). Therefore, it is questionable whether the disruption of the phenotypic effect can be interpreted as the result of PKC inhibition. Given the multitude of different PKC isoforms, inhibition via isoform-specific peptide inhibitors would be more informative (Csukai *et al.*, 1999; Mochly-Rosen *et al.*, 2012). Moreover, genetic strategies involving siRNAs or CRISPR/Cas9 technology for isoform-specific knockout are intriguing approaches for future work.

Turning to E-cadherin, we initially explored whether endocytosis and recycling markers would co-localise with intracellular E-cadherin signal on confocal microscopy images. Although occasional accumulations of E-cadherin could be observed in some conditions, the co-localisation of endocytosis markers did not follow a consistent pattern. Moreover, signal for recycling markers was barely visible in the DMSO control, suggesting that the quality of the antibodies against Rab9, Rab10 and Rab11 was poor or that recycling activity was low in all three conditions. In theory, it is conceivable that E-cadherin was already degraded at 24h, and therefore could not be detected in any endosomal compartment. It is worth assessing whether E-cadherin would co-localise with relevant markers after 3h treatment with (-)-Indolactam V and MO47. This assay could be performed under additional inhibition of endosome-lysosome fusion via bafilomycin (Gillespie *et al.*, 2013).

As a second scenario, we hypothesised that potential cleavage of E-Cadherin at its ectodomain-membrane interface would result in an increase of soluble E-cadherin in the supernatant. A significant increase of soluble E-cadherin could be detected upon treatment with (-)-Indolactam V for 24h. However, E-cadherin shedding may be a surrogate for loss of E-cadherin on the membrane since new E-cadherin molecules might be translocated to the membrane at the same time. Moreover, it has been shown that E-cadherin cleavage is induced upon apoptosis (Steinhusen *et al.*, 2001). Since (-)-Indolactam V exerts pro-apoptotic effects, it remains unclear whether the increase of soluble E-cadherin in the supernatant is due to apoptosis or induction of a new phenotype. Notably, for MO47, no significant difference could be observed. The absence of a positive control, which induces E-cadherin shedding, is an important limitation of this data set.

Analysis of cell surface E-cadherin by flow cytometry revealed that E-cadherin was expressed at similar or even higher levels on the cell surface upon treatment with (-)-

Indolactam V, suggesting that the loss of E-cadherin on the cell surface is not involved in the mechanisms of action. However, the data sets for the detection of soluble E-cadherin and the cell surface expression have not been repeated with independent biological replicates. To corroborate these findings, one could quantify the amount of E-cadherin on the cell surface via western blotting of cell membrane extractions. Further investigation into E-cadherin, including the cadherin switch from E-cadherin to N-cadherin as a hallmark of EMT, could also be informative (Wheelock et al., 2008).

Finally, the cytotoxic effects of (-)-Indolactam V were assessed using immunohistochemistry with Annexin-V followed by flow cytometry and the generation of a growth curve. (-)-Indolactam V treatment resulted in a significant shift from healthy to early and late apoptotic iPSCs. This is corroborated by clearly impaired iPSC proliferation as illustrated by the growth curve. Notably, at 72h the number of dying iPSCs outweighed the proliferation of new iPSCs, suggesting that during the first 48h iPSCs were undergoing increased apoptosis. Since MO47 was originally synthesised because of its unique advantage of increased cell viability, a comparison with (-)-Indolactam V would have been a powerful approach to distil further differences. Shortages in the compound MO47 did not allow parallel analysis, but because of its higher IC_{50} value for apoptosis, it is expected that the fraction of apoptotic cells would be much lower.

In summary, the data presented in this chapter can neither confirm nor refute any potential link between PKC activation and E-cadherin in the mechanisms of action of (-)-Indolactam V and MO47. Particularly, it remains unresolved whether E-cadherin is involved in the induction of the phenotypes.

Chapter 5: Assessing iPSC characteristics after serial treatment with MO47

5.1 Introduction

As previously discussed, poor chemical specificity harbours the risk of promisciousity with the potential for adverse off-target effects (Davies *et al.*, 2015). In particular, the application of small molecules for large-scale iPSC culturing requires the reduction of heterogeneity without comprising their pluripotency potential. Thus, the work in this chapter aims to assess the effects of MO47 treatment on iPSC characteristics.

The previous chapter illustrated the pro-apoptotic effects upon treatment with (-)-Indolactam V using an Annexin-V assay and a growth curve. Since (-)-Indolactam V's cytotoxicity rules it out as a compound worth pursuing for the application in 2D or 3D iPSC culturing, we decided to exclude (-)-Indolactam V from the work in this chapter and continued only with MO47.

iPSCs are characterised by their properties of self-renewal and pluripotency, defined by the potential to differentiate to representatives of all three germ layers (De Los Angeles *et al.*, 2015). Firstly, we assessed iPSCs according to the molecular profile of the pluripotent state using so-called core and state markers (De Los Angeles *et al.*, 2015). Secondly, we investigated pluripotency according to its functional definition, testing the spontaneous differentiation of iPSCs *in vitro* to endoderm, mesoderm and ectoderm, and also directed to specific ectodermal (cortical neurons) and mesodermal (macrophages) lineages (De Los Angeles *et al.*, 2015). Since karyotypic instability is an exclusion

criterion for the clinical use of iPSCs and hinders the reproducibility of experimental data, we finally assessed our pretreated iPSCs using SNP analysis (Carpenter *et al.*, 2009).[5]

5.2 Generating a stock of MO47 pretreated iPSCs

To assess the potential impact of MO47 in a series of different experiments, we generated a stock of iPSCs that had been cultured for 3 passages in mTesR™1 supplemented with 1µM MO47 or 0.1% DMSO (control condition). At each passage, these iPSCs were replated at the same low density as described in the methods section. iPSCs that were pretreated for 3 passages with MO47 shall thereafter be referred to as '3 cycles MO47'.

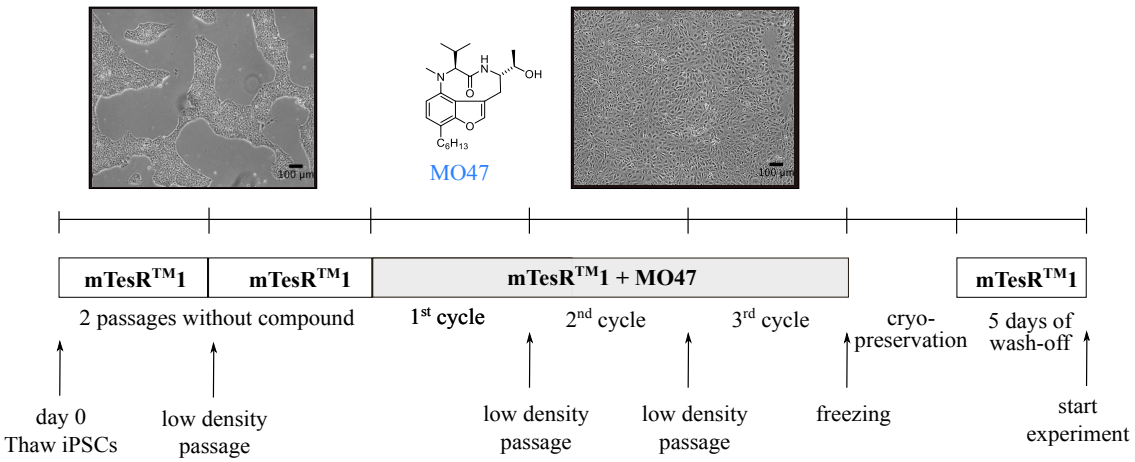

Figure 5.1 | Generating a stock of MO47 pretreated iPSCs.
iPSCs were serially treated with 1µM MO47 over 3 passages, then cryopreserved and thawed for the experiments described in this chapter.

[5] The results for the SNP analysis were pending at the completion of this work and could therefore not be included in this chapter.

5.3 Assessing proliferation through KI-67

Pluripotent stem cells harbour the characteristic of self-renewal through mitosis (Ghule *et al.*, 2011). According to this definition, every *bona fide* pluripotent iPSC culture consists exclusively of actively cycling cells. One strictly specific marker for proliferation and therefore a surrogate for self-renewal is the protein KI-67 (Gerdes *et al.*, 1984; Scholzen *et al.*, 2000). KI-67 is a chromosome periphery component that is only expressed in cycling cells. Importantly, cells entering a quiescent or G_0 state, do not exhibit the marker (Scholzen *et al.*, 2000). Thus, KI-67 can be used to determine the growth fraction of a population and detect differentiated cells that have lost their potential for self-renewal.

We hypothesised that iPSCs treated for 3 cycles with MO47 would show no difference in proliferation or increase the number of G_0 entering cells once treatment withdrawn.[6] For this purpose, DMSO and for 3 cycles with MO47 treated iPSCs were seeded in triplicates onto a 6-well plate and harvested for immunochemistry with anti-KI-67 mAb. Subsequently, stained samples were analysed using flow cytometry (Figure 5.2A). To confirm that the antibody had bound specifically to components in the nuclei, iPSCs were also analysed using confocal microscopy (Figure 5.3).

Figure 5.2B shows that MO47 pretreated iPSCs (mean±SEM: 99.2%±0.09; n=3) exhibit no significant difference in the fraction of actively cycling cells compared to DMSO pretreated iPSCs (mean±SEM: 99.2%±0.03; n=3). The percentage of proliferative cells in human dermal fibroblasts (HDF) is, as expected, lower than in iPSCs (12.3%, n=1). Figure 5.3 shows that the primary antibody binds to structures in the nuclei or specifically

[6] It was originally planned to assess the proliferation during MO47 treatment compared to DMSO by generation of a growth curve. Due to unavailability of MO47, which occurred at an early stage of this project, and persisted until the submission of this work, this assay could not be performed.

to the chromosomes during mitosis, which corresponds to observations reported in the literature (Scholzen *et al.*, 2000).

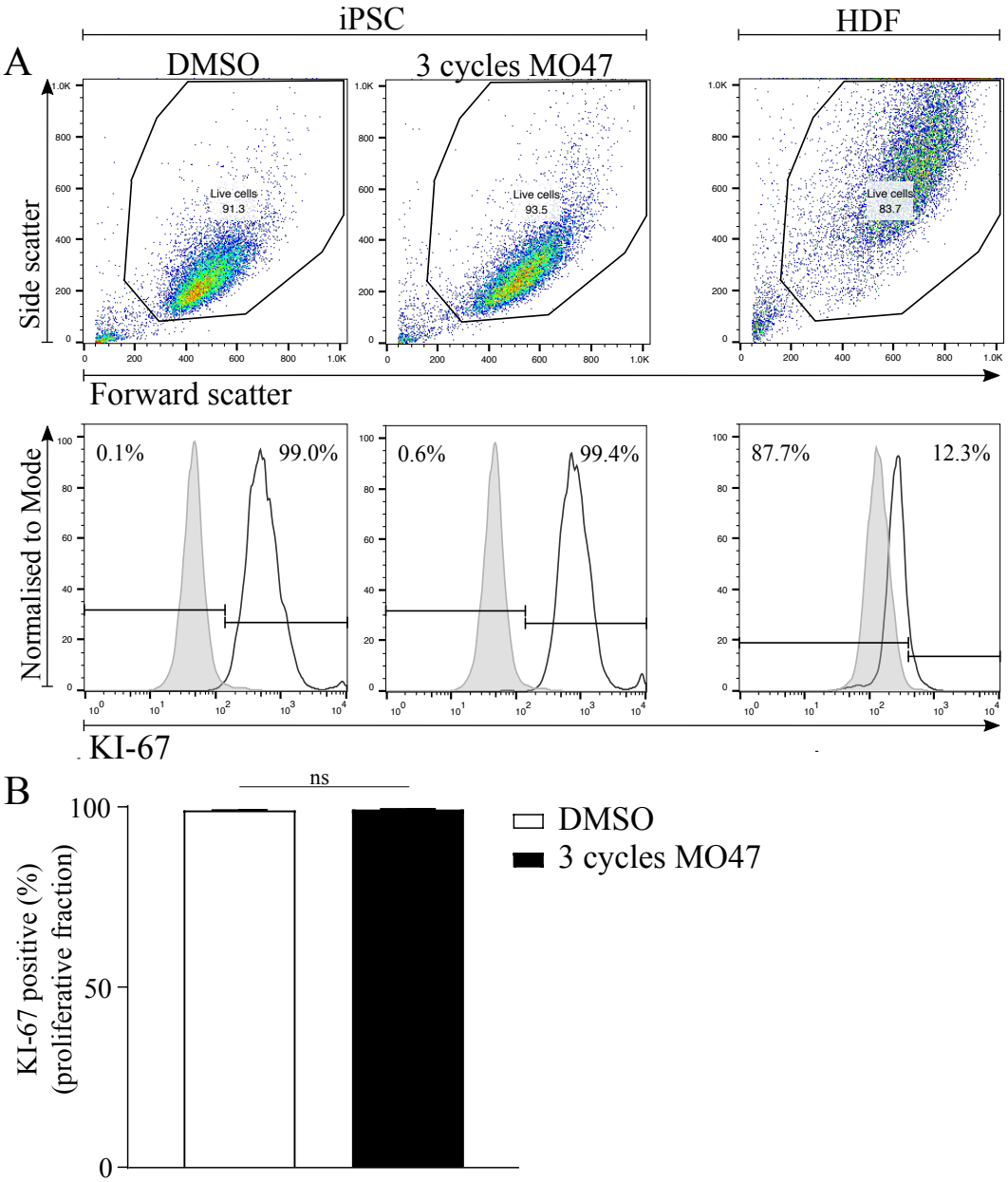

Figure 5.2 | Measuring the proliferation capacity of MO47 pretreated iPSCs using the marker KI-67 and flow cytometry.
Comparison of the fraction of actively cycling cells in DMSO and MO47 pretreated conditions and HDF. All three conditions were stained with anti-KI-67 mAB and the secondary antibody IgG Alexa Fluor 647. **(A, upper panel)** Representative flow cytometry plots for all three conditions. Debris and dead cells are gated out. **(A, lower panel)** A second gate for KI-67 positive cells is determined by staining iPSCs and HDF solely with the secondary antibody, allowing to gate KI-67 negative cells out. **(B)** Histograms for KI-67 positive populations in MO47 pretreated iPSCs (mean±SEM: 99.2±0.09; n=3), and DMSO pretreated iPSCs (mean±SEM: 99.2±0.03; n=3). Two-tailed t test, ns ($P > 0.05$), * ($P \leq 0.05$), ** ($P \leq 0.01$), *** ($P \leq 0.001$) and **** ($P \leq 0.0001$).

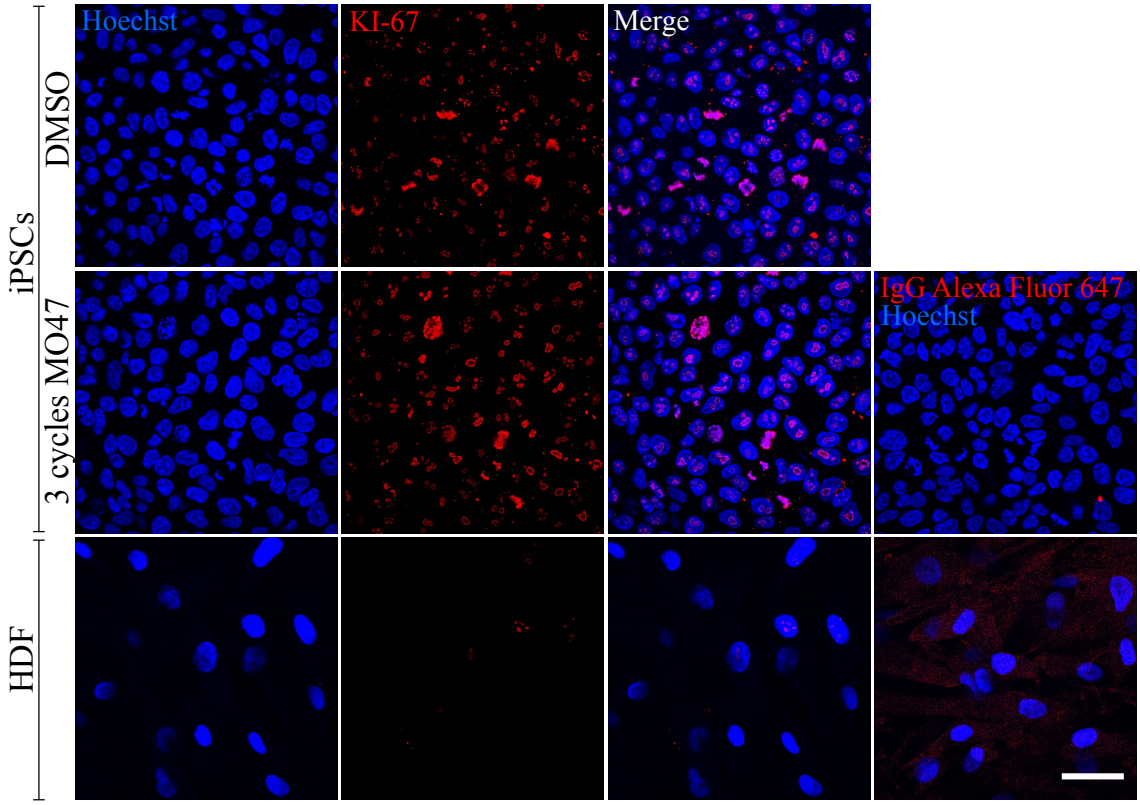

Figure 5.3 | Measuring the proliferation capacity of MO47 pretreated iPSCs using the marker KI-67 and confocal microscopy.
Comparison of actively cycling cells in DMSO and MO47 pretreated conditions and HDF. All three conditions were stained with anti-KI-67 mAB and the secondary antibody IgG Alexa Fluor 647. The expression of KI-67 in DMSO and MO47 pretreated iPSCs is characteristic. HDF display a much lower degree of actively cycling cells. Conditions that are only stained with the secondary Ab show no signal in the red channel (negative control). Magnification = 400 ×; scale bar = 50µM.

5.4 Assessing pluripotency

In addition to self-renewal, iPSC can be characterised by pluripotency, defined in *sensu stricto* by the potential to differentiate into representatives of all three germ layers (De Los Angeles *et al.*, 2015). In recent years, an additional definition has been developed, characterising pluripotency by the way it is assessed. Pluripotency can be assessed by the pluripotent state (core and state markers) and by its function (developmental potential), accordingly (De Los Angeles *et al.*, 2015).

5.4.1 Assessing molecular pluripotency through core and state markers

Pluripotent core and state markers can be used as a surrogate to assess pluripotency potential. Notably, the combinations of multiple so-called pluripotency markers is nowadays increasingly used to identify *bone fide* iPSCs clones via flow cytometry without the analysis of morphological criteria (Abujarour *et al.*, 2013). Here, Nanog, Tra-1-60, SSEA-3, SSEA-4 and CD44 were used to assess the expression of core and state pluripotent markers.

Nanog is a divergent homoeodomain protein that acts as a transcription factor upon many genes during early development (Boyer *et al.*, 2005; Chambers *et al.*, 2003). The transcription factor induces, maintains and governs pluripotency in the core regulatory circuitry together with OCT4 and SOX2 (Boyer *et al.*, 2005; De Los Angeles *et al.*, 2015). Being specific for pluripotent stem cells, Nanog is not expressed in differentiated cells (Chambers *et al.*, 2003).

Tumor rejection antigens Tra-1-60 and Tra-1-80 are redundant keratan-sulfate antigens in the transmembrane protein podocalyxin (Andrews *et al.*, 1984; International Stem Cell *et al.*, 2007; Toyoda *et al.*, 2017). Podocalyxin was first discovered on podocytes in the kidney but can also be found on endothelial cells, platelets, hematopoietic stem cells and

in brain tissue (Toyoda *et al.*, 2017). Importantly, Tra-1-60 is also highly expression on iPSCS and ESCs, and downregulates rapidly upon differentiation (Abujarour *et al.*, 2013; Schopperle *et al.*, 2007) Therefore, it has been used extensively as a positive marker for undifferentiated iPSCs.

The stage-specific surface antigens SSEA-3 and SSEA-4 are related epitopes on globo-series sphingoglycolipids and expressed on the cell surface of iPSC and hES (Andrews *et al.*, 1982; Brimble *et al.*, 2007; Kannagi *et al.*, 1983). Although both surface markers are structurally related to the lacto-series glycolipid SSEA-1, their expression follows a different pattern. During differentiation, human iPSCs and ESCs shift from a SSEA-1^- /SSEA-3^+/SSEA-4^+/ to a SSEA-1^+/SSEA-3^-/SSEA-4^- phenotype (Andrews *et al.*, 1982; Brimble *et al.*, 2007). Interestingly, the opposite is true for mouse iPSCs, a naive pluripotency model, where SSEA-1 is upregulated in the undifferentiated state (Henderson *et al.*, 2002). SSEA-3 and SSEA-4 are not essential for the maintenance of pluripotency. However, their rapid downregulation upon differentiation makes them valuable for the characterisation of pluripotency.

Cluster of differentiation CD44 or $gp90^{hermes}$ is a negative marker for human iPSCs and ESCs (Culty *et al.*, 1990; Goldstein *et al.*, 1989; Quintanilla *et al.*, 2014). The amino-terminal site of CD44 functions as a hyaluron-binding site and mediates cell-matrix interactions (Ponta *et al.*, 2003). CD44 is expressed in epithelia and lymphocytes and highly abundant on the cell surface of human parental fibroblasts (Quintanilla *et al.*, 2014). Therefore, CD44 is ideally suited as a negative control for iPSCs and a positive control for the parental HDF.

We hypothesised that 3 cycles pretreatment with MO47 would not impair pluripotency, and DMSO and MO47 pretreated iPSCs would, therefore, exhibit similar expression levels of all pluripotency markers.

Immunohistochemistry for SSEA-3, SSEA-4 and CD44 was performed on live cells with conjugated antibodies. For Nanog and Tra-1-60, cells were fixed and permeablised before staining. The relevant isotype controls for each antibody were included and the same gate was applied to all populations to select for live cells.

Figure 5.4 shows clear signal shifts in DMSO and MO47 pretreated iPSCs for staining with Nanog, Tra-1-60, SSEA-3 and SSEA-4. The binding of the antibodies was subsequently confirmed via confocal microscopy. Figure 5.5 shows the corresponding DMSO and MO47 pretreated iPSCs that were stained with Hoechst, Tra-1-60 and Nanog for confocal microscopy. Note also the typical colony-based phenotypes of the conditions: in both conditions iPSCs form clearly defined colonies with sharp edges.

In summary, the phenotypes of core and state pluripotent markers are highly consistent between DMSO and MO47 pretreated cells. In contrast, HDF display a low signal for all pluripotency markers and a strongly positive signal for CD44.

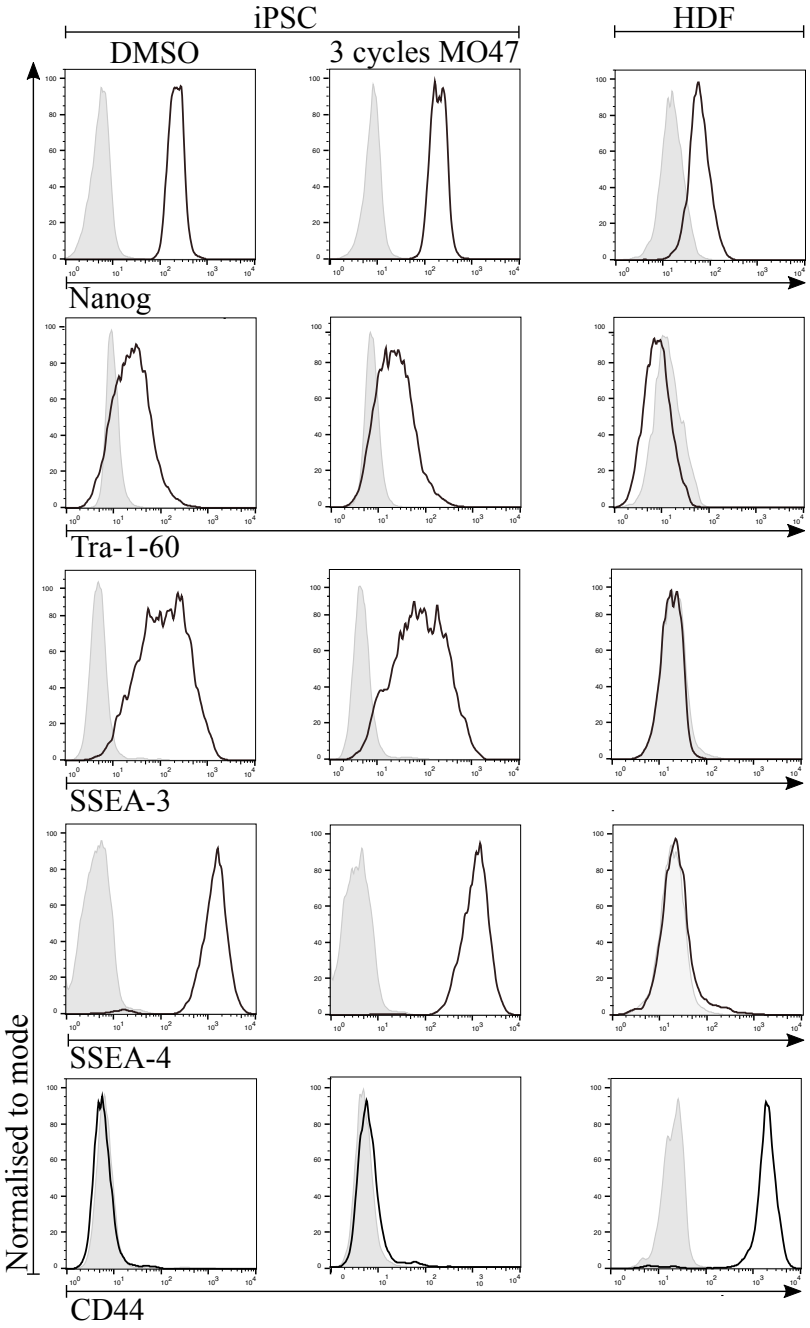

Figure 5.4 | Assessing pluripotency markers of MO47 pretreated iPSCs using flow cytometry.

Phenotypes of iPSCs pretreated with DMSO and MO47 and HDF are displayed. The expression of the pluripotency markers Nanog, Tra-1-60, SSEA-3 and SSEA-4 and the fibroblast marker CD44 were measured using flow cytometry. The same gate to select for live cells was applied to all conditions. The histograms in each plot represent one population stained with the conjugated antibodies (black line) and one population stained with the relevant isotype control (shaded grey). The localisation of the binding of these antibodies was confirmed via confocal microscopy in figure 5.5.

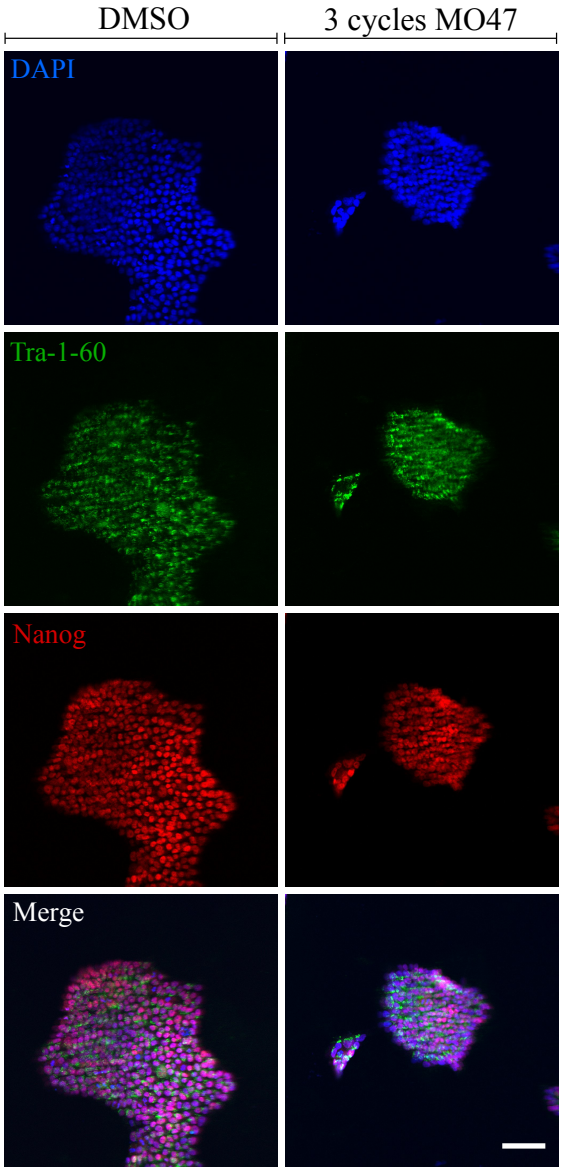

Figure 5.5 | Assessing pluripotency markers of MO47 pretreated iPSCs using confocal microscopy.
To confirm the results presented in figure 5.4, the expression of the pluripotency markers Nanog and Tra-1-60 of DMSO and MO47 pretreated iPSCs was analysed using confocal microscopy. In each condition, Nanog (nuclei) and Tra-1-60 (cell surface) are highly expressed. Confocal microscopy; magnification = 200×; scale bar = 100µm.

5.4.2 Assessing functional pluripotency through differentiation *in vivo*

To test whether iPSCs could still differentiate into representatives of all three germ layers after 3 cycles pretreatment with MO47, iPSCs were subjected to spontaneous and directed ectodermal and mesodermal differentiation (functional definition of pluripotency).

5.4.2.1 Assessing functional pluripotency through spontaneous differentiation

The formation of well-differentiated teratoma in immunodeficient mice has long been the gold standard to appreciate functional pluripotency (Daley *et al.*, 2009). However, the implantation into mice is time-consuming and inappropriate for scalable, quantitative assays (Tsankov *et al.*, 2015). One approach to circumvent teratomas is PluriTest, a quantitative assay based on the analysis of the gene expression profile (Muller *et al.*, 2011). Although this test can be used to quantify the molecular signature of pluripotency genes, it does not assess functional pluripotency, including differentiation signatures of all three germ layers (Muller *et al.*, 2011). Consequently, ScoreCard, a qRT-PCR-based assay that evaluates both pluripotency and differentiation signatures at the same time, has become the method of choice (Bock *et al.*, 2011; Tsankov *et al.*, 2015).

ScoreCard is based on 96 different TaqMan probes. Because of the high correlation between differentiation potential and differentiation efficiency as measured in this unique set of genes, ScoreCard offers a valuable quantitative approached for line-to-line comparison (Tsankov *et al.*, 2015). Moreover, ScoreCard was shown to be sensitive enough to compare the functional pluripotency of samples with distinct culture conditions, making it an ideal tool for our purposes (Tsankov *et al.*, 2015).

ScoreCard can be used for the analysis of undifferentiated, directly differentiated and spontaneously differentiated samples. Spontaneous differentiation of pluripotent stem cells is defined by the potential to generate a mixture of different stem cell fates upon

removal of essential culturing conditions that maintain pluripotency (Cohen *et al.*, 2011). For the ScoreCard assay, iPSCs are generally directed into spontaneous differentiation through the formation of embryoid bodies (EBs, the entire sequence of spontaneous differentiation has been imaged for both conditions; see Appendices, Figures V.1, V.2, V.3 and V.4). These are agglomerations of iPSCs or ESCs in 3D, which have a distinct similarity to the development of the inner cell mass, and harbour the potential to differentiate into representatives of all three germ layers (Doetschman *et al.*, 1985; Pettinato *et al.*, 2014).

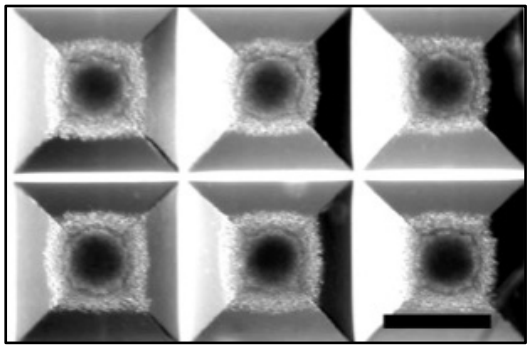

Figure 5.6 | Generation of Spin-EBs 24h after plating.
Scale bar = 200μm.

We hypothesised that serial pretreatment with MO47 would not interfere with the functional pluripotency of iPSCs, and DMSO and MO47 pretreated iPSCs would consequently exhibit the same differentiation efficiency. To this end, we analysed undifferentiated and differentiated samples (day 14 of spontaneous differentiation, Appendix Chapter 5) of DMSO and MO47 pretreated iPSCs for ScoreCard analysis.

Figure 5.6 shows the expression levels of all 4 samples for genes grouped in 4 different signatures, including pluripotency, ectodermal, mesodermal and endodermal differentiation. Figure 5.7 summarises each signature in an algorithm score compared to an already provided endogenous reference set of *bona fide* pluripotent stem cells. The Ct values for each gene are listed in Table V.1 (Appendices).

Overall, the data indicate that both DMSO and MO47 pretreated iPSCs exhibit upregulated gene signatures for all three germ layers upon spontaneous differentiation in a highly similar pattern. Moreover, their undifferentiated counterparts have consistent positive scores for pluripotency and negative scores for the three differentiation signatures.

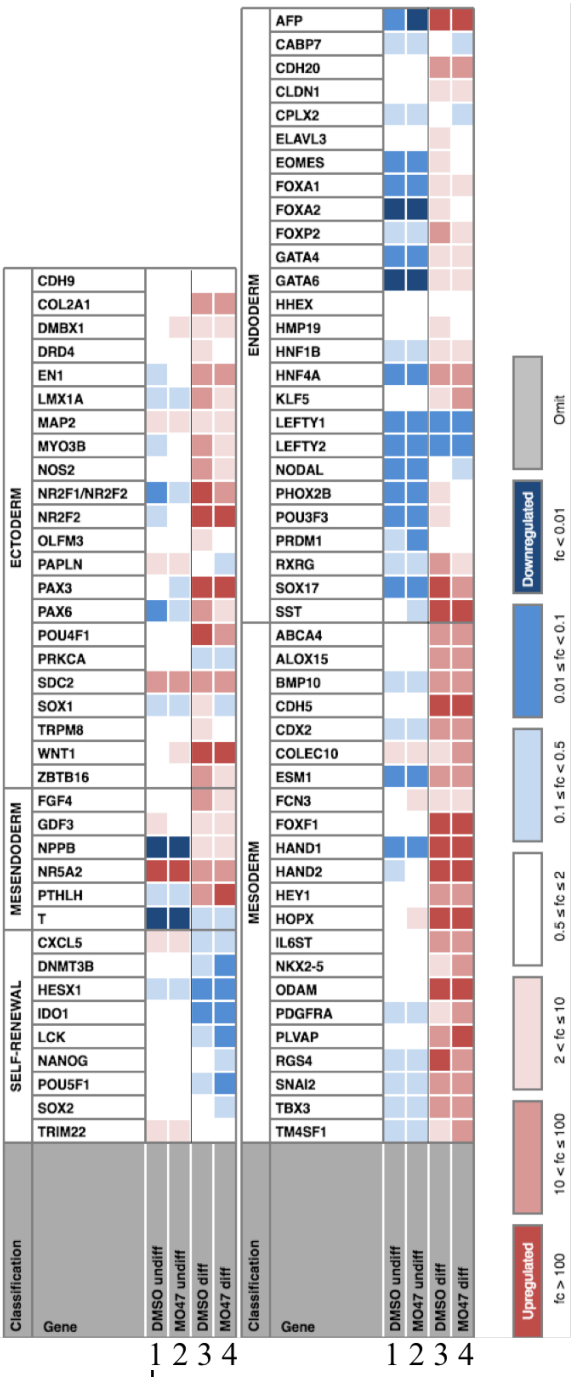

Figure 5.7 | Assessing functional pluripotency of DMSO and MO47 pretreated iPSCs using ScoreCard.

The heat map groups genes according to signatures for pluripotency and trilineage differentiation for the 4 samples: (1) DMSO pretreated undifferentiated, (2) MO47 pretreated undifferentiated, (3) DMSO pretreated and differentiated for 14 days, (4) MO47 pretreated and differentiated for 14 days. Each sample is normalised to a reference set of undifferentiated samples provided via the online software of the ScoreCard^{TM} kit. Colour-coding indicates whether a gene is upregulated (red, ≥2), downregulated (blue, <0.5) or expressed at the same level (white, ≥0.5 and <2).

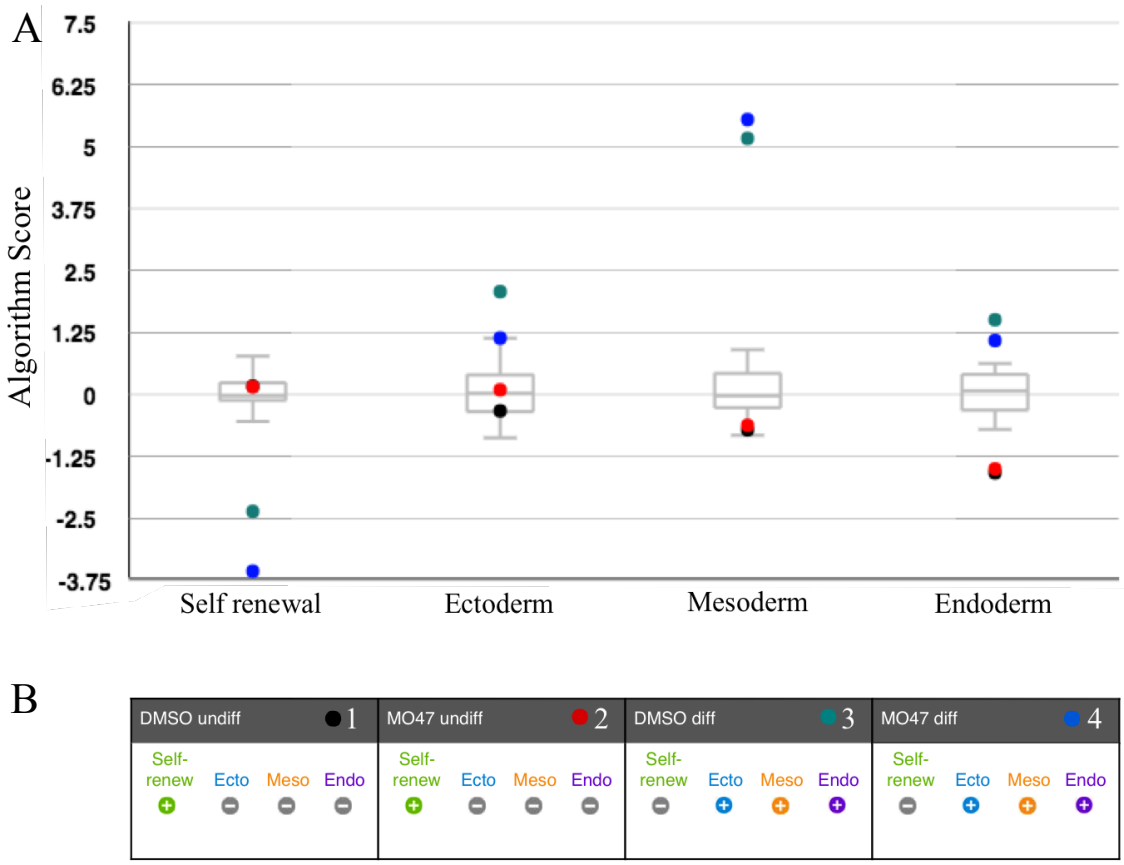

Figure 5.8 | Scores for different signatures determine the functional pluripotency for DMSO and MO47 pretreated iPSCs using ScoreCard.
(A) Box-and-whiskers plots indicate the reference signatures of undifferentiated samples as provided by the ScoreCard kit. Dots represents the algorithm scores of the included samples for each signature: DMSO pretreated undifferentiated (black), MO47 pretreated undifferentiated (red), DMSO pretreated and differentiated for 14 days (green), MO47 pretreated and differentiated for 14 days (blue). **(B)** The 4 algorithm scores determine whether a sample is overall negative or positive for an entire differentiation or pluripotency signature. Algorithm scores ≥2 indicate upregulation, <0.5 downregulation and scores ≥0.5 and <2 are highly similar to a reference set of undifferentiated pluripotent stem cells.

5.4.2.2 Assessing functional pluripotency through directed differentiation to macrophages (mesoderm)

Spontaneous differentiation of DMSO and MO47 pretreated iPSCs resulted in the upregulation of the gene signatures for all three germ layers, suggesting that MO47 pretreated iPSCs still harboured functional pluripotency. To further assess the differentiation efficiency of MO47 pretreated iPSCs to fully differentiated representatives of the mesoderm, we explored the differentiation potential to yolk sac-like adherent macrophages (pMac) (Buchrieser *et al.*, 2017). The differentiation to pMac was chosen because it promised a high degree of robustness and efficiency (Buchrieser *et al.*, 2017; van Wilgenburg *et al.*, 2013).

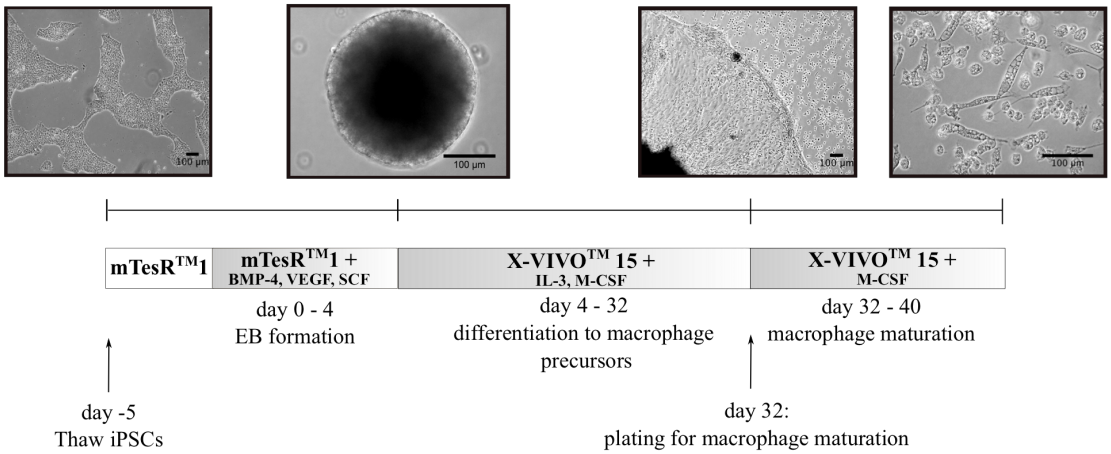

Figure 5.9 | Differentiation of pretreated iPSCs to macrophages via macrophage precursors.
EBs are generated using a spin approach and directed differentiation is initiated by the change to medium supplemented with BMP-4 (general mesodermal induction), VEGF (endothelial induction) and SCF (hematopoietic induction). Upon the formation on day 4, EBs are transferred to flasks and cultured in X-VIVO™ 15 medium supplemented with M-CSF and IL-3 (both promote myeloid differentiation). This is followed by at least 8 days of maturation and the removal of IL-3.

To this end, spin-EBs were generated, and followed by differentiation with IL-3 and M-CSF along the myeloid lineage, yielding so-called macrophage precursors (pMacpre) (Buchrieser *et al.*, 2017; van Wilgenburg *et al.*, 2013). Although in the literature previously described as “monocytes”, the term “macrophage precursors” is more

appropriate because of the MYB-independent ontogeny of the primitive myeloid cells (Buchrieser *et al.*, 2017; Haenseler *et al.*, 2017; van Wilgenburg *et al.*, 2013). A further maturation period resulted in adherent macrophages. iPSC-derived macrophages of this type can generally be characterised by their morphology of voluminous cytoplasm, membrane blebs and ruffles, and an elongated, spindle-like form (Akagawa *et al.*, 2006; Buchrieser *et al.*, 2017; Hashimoto *et al.*, 1999; van Wilgenburg *et al.*, 2013). In addition to these morphological criteria, the expression of phenotypic surface markers, including CD11, CD14 and CD45, is characteristic (Buchrieser *et al.*, 2017; Karlsson *et al.*, 2008).

CD45 is a transmembrane tyrosine phosphatase involved in various cell signalling pathways. It constitutes a positive marker for all nucleated hematopoietic cells and is highly expressed on representatives of the lymphocytic and the monocytic lineage (Penninger *et al.*, 2001; Shah *et al.*, 1988). During maturation, cells committing to the monocytic lineage express CD11b and CD14 (Kuwana *et al.*, 2003; Shah *et al.*, 1988). CD11b is a type 3 complement receptor and constitutively expressed in macrophages (Gordon *et al.*, 2014). CD14 is part of the liposaccharide receptor and a classic marker for circulating monocytes (Gordon *et al.*, 2005; Kuwana *et al.*, 2003).

The combinatorial analysis of all three surface markers, together with morphological criteria, presents a common approach to identify yolk-sac derived tissue-resident macrophages, and was also used in this study (Buchrieser *et al.*, 2017; van Wilgenburg *et al.*, 2013).

Figure 5. shows macrophages derived from DMSO and MO47 pretreated iPSCs on day 40 of differentiation. Cells with elongated, spindle-like morphology have emerged in both conditions. The cytoplasm of each cell contains multiple vesicles. Both conditions exhibit a $CD11b^{+}/CD14^{+}/CD45^{+}$ phenotype as described in the literature (Buchrieser *et al.*, 2017). In contrast, iPSCs have a $CD11b^{-}/CD14^{-}/CD45^{-}$ phenotype.

Taken together, these phenotypic data indicate that DMSO and MO47 pretreated iPSCs have successfully been differentiated to yolk-sac derived adherent macrophages.

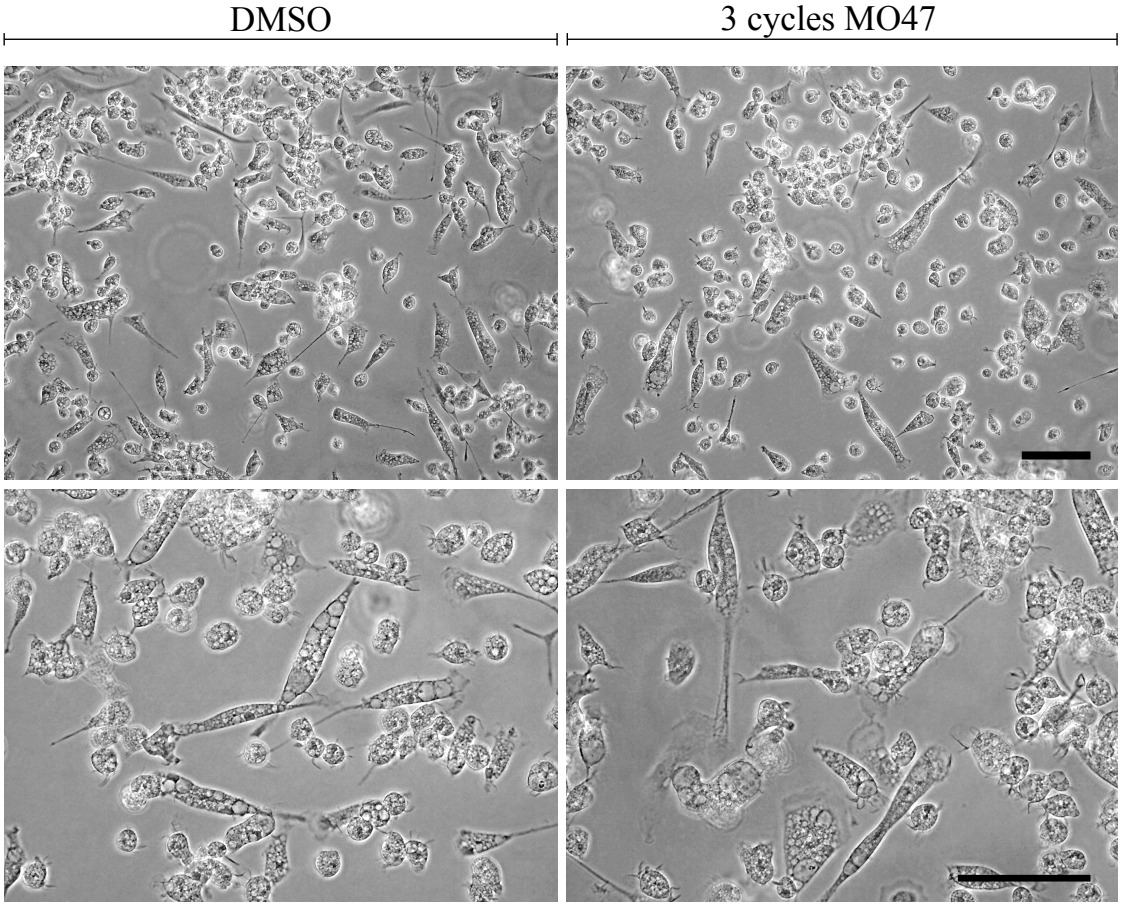

Figure 5.10 | Characterising iPSCs-derived macrophrages (pMac) using morphological critera.
Morphological phenotypes of macrophages derived from DMSO and MO47 pretreated iPSCs are analysed using phase contrast. Shown are adherent macrophages (pMac) on day 40 of differentiation along the monocytic line. A voluminous cytoplasms, membrane blebs and ruffles, and an elongated, spindle-like forms are characteristic. Phase contrast; magnifications = 200× (upper panel) and 400× (lower panel); scale bars = 100μm.

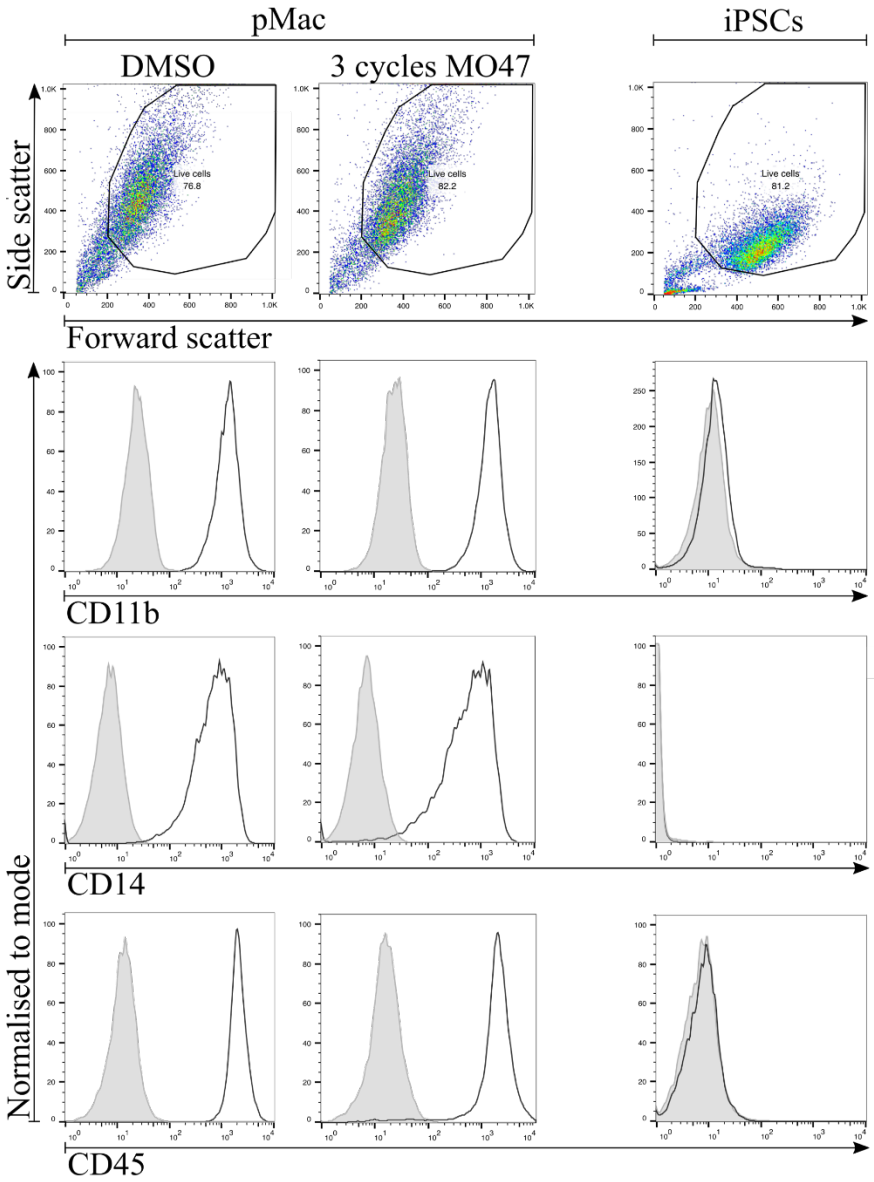

Figure 5.11 | Characterising iPSC-derived macrophages using flow cytometry.
Phenotypes of DMSO and MO47 pretreated iPSCs that have been differentiated along the myeloid line to pMac. Shown is the expression of the markers CD11b, CD14 (both monocytic markers) and CD45 (hematopoietic marker) measured on day 40 of differentiation using flow cytometry. The same gate to select for live cells was applied to each condition. The histograms in each plot represent a population stained with the conjugated antibodies (black line) and its control stained with the relevant isotype control (shaded grey).

5.4.2.3 Assessing functional pluripotency through directed differentiation to cortical neurons (ectoderm)

Spontaneous and directed differentiation of DMSO and MO47 pretreated iPSCs resulted in the upregulation of gene signatures for all three germ layers and differentiated macrophages (pMac), respectively. In order to validate the preservation of functional pluripotency for a second germ layer, we explored the differentiation of MO47 pretreated iPSCs to cortical neurons. We hypothesised that the efficiency for ectodermal differentiation would be unchanged compared to the DMSO control. We chose a differentiation strategy to cortical neurons because of its high reproducibility, efficiency and rapidity, which had previously been reported in the literature (Grutz *et al.*, 2017; Haenseler *et al.*, 2017; Shi *et al.*, 2012a; Shi *et al.*, 2012b).

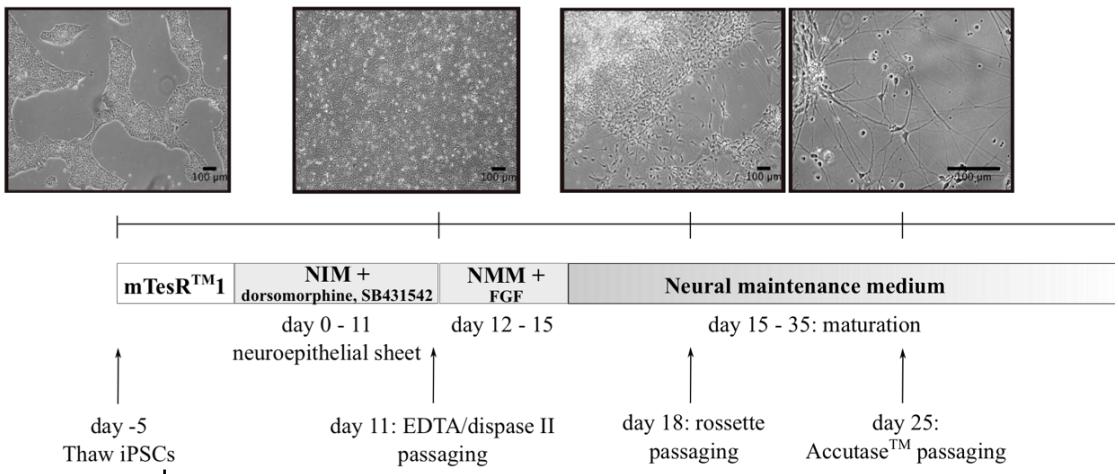

Figure 5.12 | Differentiation of iPSCs to cerebral cortex neurons.
Upon formation of a neuroepithelial after SMAD inhibition for 11 days, cells are EDTA/dispase II passaged, plated on laminin and cultured for 4 days in neural maintenance medium supplemented with FGF-2, which promotes the formation of neuronal rosettes. On day 16, neuronal progenitors form neuronal rosettes, which are subsequently passaged and cultured in NMM for maturation. On day 25, early neurons characterised by dendrites and axons emerge.

In this study, MO47 and DMSO pretreated iPSCs were differentiated to cerebral cortex neurons in a protocol adapted from Shi *et al.* (2012a). This protocol is based on a dual SMAD signalling inhibition through dorsomorphine and SB431542, which has shown to accelerate the downregulation of pluripotency markers and promote direct differentiation

towards the anterior neuroectodermal lineage (Chambers *et al.*, 2009; Kim *et al.*, 2010; Shi *et al.*, 2012a). After formation of a neuroepithelial sheet on day 11, the culture changes to an almost pure population of primary cortical progenitors, which can be monitored by PAX-6 (Chambers *et al.*, 2009).

PAX-6 is a highly conserved paired-box transcription factor with functions in gene dosage (Callaerts *et al.*, 1997; Cvekl *et al.*, 2017). Notably, the protein plays vital roles in the development of the central nervous system, the pancreas and especially the eye (Callaerts *et al.*, 1997; Cvekl *et al.*, 2017). During the differentiation to cortical neurons, PAX-6 can be harnessed as a marker to identify primitive neuroepithelial populations that can subsequently commit to the formation of neuronal rosettes (Chambers *et al.*, 2009). Neuronal rosettes consist of primitive ectodermal progenitors. Importantly, after passaging of neuronal rosettes on day 18, cells that emerge at the edges of neuronal rosettes are often positive for β-tubulin III (Shi *et al.*, 2012a).

ß-tubulin III belongs to the family of tubulins, and is expressed in the central nervous system, the peripheral nervous system and the Sertoli cells of the testes (Mariani *et al.*, 2015). TUJ1 is an antibody directed against epitopes that are unique to ß-tubulin III. Importantly, TUJ1 has been used extensively as a gold standard to confirm neuronal commitment during differentiation in recent years (Caccamo *et al.*, 1989; Mariani *et al.*, 2015; Shi *et al.*, 2012a; Shi *et al.*, 2012b).

Figure 5. shows the progressive differentiation of iPSCs to cerebral cortical neurons. In both conditions, neuronal rosettes emerged on day 16 and gave rise to primitive neurons as visible on day 27. To confirm the commitment to cortical neurons, we further analysed the populations on day 25 using immunohistochemistry staining with anti-PAX-6 and TUJ1 mAbs (Figure 5.). Cells at the edges of neuronal rosettes are positive for TUJ1. Inside the neuronal rosettes, cells are stained by anti-PAX-6 mAb.

Overall, these results show that DMSO and MO47 pretreated iPSCs form neuronal rosettes and commit to a similar extent to cerebral cortical progenitors on day 25.

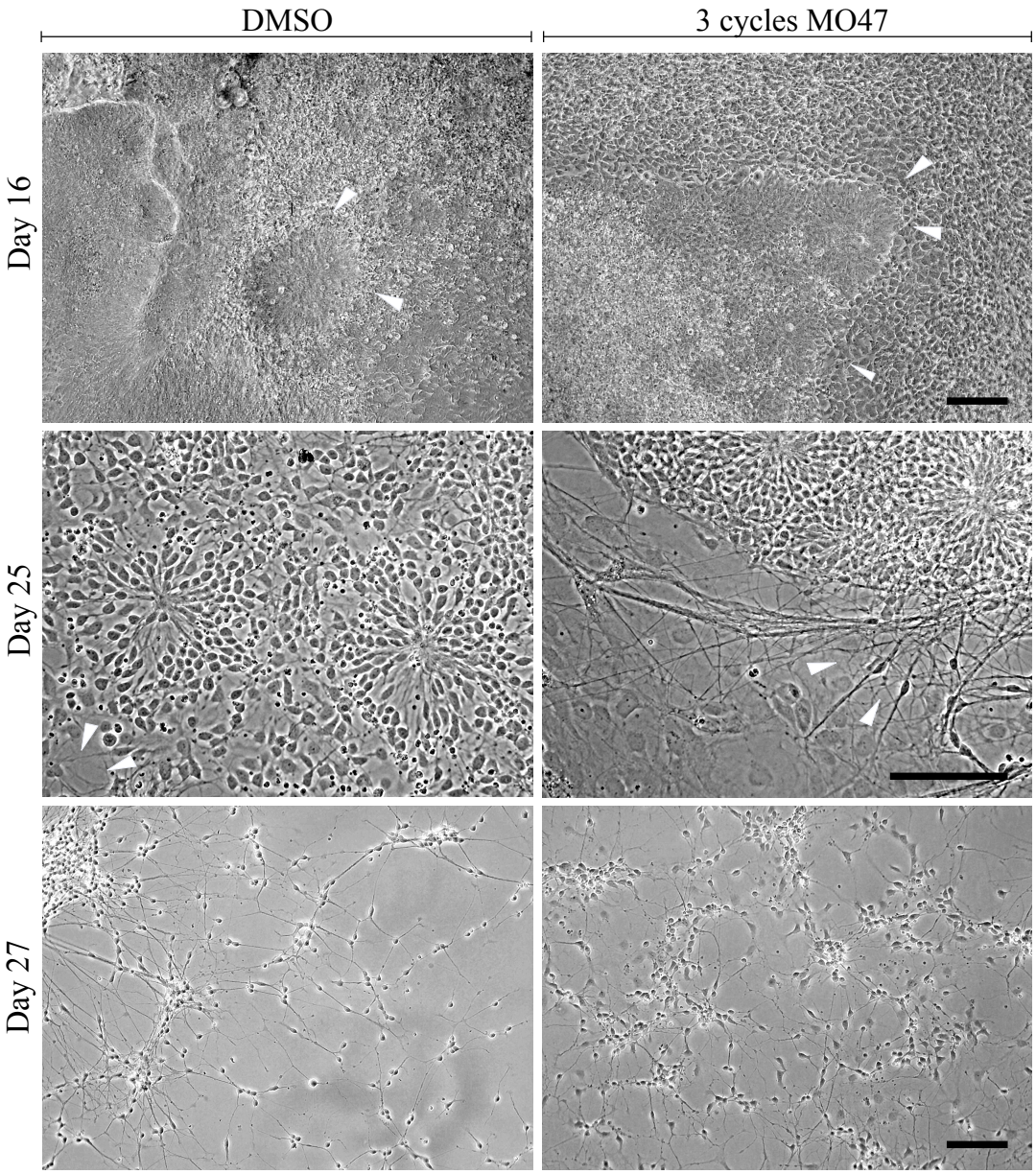

Figure 5.13 | Monitoring differentiation of MO47 pretreated iPSCs to cerebral cortical neurons using morphological criteria.
Shown are images of DMSO and MO47 pretreated iPSCs on days 16, 25 and 27. **(Upper panel)** On day 16, primitive neuroepithelial progenitors are grouped in neuronal rosettes with clear edges (white arrows) in both conditions. **(Middle panel)** On day 25, neuronal progenitors are more spread out. At the edges of the rosettes, cells with neurites can be identified (white arrows). (**Lower panel**) On day 27, a population with clearly-defined neurites has emerged in each condition. Phase contrast; magnifications = 200× (upper and lower panel) and 400× (middle panel); scale bars = 50μm.

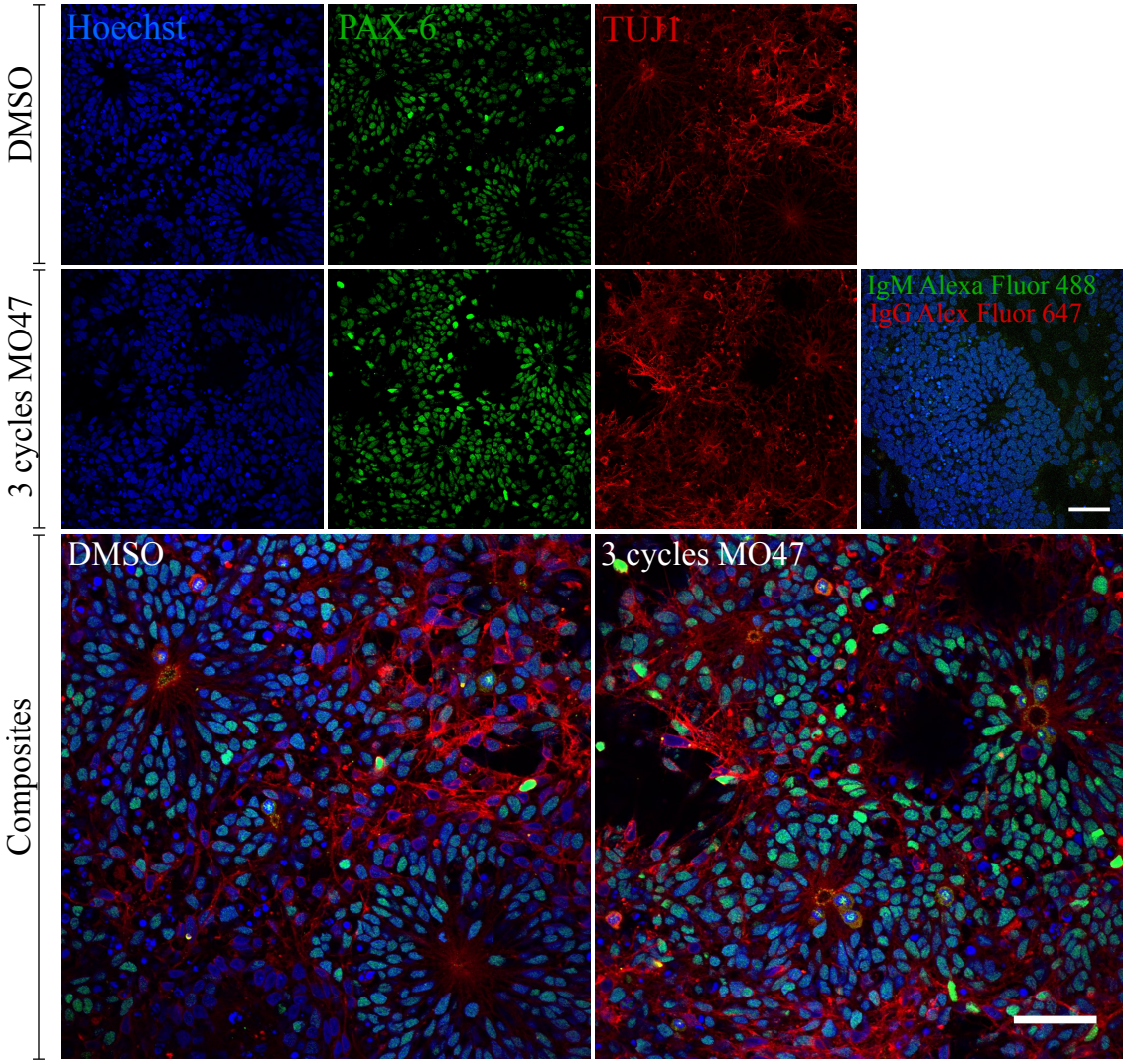

Figure 5.14 | Characterising iPSC-derived cortical neuronal progenitors using immunohistochemistry and confocal microscopy.
Shown are confocal microscopy images of primitive cortical neurons derived from DMSO and MO47 pretreated iPSCs. On day 18 of differentiation, neuronal rosettes were plated onto μ-slides and cultured in NMM until day 25. Each condition was stained with PAX-6 and TUJ1 mAbs followed by staining with secondary Abs. At the edges of neuronal rosettes TUJ1-specific neuronal progenitors have emerged in both conditions. The neuronal rosettes are positive for PAX-6. Negative controls were stained with the relevant secondary Abs. Confocal microscopy; magnifications 400×; scale bars = 500μm.

5.5 Summary and discussion

In this chapter, the self-renewal capacity and the molecularly and functionally defined pluripotency potential of iPSCs that had previously been pretreated with MO47 and DMSO (control) were assessed. MO47 pretreated iPSCs were still in an actively cycling state. On the RNA level (ScoreCard), these iPSCs still harboured functional pluripotency. When analysing functional pluripotency on the actual cell state, these iPSCs could also commit to macrophages and primitive cerebral cortical neurons upon directed differentiation. There was no observable difference in differentiation efficiency compared to control conditions (DMSO).

In a first step, a stock of DMSO and MO47 pretreated iPSCs was generated by treating iPSCs over three passages with 1μM MO47 and 0.1% DMSO, respectively. We decided to exclude (-)-Indolactam V from the work in this chapter because of its low IC_{50} value for apoptosis, and the cytotoxic effects illustrated by the Annexin-V assay in the previous chapter. Although it was possible to serially passage iPSCs upon treatment with MO47 and to harvest a large amount of iPSCs for cryopreservation, it is difficult to appreciate the adverse effects of MO47 on proliferation comprehensively without a growth curve. This lack of data constitutes an important caveat to this study. It is due to the lack of opportunity to repeat these experiments because unavailability of MO47 occurred at an early stage of this project, and persisted until the submission of this work.

Given the shortage of MO47, the work in this chapter is based on a single cell line (iPS-OX1-18). However, iPSC lines have been shown to exhibit a large line-to-line variability (Cahan *et al.*, 2013). It has recently been shown that different genetic backgrounds in iPSCs result in a high degree of molecular heterogeneity, which can account for different capacities in differentiation to representatives of the three germ layers (Kilpinen *et al.*, 2017; Narsinh *et al.*, 2011) Importantly, this heterogeneity concerns the epigenome,

transcriptome, proteome, and even the cell morphology (Kilpinen *et al.*, 2017). Therefore, further studies are required using additional cell lines. iPSCs were serially treated for 3 passages in this study, but it is possible that there may be an effect of MO47 on iPSC characteristics over many passages. iPSCs often need to be maintained in their pluripotent state for much longer periods, so it might be advisable to study chemical effects for more passages, as described elsewhere (Watanabe *et al.*, 2007; Xu *et al.*, 2010). This is especially relevant for possible effects on the karyotype and the occurrence of SNPs. Since the results for SNP analysis could not be obtained before the completion of this work, this remains an important caveat.

After the generation of a stock of MO47 pretreated iPSCs, we first compared the proliferative capacities of MO47 pretreated iPSCs to control conditions by using the marker KI-67. Importantly, we could not see any significant difference between the growth fractions of MO47 and DMSO pretreated iPSCs, suggesting that MO47 did not increase the number of post-mitotic, quiescent or G_0 entering cells. Analysis of low-cycling HDF as a negative control showed a considerably lower fraction of actively cycling cells. However, it is important to note that KI-67 is only a surrogate for cell proliferation and self-renewal as it merely labels actively cycling cells. Therefore, it is difficult to appraise possible prolongations or abbreviations of the cell cycle, resulting in a lower yield of iPSC growth. Given these limitations, the generation of growth curves during treatment and after serial treatment are compelling assays for future work.

As presented in chapter 3 of this study, the induction of a distinctly different phenotype upon treatment with MO47, prompted the question whether iPSCs were still *bona fide* pluripotent or had, instead, committed to a new cell type. Immunohistochemistry for core and state markers showed that MO47 pretreated iPSCs displayed a $Nanog^+$/Tra-1-60^+/SSEA-3^+/SSEA-4^+/$CD44^-$ phenotype in flow cytometry, which was consistent with

the control condition (DMSO). In contrast, the opposite phenotype could be observed for HDF, except for Nanog. This low signal shift for Nanog in HDF populations is in line with previous findings for the same cell-antibody combination in our laboratory. Encouragingly, we could also validate the expression and localisation of Tra-1-60 and Nanog using confocal microscopy. In summary, these data highlight the preservation of molecularly defined pluripotency upon serial treatment with MO47 (Abujarour *et al.*, 2013; De Los Angeles *et al.*, 2015).

Core and state markers are only surrogates for pluripotency and cannot be used to validate functional pluripotency, defined by differentiated to all three germ layers. ScoreCard is a quantitative approach that is increasingly replacing teratoma assays as a gold standard in the assessment of functional pluripotency because of its rapidity, better reproducibility and higher robustness (Tsankov *et al.*, 2015). Spontaneous differentiation of DMSO and MO47 pretreated iPSCs resulted in the upregulation of the signatures for all three germ layers, whereas MO47 pretreated and undifferentiated iPSCs were negative for differentiation but positive for pluripotency signatures. Moreover, the remarkable consistency within each group of differentiated (1 and 2) and undifferentiated (3 and 4) samples (Figure 5.) suggests that MO47 did not prime iPSCs to commit to one of the three germ layers.

The results derived from the ScoreCard assay confirmed that DMSO and MO47 pretreated iPSCs still harboured both molecular (pluripotency signature) and functional (differentiation signatures) pluripotency on the RNA level. However, ScoreCard only includes a specific collection of differentiation and pluripotency in each signature. Consequently, potential alterations in other markers that govern pluripotency and differentiation to the three germ layers have not been screened. A promising approach to

overcome this limitation would be RNA sequencing (RNA-seq), but this is expensive and complex in its interpretation.

It is generally questionable whether readouts on the RNA level also translate to protein function or, more importantly, to the actual cell state. It was, therefore, necessary to validate functional pluripotency also on the protein/cell state level through directed differentiation. Importantly, both DMSO and MO47 pretreated iPSCs could successfully be subjected to directed mesodermal (macrophages, pMac) and ectodermal (cerebral cortex neurons) differentiation. Based on a $CD11b^+/CD14^+/CD45^+$ phenotype with relevant morphological criteria (elongated, spindle-like form and multiple vesicles), adherent macrophages were obtained. Although this phenotype is very indicative of tissue-resident macrophages, the further validation by phagocytic activity via fluorescent zymosan as well as the expression of MHC-II is conceivable in this context (Gordon *et al.*, 2005; van Wilgenburg *et al.*, 2013). The same applies for the differentiation to cerebral cortex neurons. $TUJ1^+$ populations together with morphological criteria are compelling arguments for successful differentiation but also deserve further exploration until the post-mitotic stage of neurons.

This study also aimed to evaluate potential differences in the differentiation efficiency between MO47 pretreated iPSCs and control conditions. To this end, an experimental design including three actual biological triplicates allowing for robust quantitative data would have been informative. The readout of germ-line specific protein expression has already been used to measure the differentiation efficiency of differentiation protocols: Chambers *et al.* (2009), for example, measured the fraction of $TUJ1^+$ cells to appreciate the positive effects dual SMAD inhibition on neuronal induction.

It can further be argued that the differentiation to representatives of the endoderm would have corroborated this set of data. Importantly, (-)-Indolactam V, which is structurally

highly related to MO47, is currently used to enhance the differentiation to pancreatic progenitors (Chen *et al.*, 2009b; Johnson *et al.*, 2017). Thus, ectodermal and mesodermal differentiation were chosen over the endodermal germ layer. It is debatable whether the effects of a small molecule and its derivatives can be measured by a readout in which the compound constitutes an integral part itself.

In summary, the data sets of flow cytometry markers, RNA (ScoreCard) and cell state (directed differentiation assays) on functional pluripotency provide strong evidence on the preservation of functional pluripotency in the iPSC line OX1-18 upon treatment with MO47.

Chapter 6: Summary and final discussion

6.1 Summary of results

This research project argued for a chemical approach to overcome current limitations in iPSC 2D and 3D culturing. We hypothesised that the small molecules MO47 and (-)-Indolactam V would induce iPSC phenotypes that could be harnessed to improve culturing conditions. The results in this study suggest that (-)-Indolactam V and MO47 disrupt iPSC colonies and induce spread phenotypes in 2D culture. Further investigation is required to unravel the intricacies of the mechanisms of action and to explore the potential of these phenotypes for 2D and 3D culturing. This study further provides evidence for the preservation of key iPSC characteristics upon serial pretreatment with MO47.

Firstly, as a proof-of-principle, the phenotypes induced by (-)-Indolactam V and MO47 were assessed morphologically according to previously established criteria. Both compounds induced strong, reproducible and reversible phenotypes (Figures 3.1 and 3.2). Although we could not confirm contact-independence, the cells were no longer in tightly packed colonies (Figure 3.3). Remodelling of the actin cytoskeleton, including conspicuous stress fibres, and a decrease in cell packing were indicative of increased cell spreading (Figures 3.3 and 3.5). Despite remodelling processes, the disruption of E-cadherin mediated cell-cell adhesion could not be confirmed as focal adhesions were still present in the treated conditions (Figure 3.5).

In a second step, we endeavoured to elucidate the mechanism of actions of (-)-Indolactam V and MO47 and considered them as two distinct chemical entities. Based on the observations of the morphological changes, we hypothesised a link between PKC

activation and E-cadherin. Focusing on PKC, we confirmed the expression of cPKCs, nPKCs and aPKCs in iPSCs using qRT-PCR (Figure 4.1). Moreover, the phenotypic effects could be abrogated when treating iPSCs with (-)-Indolactam V or MO47 in combination with the PKC inhibitor Gö6983 but not with Gö6976 (Figures 4.2 and 4.3). Considering E-cadherin, the findings were neither indicative of the internalisation (Figures 4.4 and 4.5) nor the cleavage of E-cadherin at its ectodomain-membrane interface (Figure 4.6) upon treatment. Moreover, a potential link between PKC activation and E-cadherin could neither be proven nor refuted as the role of E-cadherin in the morphological change remains unresolved. Finally, (-)-Indolactam V clearly induced pro-apoptotic effects in iPSCs (Figure 4.8). Since (-)-Indolactam V's cytotoxicity rules it out as a compound worth pursuing for the application in 2D or 3D iPSC culturing, we decided to exclude it from subsequent work.

In the final chapter, self-renewal capacity, and molecular and functional pluripotency of MO47 pretreated iPSCs were assessed. MO47 pretreated iPSCs maintained an actively cycling state as assessed by the marker KI-67 (Figures 5.2 and 5.3). Assessing pluripotency markers using flow cytometry (Figure 5.4) and mRNA (ScoreCard, Figure 5.7), iPSCs still harboured molecular and functional pluripotency; upon spontaneous differentiation, these iPSCs were also positive for the gene signatures of all three germ layers (Figures 5.7 and 5.8). When analysing functional pluripotency directly through directed differentiation, MO47 pretreated iPSCs could also commit to macrophages (Figures 5.10 and 5.11) and primitive cerebral cortical neurons (Figures 5.13 and 5.14).

6.2 Implication and future challenges

This research project paves the way for further studies on MO47 and other chemical approaches in 2D and 3D iPSC culture. Importantly, the morphological studies shed a new light on small molecules and their potential to harness the plasticity of iPSCs (Davies

et al., 2015). Different treatment conditions in this study induced a spectrum of different morphologies, including colony-dependent and colony-independent phenotypes. Notably, despite their phenotypic diversity, these iPSCs were in accordance with a *bona fide* pluripotent cell state. It is conceivable that the spreading iPSCs could also be harnessed for other applications. The disruption of dense colonies might facilitate the picking of clones in 2D.

In this study, MO47 was only applied in 2D culture. Therefore, it remains open whether MO47 is amenable to scaleup and whether the biological changes seen in 2D are relevant for 3D. Clearly, 2D and 3D culturing systems must be considered as two distinct systems, and physiological differences between 2D and 3D are especially important for primary cells, which are highly sensitive to their microenvironment (Couture, 2010; Watt *et al.*, 2013). Nonetheless, the effects of MO47 would be expected to increase contact-independency in 3D and preliminary data in our group suggests that aggregates are reduced in the presence of MO47. Further assays should assess the size and number of iPSC aggregates in presence and absence of MO47, followed by tests in stirred bioreactors at increasing scale and increasing cell densities (Kropp *et al.*, 2016; Zweigerdt *et al.*, 2011). It would also be predicted that addition of MO47 would inhibit EB formation in Aggrewells^{TM}.

From a biological perspective, the question whether epithelial-mesenchymal transition-like regulatory molecular mechanisms account for the emergence of a spread, flat morphology is intriguing. Thus, other adhesive key molecules including claudin, occludin, ZO1 and ZO2, p120 cadherin, β-catenin, cross-talk to WNT signalling, as well as gene signatures indicative of a cadherin switch, deserve further attention (Lamouille *et al.*, 2014; Moreno-Bueno *et al.*, 2009; Nelson *et al.*, 2004). This might also help to elucidate the importance of the cytoskeleton and its influence on stem cell fate (Narva *et*

al., 2017). Eventually, it may be useful to extend the studies of MO47 to naïve iPSCs in order to understand mechanistic differences better. This is especially important since in mouse PSCs, a naïve pluripotency model, contact-independent cultures have already been generated using peptide inhibitors (Segal *et al.*, 2017; Soncin *et al.*, 2009).

Unravelling the mechanistic pharmacology that underlies (-)-Indolactam V and MO47 is of paramount importance since *de facto* knowing a molecule means knowing its targets (Bunnage *et al.*, 2015; Chen *et al.*, 2006). To decipher the subtle isoform specificity of the compounds, a genetic strategy, potentially via CRISPR/Cas9 knockouts, is most promising, and genetic tools have already been used in various PKC studies (Dempsey *et al.*, 2000; Heemskerk *et al.*, 2011). In addition to MO47 itself, the study of structurally related chemicals and derivatives as well as small molecules with similar effects hold great potential. Inducing a spread phenotype with MO47 may be a first cornerstone, which, in combination with other molecules, may allow further disruption of cell-cell adhesions to finally create a truly contact-independent culture. Notably, in the past, many positive effects of small molecules could only be harnessed through their synergistic effects (Ebrahimi, 2016; Liu *et al.*, 2016; Yu *et al.*, 2014).

Moreover, technical considerations of iPSC technology need to accompany the chemical and biological studies. An ideal molecule would display robust effects on iPSCs independent of its solvent. This is especially important since the repertoire of media has been increasing in recent years (Chen *et al.*, 2014). Small molecules are only amenable to scale-up if they are compatible with the medium that is used in the scaleup technology. GMP-compatible and xeno-free media, which allow for the generation of clinical-grade iPSC-derived cells, are likely to become the state of the art in the future (Chen *et al.*, 2014). Thus, in our case, testing whether MO47 is also compatible with other media such as E8, which are free of serum albumin, is of paramount importance (Chen *et al.*, 2014).

The application of small molecules in long-term culturing requires karyotypic stability of iPSCs. Finally, the stability of the chemical during long culturing periods is important.

6.3 Therapeutic implications

iPSC technology presents a real paradigm shift for modern medicine and holds considerable value for unmet clinical needs. The growing application for pathophysiological studies (Kim *et al.*, 2013; Passier *et al.*, 2016; Stepniewski *et al.*, 2015), safety pharmacology (Kandasamy *et al.*, 2015; Matsa *et al.*, 2016; Sirenko *et al.*, 2017), and drug screens (Grskovic *et al.*, 2011; Lee *et al.*, 2012) testifies to the significance of iPSC technology in research and medicine (Robinton *et al.*, 2012). The first clinical trials (Kimbrel *et al.*, 2015), including the treatment of age-related macular degeneration (Reardon *et al.*, 2014), spinal cord injuries (Assinck *et al.*, 2017), Parkinsons's disease (Cyranoski, 2017; Kimbrel *et al.*, 2015), diabetes (Chen *et al.*, 2016; Rezania *et al.*, 2014), and heart disease (Chen *et al.*, 2016) already require incredible numbers of iPSCs (Adil *et al.*, 2017; Jenkins *et al.*, 2015; Kropp *et al.*, 2016).

The increasing prevalence of many of these fundamental health issues raises the question as to how sufficient numbers of iPSCs will be manufactured for potential therapeutic applications (Jonas, 2014; Mayer-Davis *et al.*, 2017; Trounson *et al.*, 2016). Every step in the direction of more efficient culturing will increase our ability to obtain the number of desired cells (Chen *et al.*, 2014). Moreover, the potential development of new medicines in the field, including cell therapeutics, is likely to give rise to financial issues. Thus, affordable, safe and GMP-compliant technologies are necessary to increase access to treatment for everyone. The development of compounds such as MO47 will allow the field to advance and empower iPSC technology in a global context.

Appendices

Appendix Chapter 1

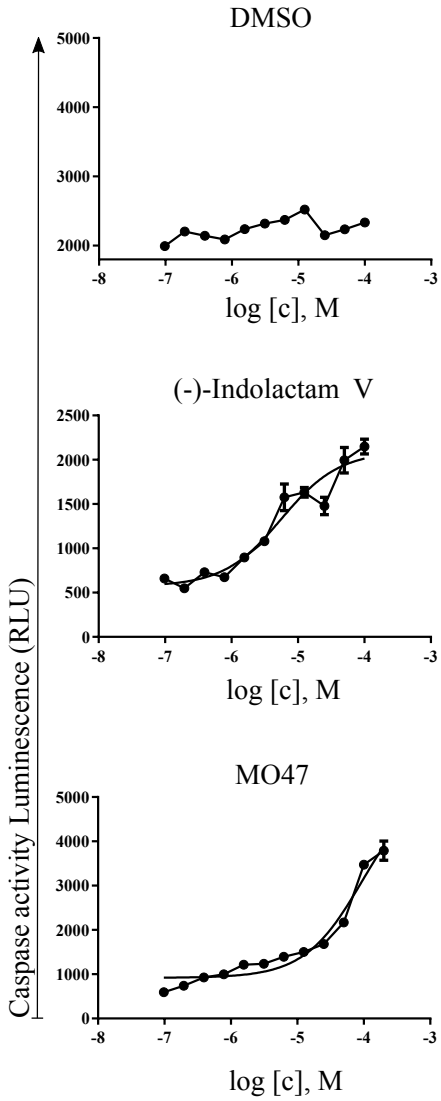

Figure III | Assessing pro-apoptotic effects of (-)-Indolactam V and MO47 via their caspase activity.

To determine the IC_{50} values for apoptosis in a cell-based assay, iPSCs were treated for 24h with (-)-Indolactam V and MO47 and the caspase activity was analysed using the Caspase-Glo® 3/7 Assay kit according to the manufacturer's protocol. The luminescence is proportional to the caspase-3 activity. The IC_{50} values for apoptosis were determined using the software Graphpad Prism. (-)-Indolactam V: IC_{50} = 5μM; MO47: IC_{50} = 94μM. The assay and its analysis were entirely performed by Dr Laurence Silpa, a post-doctoral research associate in our laboratory.

Appendix Chapter 4

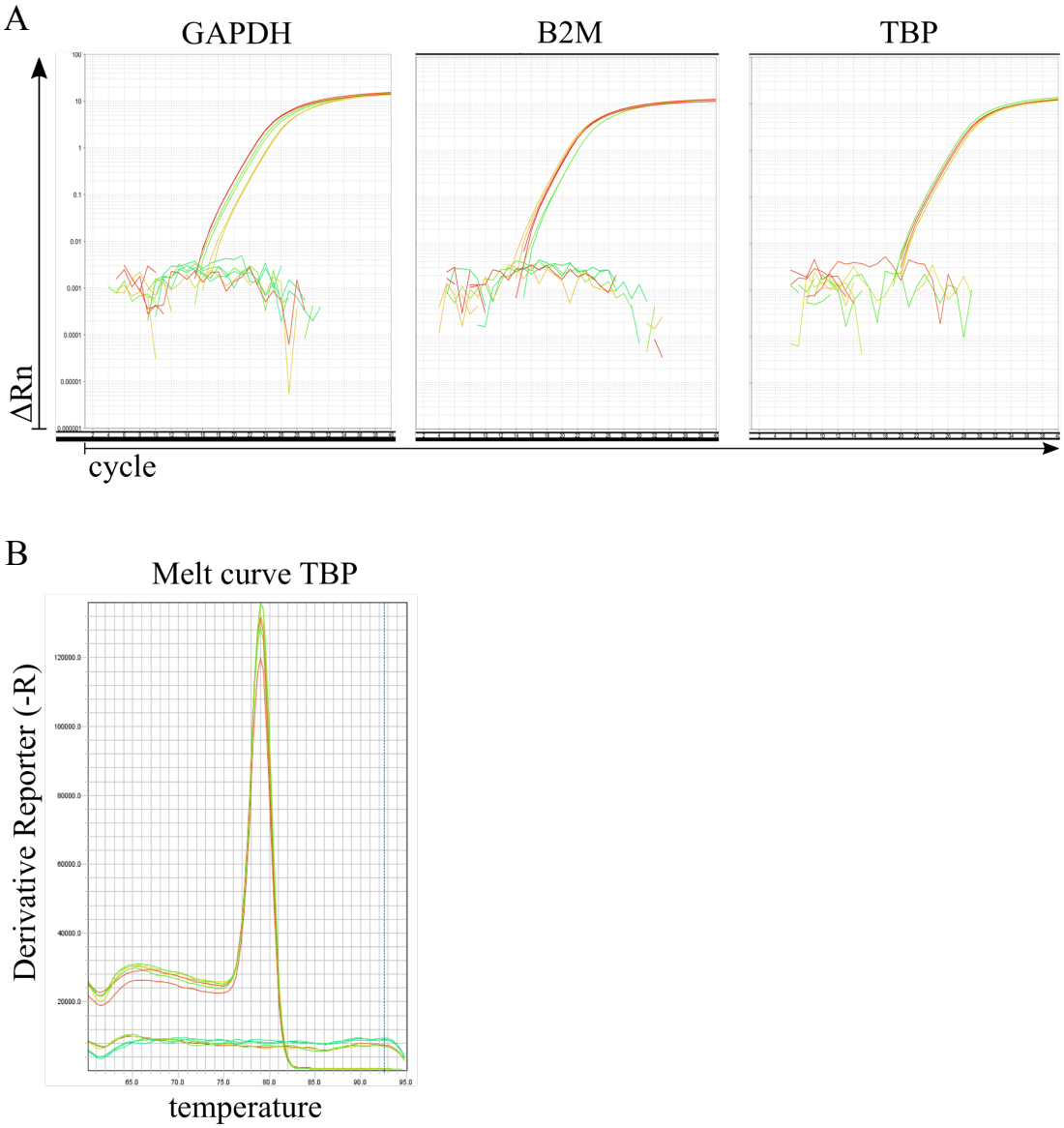

Figure IV.1 | Selecting an endogenous control for qRT-PCR.
To select an appropriate endogenous control, iPSCs were treated for 72h with 1µM (-)-Indolactam V, MO47 and 0.1% DMSO. Upon RNA extraction, cDNA was generated and loaded for qRT-PCR. The primer pairs of three different endogenous controls were tested: Glyceraldehyde 3-phosphate dehydrogenase (GAPDH), β-2 microglobulin (B2M) and TATA-binding protein (TBP). **(A)** Shown are the amplification curves of the three different endogenous controls for (-)-Indolactam V, MO47 and DMSO 72h (and their negative controls). The amplification curves for TBP are most robust. **(B)** The melt curve for TBP confirms the presence of a single amplicon.

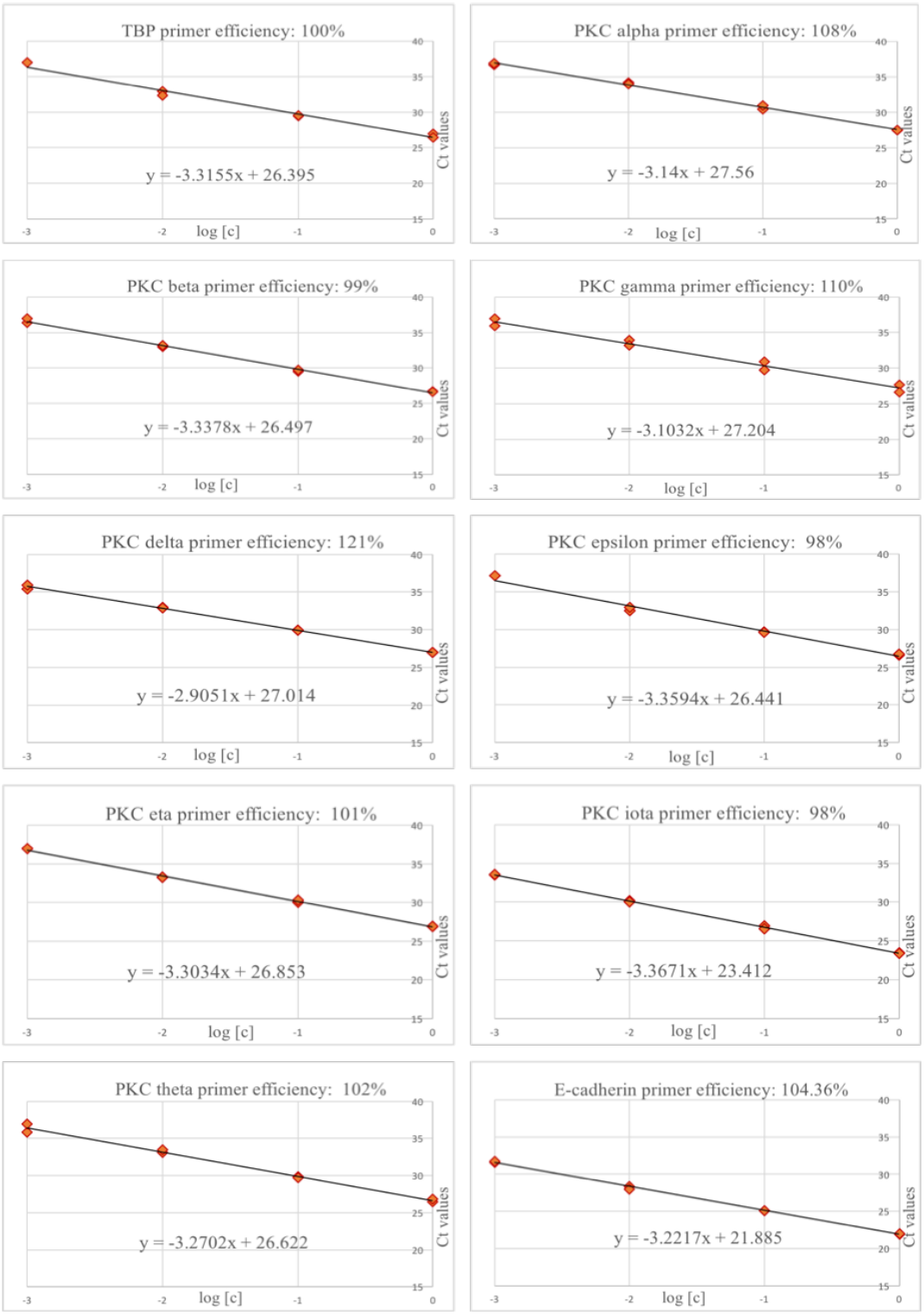

Figure IV.2 | Determining the efficiency of PKC and E-cadherin primer pairs. Shown are primer efficiency curves for the following primer pairs: PKA alpha, PKC beta, PKC gamma, PKC delta, PKC epsilon, PKC eta, PKC theta, PKC iota and E-cadherin. The efficiency of each primer pair was determined through serial cDNA dilutions (10×) from 1 to 0.001. Shown are the Ct values for each dilution. The efficiency was calculated according to the formula: $E = 10^{-1/slope}$.

Appendix Chapter 5

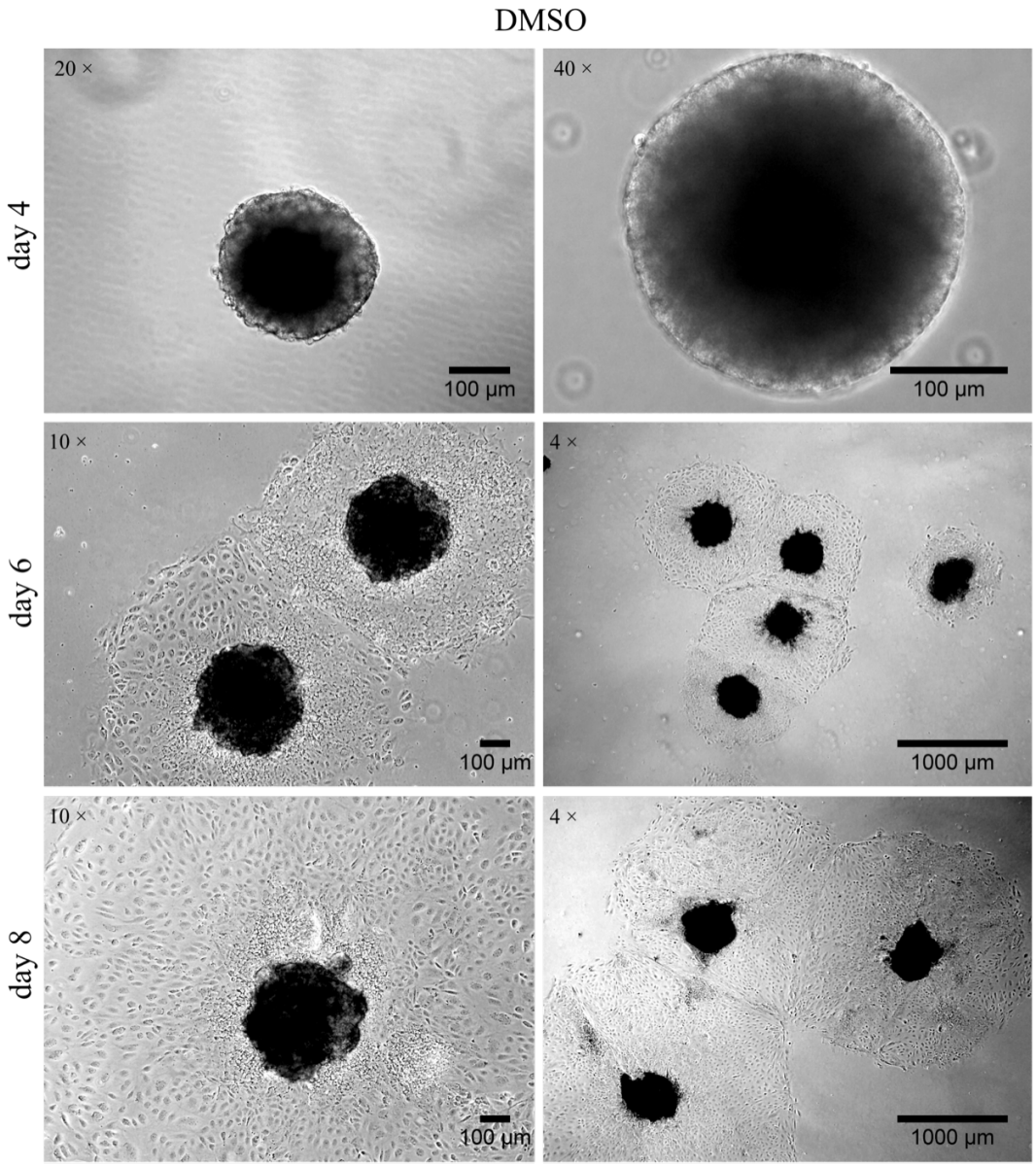

Figure V.1 | Spontaneous differentiation of DMSO pretreated iPSCs, days 4-8. Shown is the spontaneous differentiation of DMSO pretreated iPSCs. On day 4, spin-EBs are transferred from Aggrewells™ to a with Geltrex™ precoated dish (upper panel). On day 6, the EBs have attached and the cells start to grow out from the centre of the EBs (middle panel). This growth is progressive (day 8, lower panel). Phase contrast; magnifications and scale bars as indicated.

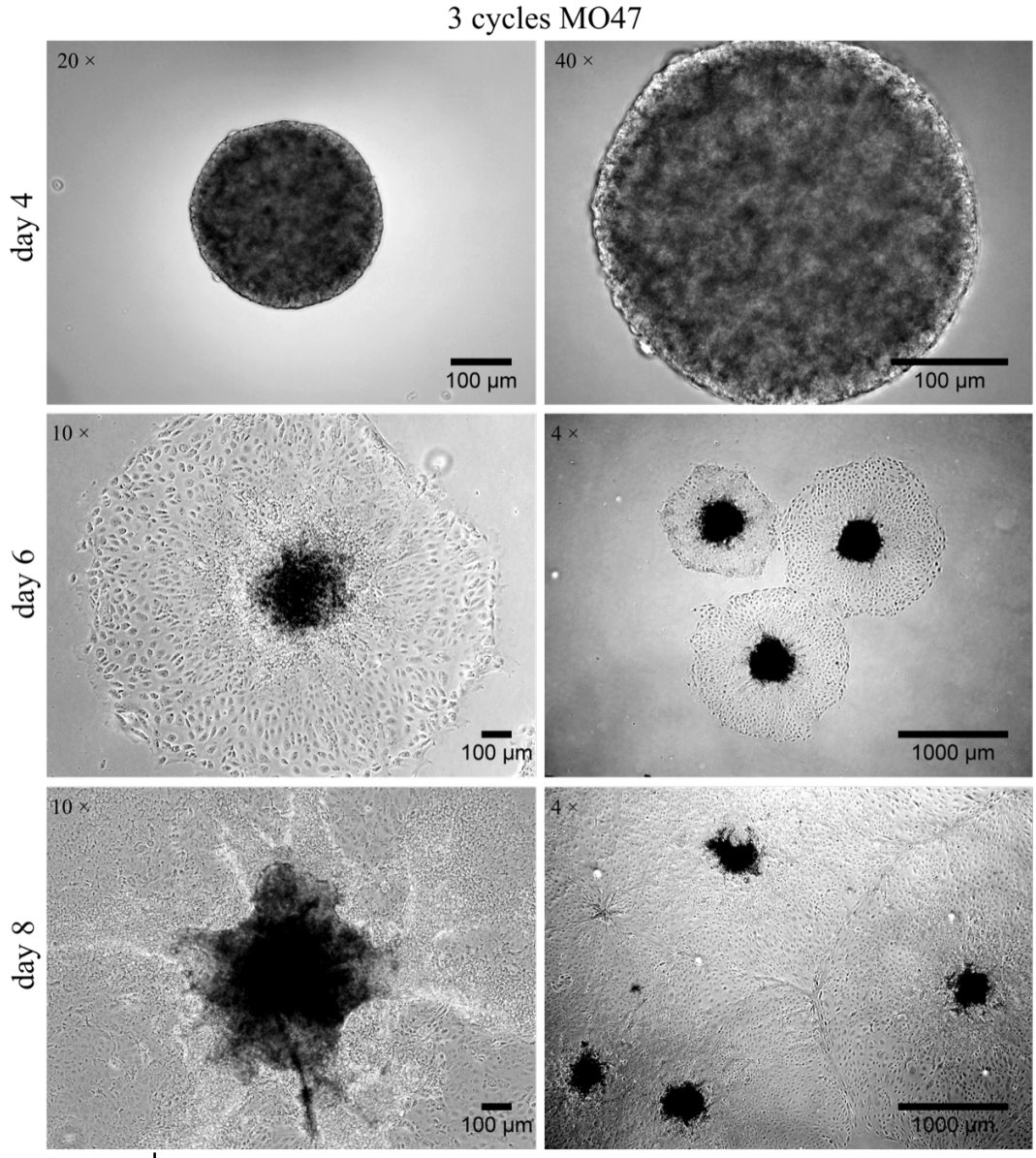

Figure V.2 | Spontaneous differentiation of MO47 pretreated iPSCs, days 4-8.
Shown is the spontaneous differentiation of MO47 pretreated iPSCs. On day 4, spin-EBs are transferred from Aggrewells™ to a with Geltrex™ precoated dish (upper panel). On day 6, the EBs have attached and cells start to grow out from the centre of the EBs (middle panel). This growth is progressive (day 8, lower panel). Phase contrast; magnifications and scale bars as indicated.

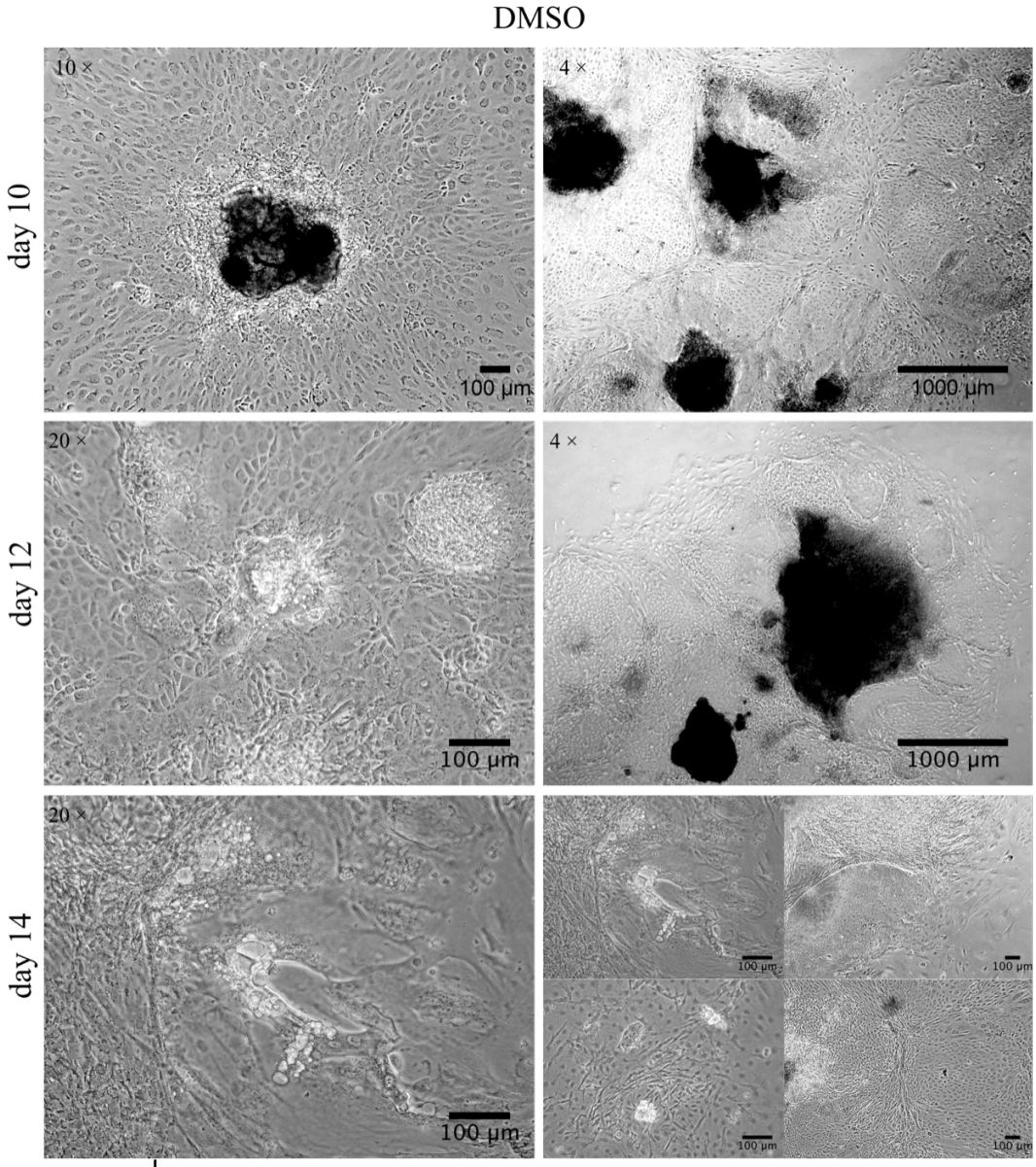

Figure V.3 | Spontaneous differentiation of DMSO pretreated iPSCs, days 10-14. Shown is the spontaneous differentiation of DMSO pretreated iPSCs. On day 10 (upper panel), different cell morphologies can be identified. The cells around the EBs are tightly packed. On day 12 (middle panel), the cell density has increased and the cell populations become increasingly heterogenous. Several populations are marked by white fat cells, which are indicative of adipocytes (mesoderm). On day 14 (lower panel), the morphological heterogeneity is even more conspicuous, suggesting the continuation of spontaneous differentiation. Phase contrast; magnifications and scale bars as indicated.

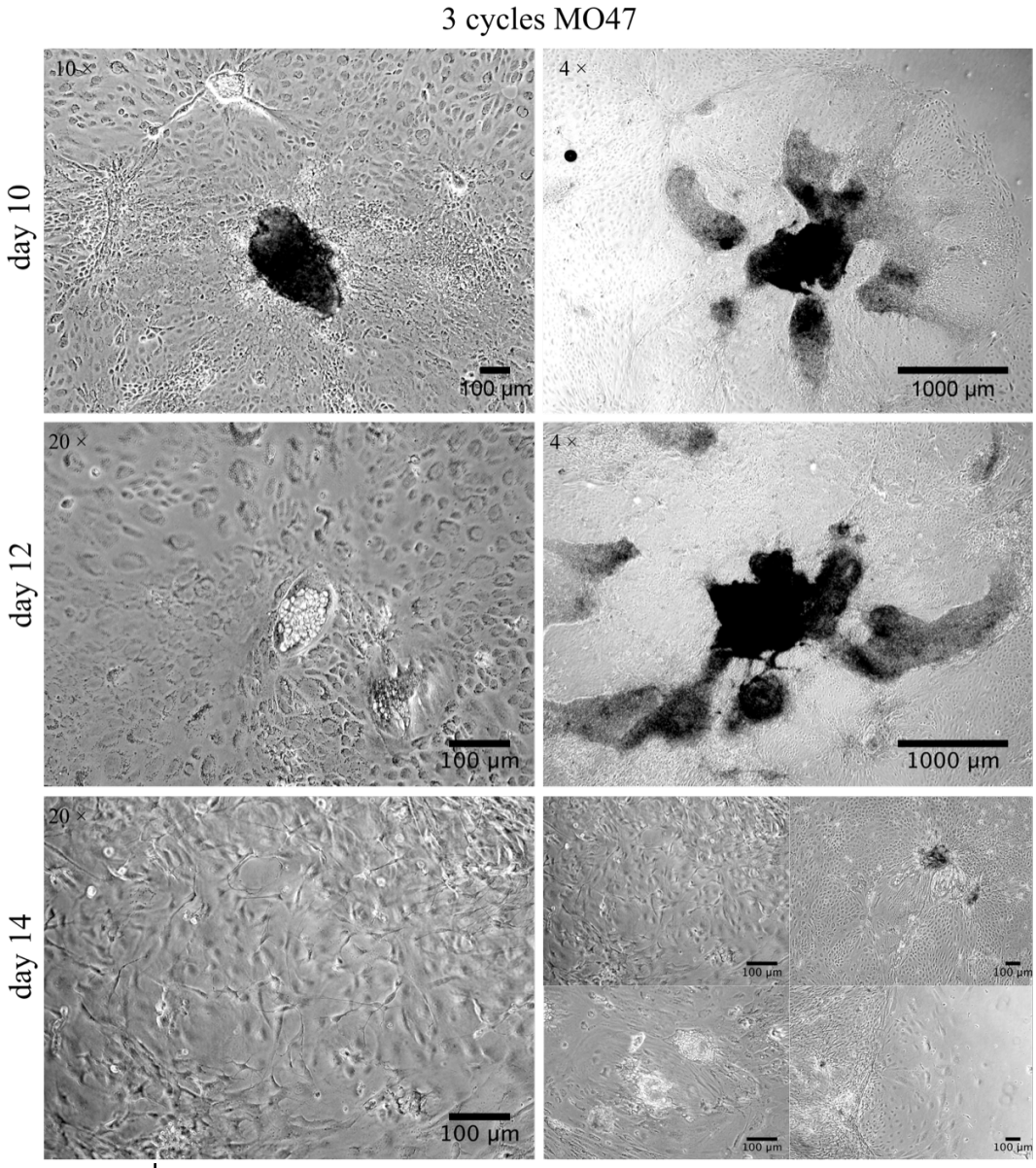

Figure V.4 | Spontaneous differentiation of MO47 pretreated iPSCs, days 10-14. Shown is the spontaneous differentiation of MO47 pretreated iPSCs. On day 10 (upper panel), different cell morphologies around the centre of the EBs can be identified. The cells are tightly packed. On day 12 (middle panel), the entire population appears to be more heterogenous. Populations bearing white fat cells in the centre are indicative of adipocytes (mesoderm). On day 14 (lower panel), the morphological heterogeneity is even more conspicuous. In addition to fat white cells, populations with neurite-like morphology can be identified (lower panel, left). Phase contrast; magnifications and scale bars as indicated.

Table V.1 | ScoreCard assay Ct values

Gene	Category	DMSO undiff. (1)	MO47 undiff. (2)	DMSO diff. (3)	MO47 diff. (4)
ACTB	Controls	19.16	19.19	19.23	18.98
ACTB	Controls	24.23	22.85	22.97	22.39
ACTB	Controls	23.72	22.96	22.70	21.80
ACTB	Controls	19.56	19.56	19.57	18.99
CTCF	Controls	25.94	25.96	26.37	26.28
EP300	Controls	25.85	25.94	26.58	26.30
SMAD1	Controls	27.78	27.97	27.66	27.75
CDH9	Ectoderm	33.41	32.42	32.90	32.92
COL2A1	Ectoderm	30.35	29.92	25.95	27.21
DMBX1	Ectoderm	32.97	30.87	31.26	31.06
DRD4	Ectoderm	28.41	27.91	26.97	28.57
EN1	Ectoderm	36.95	35.97	31.10	31.74
LMX1A	Ectoderm	35.95	34.71	28.41	31.49
MAP2	Ectoderm	29.27	28.83	27.96	29.76
MYO3B	Ectoderm	37.02	35.91	31.57	32.42
NOS2	Ectoderm	30.83	30.97	27.86	29.43
NR2F1/NR2F2	Ectoderm	36.96	34.30	24.14	26.39
NR2F2	Ectoderm	36.96	35.25	25.01	24.73
OLFM3	Ectoderm	33.95	33.54	30.16	32.80
PAPLN	Ectoderm	28.79	27.98	31.11	31.48
PAX3	Ectoderm	36.99	40.00	25.88	28.34
PAX6	Ectoderm	35.84	34.23	26.98	29.86
POU4F1	Ectoderm	34.87	35.07	28.98	30.98
PRKCA	Ectoderm	27.19	26.92	28.44	28.69
SDC2	Ectoderm	25.01	25.47	25.74	25.91
SOX1	Ectoderm	36.93	35.90	33.08	36.96
TRPM8	Ectoderm	36.48	35.97	34.36	35.84
WNT1	Ectoderm	37.01	35.77	25.83	27.67
ZBTB16	Ectoderm	33.83	33.97	27.74	30.43
AFP	Endoderm	37.05	40.00	24.24	22.16
CABP7	Endoderm	33.65	33.65	32.07	32.99
CDH20	Endoderm	34.44	34.92	28.96	30.57
CLDN1	Endoderm	29.88	29.91	27.96	28.30
CPLX2	Endoderm	31.86	31.66	29.92	31.41
ELAVL3	Endoderm	31.59	31.98	29.65	30.77
EOMES	Endoderm	34.92	34.89	27.94	28.54
FOXA1	Endoderm	35.69	35.99	29.30	29.62
FOXA2	Endoderm	35.78	37.01	27.09	27.90
FOXP2	Endoderm	35.76	35.94	30.30	31.01
GATA4	Endoderm	33.56	34.29	26.95	26.38
GATA6	Endoderm	35.81	35.63	26.30	25.92
HHEX	Endoderm	30.19	29.64	29.99	29.98
HMP19	Endoderm	34.72	34.95	33.81	34.60
HNF1B	Endoderm	33.85	33.77	29.90	29.96
HNF4A	Endoderm	36.99	35.41	25.44	25.02
KLF5	Endoderm	32.64	32.61	28.94	28.47
LEFTY1	Endoderm	33.95	33.77	33.81	34.39
LEFTY2	Endoderm	33.92	34.49	32.62	33.00
NODAL	Endoderm	30.95	31.87	27.95	28.94
PHOX2B	Endoderm	40.00	40.00	34.60	35.99

Table V.1 | ScoreCard assay Ct values (continued)

Gene	Category	DMSO undiff. (1)	MO47 undiff. (2)	DMSO diff. (3)	MO47 diff. (4)
FGF4	Mesendoderm	32.20	32.49	29.07	29.96
GDF3	Mesendoderm	29.43	29.94	27.50	28.98
NPPB	Mesendoderm	36.97	35.53	25.24	24.47
NR5A2	Mesendoderm	28.82	28.81	31.66	31.96
PTHLH	Mesendoderm	35.66	36.97	29.70	27.40
T	Mesendoderm	35.99	35.50	30.08	30.07
ABCA4	Mesoderm	35.93	35.62	29.12	29.45
ALOX15	Mesoderm	30.67	30.53	26.94	25.70
BMP10	Mesoderm	40.00	40.00	32.98	32.92
CDH5	Mesoderm	34.83	35.01	26.87	26.01
CDX2	Mesoderm	35.38	35.99	27.38	28.00
COLEC10	Mesoderm	33.67	33.73	31.95	29.88
ESM1	Mesoderm	40.00	40.00	29.95	29.96
FCN3	Mesoderm	32.89	32.63	31.95	31.49
FOXF1	Mesoderm	36.42	36.95	27.57	26.74
HAND1	Mesoderm	36.43	36.96	22.91	22.47
HAND2	Mesoderm	36.71	35.92	25.97	25.04
HEY1	Mesoderm	32.24	31.94	26.68	27.42
HOPX	Mesoderm	37.21	35.56	23.10	22.51
IL6ST	Mesoderm	29.88	29.97	25.99	24.87
NKX2-5	Mesoderm	35.56	35.95	32.43	31.67
ODAM	Mesoderm	36.78	37.10	27.60	28.33
PDGFRA	Mesoderm	32.76	32.51	26.96	26.73
PLVAP	Mesoderm	33.71	33.96	28.14	26.98
RGS4	Mesoderm	34.53	34.94	26.93	26.88
SNAI2	Mesoderm	32.83	33.24	25.95	25.28
TBX3	Mesoderm	33.03	32.57	24.19	23.94
TM4SF1	Mesoderm	34.40	34.86	28.99	27.87
CD44	Other	40.00	40.00	40.00	40.00
JARID2	Other	23.90	23.59	25.38	25.97
MYC	Other	25.96	25.49	26.96	25.89
SEV	Other	40.00	40.00	40.00	40.00
CXCL5	Self-renewal	25.96	26.30	30.56	31.29
DNMT3B	Self-renewal	20.68	20.87	22.95	23.89
HESX1	Self-renewal	29.39	29.33	31.75	31.94
IDO1	Self-renewal	25.93	25.93	30.61	31.62
LCK	Self-renewal	25.73	25.95	29.68	30.65
NANOG	Self-renewal	24.93	24.92	26.06	27.41
POU5F1	Self-renewal	28.47	28.60	31.21	31.95
SOX2	Self-renewal	23.19	22.95	24.57	26.78
TRIM22	Self-renewal	25.92	26.55	28.58	28.18

Bibliography

Abujarour R, Valamehr B, Robinson M, Rezner B, Vranceanu F, & Flynn P (2013). Optimized surface markers for the prospective isolation of high-quality hiPSCs using flow cytometry selection. Sci Rep 3**:** 1179.

Adil MM, & Schaffer DV (2017). Expansion of human pluripotent stem cells. Current Opinion in Chemical Engineering 15**:** 24-35.

Akagawa KS, Komuro I, Kanazawa H, Yamazaki T, Mochida K, & Kishi F (2006). Functional heterogeneity of colony-stimulating factor-induced human monocyte-derived macrophages. Respirology 11 Suppl**:** S32-36.

Akhtar N, & Hotchin NA (2001). RAC1 regulates adherens junctions through endocytosis of E-cadherin. Molecular Biology of the Cell 12**:** 847-862.

Alvi F, Idkowiak-Baldys J, Baldys A, Raymond JR, & Hannun YA (2007). Regulation of membrane trafficking and endocytosis by protein kinase C: emerging role of the pericentrion, a novel protein kinase C-dependent subset of recycling endosomes. Cell Mol Life Sci 64**:** 263-270.

Andrews PW, Banting G, Damjanov I, Arnaud D, & Avner P (1984). Three monoclonal antibodies defining distinct differentiation antigens associated with different high molecular weight polypeptides on the surface of human embryonal carcinoma cells. Hybridoma 3**:** 347-361.

Andrews PW, Goodfellow PN, Shevinsky LH, Bronson DL, & Knowles BB (1982). Cell-surface antigens of a clonal human embryonal carcinoma cell line: morphological and antigenic differentiation in culture. Int J Cancer 29**:** 523-531.

Anilkumar N (2003). Interaction of fascin and protein kinase Cα: a novel intersection in cell adhesion and motility. EMBO Journal 22**:** 5390-5402.

Arrowsmith CH, Audia JE, Austin C, Baell J, Bennett J, Blagg J*, et al.* (2015). The promise and peril of chemical probes. Nat Chem Biol 11**:** 536-541.

Assinck P, Duncan GJ, Hilton BJ, Plemel JR, & Tetzlaff W (2017). Cell transplantation therapy for spinal cord injury. Nat Neurosci 20**:** 637-647.

Awadelkarim KD, Callens C, Rosse C, Susini A, Vacher S, Rouleau E*, et al.* (2012). Quantification of PKC family genes in sporadic breast cancer by qRT-PCR: evidence that PKCiota/lambda overexpression is an independent prognostic factor. Int J Cancer 131**:** 2852-2862.

Baell J, & Walters MA (2014). Chemistry: Chemical con artists foil drug discovery. Nature 513**:** 481-483.

Ben-David U, Gan QF, Golan-Lev T, Arora P, Yanuka O, Oren YS*, et al.* (2013). Selective elimination of human pluripotent stem cells by an oleate synthesis inhibitor discovered in a high-throughput screen. Cell Stem Cell 12**:** 167-179.

Bock C, Kiskinis E, Verstappen G, Gu H, Boulting G, Smith ZD*, et al.* (2011). Reference Maps of human ES and iPS cell variation enable high-throughput characterization of pluripotent cell lines. Cell 144**:** 439-452.

Boyer LA, Lee TI, Cole MF, Johnstone SE, Levine SS, Zucker JP*, et al.* (2005). Core transcriptional regulatory circuitry in human embryonic stem cells. Cell 122**:** 947-956.

Brimble SN, Sherrer ES, Uhl EW, Wang E, Kelly S, Merrill AH, Jr.*, et al.* (2007). The cell surface glycosphingolipids SSEA-3 and SSEA-4 are not essential for human ESC pluripotency. Stem Cells 25**:** 54-62.

Brodie C (2003). Regulation of cell apoptosis by protein kinase c δ. Apoptosis : An International Journal on Programmed Cell Death 8**:** 19-27.

Bucci C, Thomsen P, Nicoziani P, McCarthy J, & van Deurs B (2000). Rab7: a key to lysosome biogenesis. Mol Biol Cell 11**:** 467-480.

Buchrieser J, James W, & Moore MD (2017). Human Induced Pluripotent Stem Cell-Derived Macrophages Share Ontogeny with MYB-Independent Tissue-Resident Macrophages. Stem Cell Reports 8**:** 334-345.

Bunnage ME, Gilbert AM, Jones LH, & Hett EC (2015). Know your target, know your molecule. Nat Chem Biol 11**:** 368-372.

Caccamo D, Katsetos CD, Herman MM, Frankfurter A, Collins VP, & Rubinstein LJ (1989). Immunohistochemistry of a spontaneous murine ovarian teratoma with neuroepithelial differentiation. Neuron-associated beta-tubulin as a marker for primitive neuroepithelium. Laboratory Investigation 60**:** 390-398.

Cahan P, & Daley GQ (2013). Origins and implications of pluripotent stem cell variability and heterogeneity. Nat Rev Mol Cell Biol 14**:** 357-368.

Callaerts P, Halder G, & Gehring WJ (1997). PAX-6 in development and evolution. Annu Rev Neurosci 20**:** 483-532.

Cao N, Huang Y, Zheng J, Spencer CI, Zhang Y, Fu JD*, et al.* (2016). Conversion of human fibroblasts into functional cardiomyocytes by small molecules. Science 352**:** 1216-1220.

Carpenter MK, Frey-Vasconcells J, & Rao MS (2009). Developing safe therapies from human pluripotent stem cells. Nat Biotechnol 27**:** 606-613.

Cavallaro U, & Dejana E (2011). Adhesion molecule signalling: not always a sticky business. Nat Rev Mol Cell Biol 12**:** 189-197.

Chambers I, Colby D, Robertson M, Nichols J, Lee S, Tweedie S*, et al.* (2003). Functional expression cloning of Nanog, a pluripotency sustaining factor in embryonic stem cells. Cell 113**:** 643-655.

Chambers SM, Fasano CA, Papapetrou EP, Tomishima M, Sadelain M, & Studer L (2009). Highly efficient neural conversion of human ES and iPS cells by dual inhibition of SMAD signaling. Nat Biotechnol 27**:** 275-280.

Chan EM, Ratanasirintrawoot S, Park IH, Manos PD, Loh YH, Huo H*, et al.* (2009). Live cell imaging distinguishes bona fide human iPS cells from partially reprogrammed cells. Nat Biotechnol 27**:** 1033-1037.

Chen CL, & Chen HC (2009a). Functional suppression of E-cadherin by protein kinase Cdelta. J Cell Sci 122**:** 513-523.

Chen G, Hou Z, Gulbranson DR, & Thomson JA (2010). Actin-myosin contractility is responsible for the reduced viability of dissociated human embryonic stem cells. Cell Stem Cell 7**:** 240-248.

Chen IY, Matsa E, & Wu JC (2016). Induced pluripotent stem cells: at the heart of cardiovascular precision medicine. Nat Rev Cardiol 13**:** 333-349.

Chen KG, Mallon BS, McKay RD, & Robey PG (2014). Human pluripotent stem cell culture: considerations for maintenance, expansion, and therapeutics. Cell Stem Cell 14**:** 13-26.

Chen S, Borowiak M, Fox JL, Maehr R, Osafune K, Davidow L*, et al.* (2009b). A small molecule that directs differentiation of human ESCs into the pancreatic lineage. Nat Chem Biol 5**:** 258-265.

Chen S, Do JT, Zhang Q, Yao S, Yan F, Peters EC*, et al.* (2006). Self-renewal of embryonic stem cells by a small molecule. Proc Natl Acad Sci U S A 103**:** 17266-17271.

Cohen DE, & Melton D (2011). Turning straw into gold: directing cell fate for regenerative medicine. Nat Rev Genet 12**:** 243-252.

Couture LA (2010). Scalable pluripotent stem cell culture. Nat Biotechnol 28**:** 562-563.

Csukai M, & Mochly-Rosen D (1999). Pharmacologic modulation of protein kinase C isozymes: the role of RACKs and subcellular localisation. Pharmacol Res 39**:** 253-259.

Culty M, Miyake K, Kincade PW, Silorski E, Butcher EC, & Underhill C (1990). The Hyaluronate Receptor Is a Member of the Cd44 (H-Cam) Family of Cell-Surface Glycoproteins. Journal of Cell Biology 111**:** 2765-2774.

Cvekl A, & Callaerts P (2017). PAX6: 25th anniversary and more to learn. Exp Eye Res 156**:** 10-21.

Cyranoski D (2017). Trials of embryonic stem cells to launch in China. Nature 546**:** 15-16.

Daley GQ, Lensch MW, Jaenisch R, Meissner A, Plath K, & Yamanaka S (2009). Broader implications of defining standards for the pluripotency of iPSCs. Cell Stem Cell 4**:** 200-201; author reply 202.

Davidson AJ, & Wood W (2016). Unravelling the Actin Cytoskeleton: A New Competitive Edge? Trends Cell Biol 26**:** 569-576.

Davies SG, Kennewell PD, Russell AJ, Seden PT, Westwood R, & Wynne GM (2015). Stemistry: the control of stem cells in situ using chemistry. J Med Chem 58**:** 2863-2894.

Davis MI, Hunt JP, Herrgard S, Ciceri P, Wodicka LM, Pallares G*, et al.* (2011). Comprehensive analysis of kinase inhibitor selectivity. Nat Biotechnol 29**:** 1046-1051.

De Los Angeles A, Ferrari F, Xi R, Fujiwara Y, Benvenisty N, Deng H*, et al.* (2015). Hallmarks of pluripotency. Nature 525**:** 469-478.

Delaszlo SE, Ley SV, & Porter RA (1986). Synthetic Approaches to the Teleocidin-Related Tumor Promoters - a Total Synthesis of (+/-)-Indolactam-V. Journal of the Chemical Society-Chemical Communications**:** 344-346.

Dempsey EC, Newton AC, Mochly-Rosen D, Fields AP, Reyland ME, Insel PA*, et al.* (2000). Protein kinase C isozymes and the regulation of diverse cell responses. Am J Physiol Lung Cell Mol Physiol 279**:** L429-438.

Desbordes SC, & Studer L (2013). Adapting human pluripotent stem cells to high-throughput and high-content screening. Nat Protoc 8**:** 111-130.

Doetschman TC, Eistetter H, Katz M, Schmidt W, & Kemler R (1985). The in vitro development of blastocyst-derived embryonic stem cell lines: formation of visceral yolk sac, blood islands and myocardium. J Embryol Exp Morphol 87**:** 27-45.

Dowling CM, & Kiely PA (2015). Targeting Protein Kinase C Downstream of Growth Factor and Adhesion Signalling. Cancers (Basel) 7**:** 1271-1291.

Eastham AM, Spencer H, Soncin F, Ritson S, Merry CL, Stern PL*, et al.* (2007). Epithelial-mesenchymal transition events during human embryonic stem cell differentiation. Cancer Res 67**:** 11254-11262.

Ebrahimi B (2016). Chemical-only reprogramming to pluripotency. Frontiers in Biology 11**:** 75-84.

English AR, & Voeltz GK (2013). Rab10 GTPase regulates ER dynamics and morphology. Nature Cell Biology 15**:** 169-178.

Etzrodt M, Endele M, & Schroeder T (2014). Quantitative single-cell approaches to stem cell research. Cell Stem Cell 15**:** 546-558.

Fatehullah A, Tan SH, & Barker N (2016). Organoids as an in vitro model of human development and disease. Nat Cell Biol 18**:** 246-254.

Feng Y, Press B, & Wandinger-Ness A (1995). Rab 7: an important regulator of late endocytic membrane traffic. J Cell Biol 131**:** 1435-1452.

Frye SV (2010). The art of the chemical probe. Nat Chem Biol 6**:** 159-161.

Galvez T, Gilleron J, Zerial M, & O'Sullivan GA (2012). SnapShot: Mammalian Rab proteins in endocytic trafficking. Cell 151**:** 234-234 e232.

Ganellin CR, Jefferis R, & Roberts SM (2013). Introduction to Biological and Small Molecule Drug Research and Development Theory and Case Studies Preface. Introduction to Biological and Small Molecule Drug Research and Development: Theory and Case Studies**:** Xix-Xx.

Geiger B, Spatz JP, & Bershadsky AD (2009). Environmental sensing through focal adhesions. Nat Rev Mol Cell Biol 10**:** 21-33.

Gerdes J, Lemke H, Baisch H, Wacker HH, Schwab U, & Stein H (1984). Cell cycle analysis of a cell proliferation-associated human nuclear antigen defined by the monoclonal antibody Ki-67. J Immunol 133**:** 1710-1715.

Ghule PN, Medina R, Lengner CJ, Mandeville M, Qiao M, Dominski Z*, et al.* (2011). Reprogramming the pluripotent cell cycle: restoration of an abbreviated G1 phase in human induced pluripotent stem (iPS) cells. J Cell Physiol 226**:** 1149-1156.

Gillespie EJ, Ho CL, Balaji K, Clemens DL, Deng G, Wang YE*, et al.* (2013). Selective inhibitor of endosomal trafficking pathways exploited by multiple toxins and viruses. Proceedings of the National Academy of Sciences of the United States of America 110**:** E4904-4912.

Goerke A (2002). Induction of apoptosis by protein kinase C delta is independent of its kinase activity. Journal of biological chemistry 277**:** 32054-32062.

Goldstein LA, Zhou DF, Picker LJ, Minty CN, Bargatze RF, Ding JF*, et al.* (1989). A human lymphocyte homing receptor, the hermes antigen, is related to cartilage proteoglycan core and link proteins. Cell 56**:** 1063-1072.

Gordon S, Pluddemann A, & Martinez Estrada F (2014). Macrophage heterogeneity in tissues: phenotypic diversity and functions. Immunol Rev 262**:** 36-55.

Gordon S, & Taylor PR (2005). Monocyte and macrophage heterogeneity. Nat Rev Immunol 5**:** 953-964.

Griner EM, & Kazanietz MG (2007). Protein kinase C and other diacylglycerol effectors in cancer. Nat Rev Cancer 7**:** 281-294.

Grosshans BL, Ortiz D, & Novick P (2006). Rabs and their effectors: achieving specificity in membrane traffic. Proceedings of the National Academy of Sciences of the United States of America 103**:** 11821-11827.

Grskovic M, Javaherian A, Strulovici B, & Daley GQ (2011). Induced pluripotent stem cells--opportunities for disease modelling and drug discovery. Nat Rev Drug Discov 10**:** 915-929.

Grutz K, Seibler P, Weissbach A, Lohmann K, Carlisle FA, Blake DJ*, et al.* (2017). Faithful SGCE imprinting in iPSC-derived cortical neurons: an endogenous cellular model of myoclonus-dystonia. Sci Rep 7**:** 41156.

Gumbiner BM (1996). Cell adhesion: the molecular basis of tissue architecture and morphogenesis. Cell 84**:** 345-357.

Gumbiner BM (2005). Regulation of cadherin-mediated adhesion in morphogenesis. Nat Rev Mol Cell Biol 6**:** 622-634.

Haenseler W, Sansom SN, Buchrieser J, Newey SE, Moore CS, Nicholls FJ*, et al.* (2017). A Highly Efficient Human Pluripotent Stem Cell Microglia Model Displays a Neuronal-Co-culture-Specific Expression Profile and Inflammatory Response. Stem Cell Reports 8**:** 1727-1742.

Hamon M, Bierne H, & Cossart P (2006). Listeria monocytogenes: a multifaceted model. Nature Reviews Microbiology 4**:** 423-434.

Hashimoto S, Suzuki T, Dong HY, Yamazaki N, & Matsushima K (1999). Serial analysis of gene expression in human monocytes and macrophages. Blood 94**:** 837-844.

Hay ED (1995). An overview of epithelio-mesenchymal transformation. Acta Anat (Basel) 154**:** 8-20.

Healy L, Ruban L, & SpringerLink (Online service) (2015) *Atlas of Human Pluripotent Stem Cells in Culture*. Springer US : Imprint: Springer,. Boston, MA. Available from Full text from SpringerLink http://dx.doi.org/10.1007/978-1-4899-7507-2.

Heemskerk JW, Harper MT, Cosemans JM, & Poole AW (2011). Unravelling the different functions of protein kinase C isoforms in platelets. FEBS Lett 585**:** 1711-1716.

Heikkila J, & Akerman KE (1989). (-)-Indolactam V activates protein kinase C and induces changes in muscarinic receptor functions in SH-SY5Y human neuroblastoma cells. Biochem Biophys Res Commun 162**:** 1207-1213.

Henderson JK, Draper JS, Baillie HS, Fishel S, Thomson JA, Moore H*, et al.* (2002). Preimplantation human embryos and embryonic stem cells show comparable expression of stage-specific embryonic antigens. Stem Cells 20**:** 329-337.

Hendriks WT, Warren CR, & Cowan CA (2016). Genome Editing in Human Pluripotent Stem Cells: Approaches, Pitfalls, and Solutions. Cell Stem Cell 18**:** 53-65.

Hirota M, Suganuma M, Yoshizawa S, Horiuchi T, Nakayasu M, Hasegawa M*, et al.* (1987). Synthetic analogues (indolactams) of (-)-indolactam-V are new congeners of the teleocidin class of tumor promoters. Jpn J Cancer Res 78**:** 577-582.

Hockemeyer D, & Jaenisch R (2016). Induced Pluripotent Stem Cells Meet Genome Editing. Cell Stem Cell 18**:** 573-586.

Hughes CS, Postovit LM, & Lajoie GA (2010). Matrigel: a complex protein mixture required for optimal growth of cell culture. Proteomics 10**:** 1886-1890.

Igumenova TI (2015). Dynamics and Membrane Interactions of Protein Kinase C. Biochemistry 54**:** 4953-4968.

International Stem Cell Banking I (2009). Consensus guidance for banking and supply of human embryonic stem cell lines for research purposes. Stem Cell Rev 5**:** 301-314.

International Stem Cell I, Adewumi O, Aflatoonian B, Ahrlund-Richter L, Amit M, Andrews PW*, et al.* (2007). Characterization of human embryonic stem cell lines by the International Stem Cell Initiative. Nat Biotechnol 25**:** 803-816.

Ivanov AI, Nusrat A, & Parkos CA (2004). Endocytosis of epithelial apical junctional proteins by a clathrin-mediated pathway into a unique storage compartment. Mol Biol Cell 15**:** 176-188.

Jenkins MJ, & Farid SS (2015). Human pluripotent stem cell-derived products: advances towards robust, scalable and cost-effective manufacturing strategies. Biotechnol J 10**:** 83-95.

Johnson TC, & Siegel D (2017). Directing Stem Cell Fate: The Synthetic Natural Product Connection. Chem Rev.

Jonas JB (2014). Global prevalence of age-related macular degeneration. The Lancet Global Health 2**:** e65-e66.

Kandasamy K, Chuah JK, Su R, Huang P, Eng KG, Xiong S*, et al.* (2015). Prediction of drug-induced nephrotoxicity and injury mechanisms with human induced pluripotent stem cell-derived cells and machine learning methods. Sci Rep 5**:** 12337.

Kannagi R, Cochran NA, Ishigami F, Hakomori S, Andrews PW, Knowles BB*, et al.* (1983). Stage-specific embryonic antigens (SSEA-3 and -4) are epitopes of a unique globo-series ganglioside isolated from human teratocarcinoma cells. EMBO J 2**:** 2355-2361.

Karlsson KR, Cowley S, Martinez FO, Shaw M, Minger SL, & James W (2008). Homogeneous monocytes and macrophages from human embryonic stem cells following coculture-free differentiation in M-CSF and IL-3. Exp Hematol 36**:** 1167-1175.

Kato R, Matsumoto M, Sasaki H, Joto R, Okada M, Ikeda Y*, et al.* (2016). Parametric analysis of colony morphology of non-labelled live human pluripotent stem cells for cell quality control. Sci Rep 6**:** 34009.

Kelly EE, Horgan CP, & McCaffrey MW (2012). Rab11 proteins in health and disease. Biochemical Society Transactions 40**:** 1360-1367.

Kempf H, Andree B, & Zweigerdt R (2016). Large-scale production of human pluripotent stem cell derived cardiomyocytes. Adv Drug Deliv Rev 96**:** 18-30.

Kilpinen H, Goncalves A, Leha A, Afzal V, Alasoo K, Ashford S*, et al.* (2017). Common genetic variation drives molecular heterogeneity in human iPSCs. Nature 546**:** 370-375.

Kim C, Wong J, Wen J, Wang S, Wang C, Spiering S*, et al.* (2013). Studying arrhythmogenic right ventricular dysplasia with patient-specific iPSCs. Nature 494**:** 105-110.

Kim DS, Lee JS, Leem JW, Huh YJ, Kim JY, Kim HS*, et al.* (2010). Robust enhancement of neural differentiation from human ES and iPS cells regardless of their innate difference in differentiation propensity. Stem Cell Rev 6**:** 270-281.

Kim J, & Iyer VR (2004). Global role of TATA box-binding protein recruitment to promoters in mediating gene expression profiles. Mol Cell Biol 24**:** 8104-8112.

Kimbrel EA, & Lanza R (2015). Current status of pluripotent stem cells: moving the first therapies to the clinic. Nat Rev Drug Discov 14**:** 681-692.

Kitajima Y, Aoyama Y, & Seishima M (1999). Transmembrane Signaling for Adhesive Regulation of Desmosomes and Hemidesmosomes, and for Cell-Cell Detachment Induced by Pemphigus IgG in Cultured Keratinocytes: Involvement of Protein Kinase C. Journal of Investigative Dermatology Symposium Proceedings 4**:** 137-144.

Knowles GC, & McCulloch CA (1992). Simultaneous localization and quantification of relative G and F actin content: optimization of fluorescence labeling methods. J Histochem Cytochem 40**:** 1605-1612.

Koopman G, Reutelingsperger CP, Kuijten GA, Keehnen RM, Pals ST, & van Oers MH (1994). Annexin V for flow cytometric detection of phosphatidylserine expression on B cells undergoing apoptosis. Blood 84**:** 1415-1420.

Kozikowski A (1994). Synthesis of the benzofuran analogue of ILV, a new protein kinase C (PKC) activator. Bioorganic and medicinal chemistry letters 4**:** 637-640.

Kozikowski AP, Ma D, Du L, Lewin NE, & Bumberg PM (1995). Effect of alteration of the heterocyclic nucleus of ILV on its isoform selectivity for PKC. Palladium catalyzed route to benzofuran analogues of ILV. Farmaco 50**:** 425-430.

Kropp C, Kempf H, Halloin C, Robles-Diaz D, Franke A, Scheper T*, et al.* (2016). Impact of Feeding Strategies on the Scalable Expansion of Human Pluripotent Stem Cells in Single-Use Stirred Tank Bioreactors. Stem Cells Transl Med 5**:** 1289-1301.

Kumari S, Mg S, & Mayor S (2010). Endocytosis unplugged: multiple ways to enter the cell. Cell Res 20**:** 256-275.

Kuwana M, Okazaki Y, Kodama H, Izumi K, Yasuoka H, Ogawa Y*, et al.* (2003). Human circulating CD14+ monocytes as a source of progenitors that exhibit mesenchymal cell differentiation. J Leukoc Biol 74**:** 833-845.

Kyuno D, Kojima T, Yamaguchi H, Ito T, Kimura Y, Imamura M*, et al.* (2013). Protein kinase Calpha inhibitor protects against downregulation of claudin-1 during epithelial-mesenchymal transition of pancreatic cancer. Carcinogenesis 34**:** 1232-1243.

Labernadie A, Kato T, Brugues A, Serra-Picamal X, Derzsi S, Arwert E*, et al.* (2017). A mechanically active heterotypic E-cadherin/N-cadherin adhesion enables fibroblasts to drive cancer cell invasion. Nat Cell Biol 19**:** 224-237.

Lamouille S, Xu J, & Derynck R (2014). Molecular mechanisms of epithelial-mesenchymal transition. Nat Rev Mol Cell Biol 15**:** 178-196.

Langle D, Halver J, Rathmer B, Willems E, & Schade D (2014). Small molecules targeting in vivo tissue regeneration. ACS Chem Biol 9**:** 57-71.

Lee G, Ramirez CN, Kim H, Zeltner N, Liu B, Radu C*, et al.* (2012). Large-scale screening using familial dysautonomia induced pluripotent stem cells identifies compounds that rescue IKBKAP expression. Nat Biotechnol 30**:** 1244-1248.

Leeson P (2012). Drug discovery: Chemical beauty contest. Nature 481**:** 455-456.

Lei Y, & Schaffer DV (2013). A fully defined and scalable 3D culture system for human pluripotent stem cell expansion and differentiation. Proc Natl Acad Sci U S A 110**:** E5039-5048.

Li L, Bennett SA, & Wang L (2012a). Role of E-cadherin and other cell adhesion molecules in survival and differentiation of human pluripotent stem cells. Cell Adh Migr 6**:** 59-70.

Li M, & Belmonte JC (2017). Ground rules of the pluripotency gene regulatory network. Nat Rev Genet 18**:** 180-191.

Li W, Jiang K, & Ding S (2012b). Concise review: A chemical approach to control cell fate and function. Stem Cells 30**:** 61-68.

Li W, Jiang K, Wei W, Shi Y, & Ding S (2013a). Chemical approaches to studying stem cell biology. Cell Res 23**:** 81-91.

Li W, Li K, Wei W, & Ding S (2013b). Chemical approaches to stem cell biology and therapeutics. Cell Stem Cell 13**:** 270-283.

Lin T, & Wu S (2015). Reprogramming with Small Molecules instead of Exogenous Transcription Factors. Stem Cells Int 2015**:** 794632.

Lipinski CA, Lombardo F, Dominy BW, & Feeney PJ (2012). Experimental and computational approaches to estimate solubility and permeability in drug discovery and development settings. Advanced Drug Delivery Reviews 64**:** 4-17.

Liu K, Yu C, Xie M, Li K, & Ding S (2016). Chemical Modulation of Cell Fate in Stem Cell Therapeutics and Regenerative Medicine. Cell Chem Biol 23**:** 893-916.

Livak KJ, & Schmittgen TD (2001). Analysis of relative gene expression data using real-time quantitative PCR and the 2(-Delta Delta C(T)) Method. Methods 25**:** 402-408.

Logue SE, Elgendy M, & Martin SJ (2009). Expression, purification and use of recombinant annexin V for the detection of apoptotic cells. Nat Protoc 4**:** 1383-1395.

Lombardi D, Soldati T, Riederer MA, Goda Y, Zerial M, & Pfeffer SR (1993). Rab9 functions in transport between late endosomes and the trans Golgi network. EMBO Journal 12**:** 677-682.

Lowry WE, Richter L, Yachechko R, Pyle AD, Tchieu J, Sridharan R*, et al.* (2008). Generation of human induced pluripotent stem cells from dermal fibroblasts. Proc Natl Acad Sci U S A 105**:** 2883-2888.

Mani SA, Guo W, Liao MJ, Eaton EN, Ayyanan A, Zhou AY*, et al.* (2008). The epithelial-mesenchymal transition generates cells with properties of stem cells. Cell 133**:** 704-715.

Maretzky T, Reiss K, Ludwig A, Buchholz J, Scholz F, Proksch E*, et al.* (2005). ADAM10 mediates E-cadherin shedding and regulates epithelial cell-cell

adhesion, migration, and beta-catenin translocation. Proc Natl Acad Sci U S A 102**:** 9182-9187.

Mariani M, Karki R, Spennato M, Pandya D, He S, Andreoli M*, et al.* (2015). Class III beta-tubulin in normal and cancer tissues. Gene 563**:** 109-114.

Martin SJ, Reutelingsperger CP, McGahon AJ, Rader JA, van Schie RC, LaFace DM*, et al.* (1995). Early redistribution of plasma membrane phosphatidylserine is a general feature of apoptosis regardless of the initiating stimulus: inhibition by overexpression of Bcl-2 and Abl. J Exp Med 182**:** 1545-1556.

Martiny-Baron G, Kazanietz MG, Mischak H, Blumberg PM, Kochs G, Hug H*, et al.* (1993). Selective inhibition of protein kinase C isozymes by the indolocarbazole Go 6976. J Biol Chem 268**:** 9194-9197.

Matsa E, Burridge PW, Yu KH, Ahrens JH, Termglinchan V, Wu H*, et al.* (2016). Transcriptome Profiling of Patient-Specific Human iPSC-Cardiomyocytes Predicts Individual Drug Safety and Efficacy Responses In Vitro. Cell Stem Cell 19**:** 311-325.

Mayer-Davis EJ, Lawrence JM, Dabelea D, Divers J, Isom S, Dolan L*, et al.* (2017). Incidence Trends of Type 1 and Type 2 Diabetes among Youths, 2002-2012. N Engl J Med 376**:** 1419-1429.

McFedries A, Schwaid A, & Saghatelian A (2013). Methods for the elucidation of protein-small molecule interactions. Chem Biol 20**:** 667-673.

Mochly-Rosen D (1995). Localization of protein kinases by anchoring proteins: a theme in signal transduction. Science 268**:** 247-251.

Mochly-Rosen D, Das K, & Grimes KV (2012). Protein kinase C, an elusive therapeutic target? Nat Rev Drug Discov 11**:** 937-957.

Moreno-Bueno G, Peinado H, Molina P, Olmeda D, Cubillo E, Santos V*, et al.* (2009). The morphological and molecular features of the epithelial-to-mesenchymal transition. Nat Protoc 4**:** 1591-1613.

Muller FJ, Schuldt BM, Williams R, Mason D, Altun G, Papapetrou EP*, et al.* (2011). A bioinformatic assay for pluripotency in human cells. Nat Methods 8**:** 315-317.

Mullins RD, Heuser JA, & Pollard TD (1998). The interaction of Arp2/3 complex with actin: nucleation, high affinity pointed end capping, and formation of branching networks of filaments. Proc Natl Acad Sci U S A 95**:** 6181-6186.

Murriel CL, Churchill E, Inagaki K, Szweda LI, & Mochly-Rosen D (2004). Protein kinase Cdelta activation induces apoptosis in response to cardiac ischemia and reperfusion damage: a mechanism involving BAD and the mitochondria. J Biol Chem 279**:** 47985-47991.

Narsinh KH, Sun N, Sanchez-Freire V, Lee AS, Almeida P, Hu S*, et al.* (2011). Single cell transcriptional profiling reveals heterogeneity of human induced pluripotent stem cells. J Clin Invest 121**:** 1217-1221.

Narva E, Stubb A, Guzman C, Blomqvist M, Balboa D, Lerche M*, et al.* (2017). A Strong Contractile Actin Fence and Large Adhesions Direct Human Pluripotent Colony Morphology and Adhesion. Stem Cell Reports 9**:** 67-76.

Naumanen P, Lappalainen P, & Hotulainen P (2008). Mechanisms of actin stress fibre assembly. J Microsc 231**:** 446-454.

Nelson WJ, & Nusse R (2004). Convergence of Wnt, beta-catenin, and cadherin pathways. Science 303**:** 1483-1487.

Newton AC (2001). Protein Kinase C: Structural and Spatial Regulation by Phosphorylation, Cofactors, and Macromolecular Interactions. Chemical Reviews 101**:** 2353-2364.

Newton AC (2009). Lipid activation of protein kinases. J Lipid Res 50 Suppl**:** S266-271.

Newton AC (2010). Protein kinase C: poised to signal. Am J Physiol Endocrinol Metab 298**:** E395-402.

Nichols J, & Smith A (2009). Naive and primed pluripotent states. Cell Stem Cell 4**:** 487-492.

Niessen CM, Leckband D, & Yap AS (2011). Tissue organization by cadherin adhesion molecules: dynamic molecular and cellular mechanisms of morphogenetic regulation. Physiol Rev 91**:** 691-731.

Nose A (1990). Localization of specificity determining sites in cadherin cell adhesion molecules. Cell 61**:** 147-155.

Ohgushi M, Matsumura M, Eiraku M, Murakami K, Aramaki T, Nishiyama A*, et al.* (2010). Molecular pathway and cell state responsible for dissociation-induced apoptosis in human pluripotent stem cells. Cell Stem Cell 7**:** 225-239.

Overduin M, Harvey TS, Bagby S, Tong KI, Yau P, Takeichi M*, et al.* (1995). Solution structure of the epithelial cadherin domain responsible for selective cell adhesion. Science 267**:** 386-389.

Palacios F, Tushir JS, Fujita Y, & D'Souza-Schorey C (2005). Lysosomal targeting of E-cadherin: a unique mechanism for the down-regulation of cell-cell adhesion during epithelial to mesenchymal transitions. Mol Cell Biol 25**:** 389-402.

Parisini E, Higgins JM, Liu JH, Brenner MB, & Wang JH (2007). The crystal structure of human E-cadherin domains 1 and 2, and comparison with other cadherins in the context of adhesion mechanism. J Mol Biol 373**:** 401-411.

Parsons JT, Horwitz AR, & Schwartz MA (2010). Cell adhesion: integrating cytoskeletal dynamics and cellular tension. Nat Rev Mol Cell Biol 11**:** 633-643.

Passier R, Orlova V, & Mummery C (2016). Complex Tissue and Disease Modeling using hiPSCs. Cell Stem Cell 18**:** 309-321.

Penninger JM, Irie-Sasaki J, Sasaki T, & Oliveira-dos-Santos AJ (2001). CD45: new jobs for an old acquaintance. Nat Immunol 2**:** 389-396.

Pettinato G, Wen X, & Zhang N (2014). Formation of well-defined embryoid bodies from dissociated human induced pluripotent stem cells using microfabricated cell-repellent microwell arrays. Sci Rep 4**:** 7402.

Ponta H, Sherman L, & Herrlich PA (2003). CD44: from adhesion molecules to signalling regulators. Nat Rev Mol Cell Biol 4**:** 33-45.

Quintanilla RH, Jr., Asprer JS, Vaz C, Tanavde V, & Lakshmipathy U (2014). CD44 is a negative cell surface marker for pluripotent stem cell identification during human fibroblast reprogramming. PLoS One 9**:** e85419.

Qvit N, & Mochly-Rosen D (2014). The many hats of protein kinase Cdelta: one enzyme with many functions. Biochem Soc Trans 42**:** 1529-1533.

Reardon S, & Cyranoski D (2014). Japan stem-cell trial stirs envy. Nature 513**:** 287-288.

Redmer T, Diecke S, Grigoryan T, Quiroga-Negreira A, Birchmeier W, & Besser D (2011). E-cadherin is crucial for embryonic stem cell pluripotency and can replace OCT4 during somatic cell reprogramming. EMBO Rep 12**:** 720-726.

Reyland ME (2007). Protein kinase Cδ and apoptosis. Biochemical Society transactions 35**:** 1001-1004.

Rezania A, Bruin JE, Arora P, Rubin A, Batushansky I, Asadi A*, et al.* (2014). Reversal of diabetes with insulin-producing cells derived in vitro from human pluripotent stem cells. Nat Biotechnol 32**:** 1121-1133.

Robinton DA, & Daley GQ (2012). The promise of induced pluripotent stem cells in research and therapy. Nature 481**:** 295-305.

Rosner M, & Hengstschlager M (2016). Letter to the Editor: Human Pluripotent Stem Cells Release Oncogenic Soluble E-Cadherin. Stem Cells 34**:** 2443-2446.

Rosowski KA, Mertz AF, Norcross S, Dufresne ER, & Horsley V (2015). Edges of human embryonic stem cell colonies display distinct mechanical properties and differentiation potential. Sci Rep 5**:** 14218.

Rosse C, Linch M, Kermorgant S, Cameron AJ, Boeckeler K, & Parker PJ (2010). PKC and the control of localized signal dynamics. Nat Rev Mol Cell Biol 11**:** 103-112.

Saftig P, & Klumperman J (2009). Lysosome biogenesis and lysosomal membrane proteins: trafficking meets function. Nature Reviews Molecular Cell Biology 10**:** 623-635.

Schenone M, Dancik V, Wagner BK, & Clemons PA (2013). Target identification and mechanism of action in chemical biology and drug discovery. Nat Chem Biol 9**:** 232-240.

Scholzen T, & Gerdes J (2000). The Ki-67 protein: from the known and the unknown. J Cell Physiol 182**:** 311-322.

Schopperle WM, & DeWolf WC (2007). The TRA-1-60 and TRA-1-81 human pluripotent stem cell markers are expressed on podocalyxin in embryonal carcinoma. Stem Cells 25**:** 723-730.

Segal JM, & Ward CM (2017). Novel peptides for deciphering structural and signalling functions of E-cadherin in mouse embryonic stem cells. Sci Rep 7**:** 41827.

Shah VO, Civin CI, & Loken MR (1988). Flow cytometric analysis of human bone marrow. IV. Differential quantitative expression of T-200 common leukocyte antigen during normal hemopoiesis. Journal of Immunology 140**:** 1861-1867.

Shi Y, Inoue H, Wu JC, & Yamanaka S (2017). Induced pluripotent stem cell technology: a decade of progress. Nat Rev Drug Discov 16**:** 115-130.

Shi Y, Kirwan P, & Livesey FJ (2012a). Directed differentiation of human pluripotent stem cells to cerebral cortex neurons and neural networks. Nat Protoc 7**:** 1836-1846.

Shi Y, Kirwan P, Smith J, Robinson HP, & Livesey FJ (2012b). Human cerebral cortex development from pluripotent stem cells to functional excitatory synapses. Nat Neurosci 15**:** 477-486, S471.

Simons K, & Zerial M (1993). Rab proteins and the road maps for intracellular transport. Neuron 11**:** 789-799.

Singh A, Suri S, Lee T, Chilton JM, Cooke MT, Chen W*, et al.* (2013). Adhesion strength-based, label-free isolation of human pluripotent stem cells. Nat Methods 10**:** 438-444.

Sirenko O, Grimm FA, Ryan KR, Iwata Y, Chiu WA, Parham F*, et al.* (2017). In vitro cardiotoxicity assessment of environmental chemicals using an organotypic human induced pluripotent stem cell-derived model. Toxicol Appl Pharmacol 322**:** 60-74.

Soncin F, Mohamet L, Eckardt D, Ritson S, Eastham AM, Bobola N*, et al.* (2009). Abrogation of E-cadherin-mediated cell-cell contact in mouse embryonic stem cells results in reversible LIF-independent self-renewal. Stem Cells 27**:** 2069-2080.

Stanley ER, Berg KL, Einstein DB, Lee PS, & Yeung YG (1994). The biology and action of colony stimulating factor-1. Stem Cells 12 Suppl 1**:** 15-24; discussion 25.

Steinberg SF (2008). Structural basis of protein kinase C isoform function. Physiol Rev 88**:** 1341-1378.

Steinhusen U, Weiske J, Badock V, Tauber R, Bommert K, & Huber O (2001). Cleavage and shedding of E-cadherin after induction of apoptosis. J Biol Chem 276**:** 4972-4980.

Stepniewski J, Kachamakova-Trojanowska N, Ogrocki D, Szopa M, Matlok M, Beilharz M*, et al.* (2015). Induced pluripotent stem cells as a model for diabetes investigation. Scientific Reports 5.

Svitkina TM, & Borisy GG (1999). Arp2/3 complex and actin depolymerizing factor/cofilin in dendritic organization and treadmilling of actin filament array in lamellipodia. Journal of Cell Biology 145**:** 1009-1026.

Takahashi K, Tanabe K, Ohnuki M, Narita M, Ichisaka T, Tomoda K*, et al.* (2007). Induction of pluripotent stem cells from adult human fibroblasts by defined factors. Cell 131**:** 861-872.

Takahashi K, & Yamanaka S (2006). Induction of pluripotent stem cells from mouse embryonic and adult fibroblast cultures by defined factors. Cell 126**:** 663-676.

Takeichi M (1977). Functional correlation between cell adhesive properties and some cell surface proteins. The Journal of cell biology 75**:** 464-474.

Thatava T, Nelson TJ, Edukulla R, Sakuma T, Ohmine S, Tonne JM*, et al.* (2011). Indolactam V/GLP-1-mediated differentiation of human iPS cells into glucose-responsive insulin-secreting progeny. Gene Ther 18**:** 283-293.

Thorn K (2016). A quick guide to light microscopy in cell biology. Mol Biol Cell 27**:** 219-222.

Toyoda H, Nagai Y, Kojima A, & Kinoshita-Toyoda A (2017). Podocalyxin as a major pluripotent marker and novel keratan sulfate proteoglycan in human embryonic and induced pluripotent stem cells. Glycoconj J 34**:** 139-145.

Trounson A, & DeWitt ND (2016). Pluripotent stem cells progressing to the clinic. Nat Rev Mol Cell Biol 17**:** 194-200.

Tsankov AM, Akopian V, Pop R, Chetty S, Gifford CA, Daheron L*, et al.* (2015). A qPCR ScoreCard quantifies the differentiation potential of human pluripotent stem cells. Nat Biotechnol 33**:** 1182-1192.

van Roy F, & Berx G (2008). The cell-cell adhesion molecule E-cadherin. Cell Mol Life Sci 65**:** 3756-3788.

van Wilgenburg B, Browne C, Vowles J, & Cowley SA (2013). Efficient, long term production of monocyte-derived macrophages from human pluripotent stem cells under partly-defined and fully-defined conditions. PLoS One 8**:** e71098.

Veber DF, Johnson SR, Cheng HY, Smith BR, Ward KW, & Kopple KD (2002). Molecular properties that influence the oral bioavailability of drug candidates. Journal of Medicinal Chemistry 45**:** 2615-2623.

Wakao S, Kitada M, Kuroda Y, Ogura F, Murakami T, Niwa A*, et al.* (2012). Morphologic and gene expression criteria for identifying human induced pluripotent stem cells. PLoS One 7**:** e48677.

Watanabe K, Ueno M, Kamiya D, Nishiyama A, Matsumura M, Wataya T*, et al.* (2007). A ROCK inhibitor permits survival of dissociated human embryonic stem cells. Nat Biotechnol 25**:** 681-686.

Watt FM, & Huck WT (2013). Role of the extracellular matrix in regulating stem cell fate. Nat Rev Mol Cell Biol 14**:** 467-473.

Weinberger L, Ayyash M, Novershtern N, & Hanna JH (2016). Dynamic stem cell states: naive to primed pluripotency in rodents and humans. Nat Rev Mol Cell Biol 17**:** 155-169.

Workman P, & Collins I (2010). Probing the probes: fitness factors for small molecule tools. Chem Biol 17**:** 561-577.

Wu J, Fan Y, & Tzanakakis ES (2015a). Increased Culture Density Is Linked to Decelerated Proliferation, Prolonged G1Phase, and Enhanced Propensity for Differentiation of Self-Renewing Human Pluripotent Stem Cells. Stem Cells and Development 24**:** 892-903.

Wu J, & Izpisua Belmonte JC (2015b). Dynamic Pluripotent Stem Cell States and Their Applications. Cell Stem Cell 17**:** 509-525.

Wu-Zhang AX, & Newton AC (2013). Protein kinase C pharmacology: refining the toolbox. Biochem J 452**:** 195-209.

Xu Y, Shi Y, & Ding S (2008). A chemical approach to stem-cell biology and regenerative medicine. Nature 453**:** 338-344.

Xu Y, Zhu X, Hahm HS, Wei W, Hao E, Hayek A*, et al.* (2010). Revealing a core signaling regulatory mechanism for pluripotent stem cell survival and self-renewal by small molecules. Proc Natl Acad Sci U S A 107**:** 8129-8134.

Yang YC, Ciarletta AB, Temple PA, Chung MP, Kovacic S, Witek-Giannotti JS*, et al.* (1986). Human IL-3 (multi-CSF): identification by expression cloning of a novel hematopoietic growth factor related to murine IL-3. Cell 47**:** 3-10.

Yang YP, & Wright C (2009). Chemicals turn human embryonic stem cells towards beta cells. Nat Chem Biol 5**:** 195-196.

Yu C, Liu K, Tang S, & Ding S (2014). Chemical approaches to cell reprogramming. Curr Opin Genet Dev 28**:** 50-56.

Zeigerer A, Gilleron J, Bogorad RL, Marsico G, Nonaka H, Seifert S*, et al.* (2012). Rab5 is necessary for the biogenesis of the endolysosomal system in vivo. Nature 485**:** 465-470.

Zhang X, Ding L, & Sandford AJ (2005). Selection of reference genes for gene expression studies in human neutrophils by real-time PCR. BMC Mol Biol 6**:** 4.

Zhang Y, Li W, Laurent T, & Ding S (2012). Small molecules, big roles -- the chemical manipulation of stem cell fate and somatic cell reprogramming. J Cell Sci 125**:** 5609-5620.

Zhu T, Tsuji T, & Chen C (2010). Roles of PKC isoforms in the induction of apoptosis elicited by aberrant Ras. Oncogene 29**:** 1050-1061.

Zweigerdt R, Olmer R, Singh H, Haverich A, & Martin U (2011). Scalable expansion of human pluripotent stem cells in suspension culture. Nat Protoc 6**:** 689-700.